Design and Controllability of Plug-in Hybrid Electric Vehicle (PHEV) Charging Facilities Integrated with Renewable Energy Resources

A Dissertation

Presented to

the Faculty of the Department of Electrical and Computer Engineering

University of Houston

In Partial Fulfillment

of the Requirements for the Degree

Doctor of Philosophy

in Electrical Engineering

by

Preetham Goli

December 2014

Design and Controllability of Plug-in Hybrid Electric Vehicle (PHEV) Charging Facilities Integrated with Renewable Energy Resources

Preetham Goli

Approved:

Chair of the Committee
Dr. Wajiha Shireen, Professor,
Electrical and Computer Engineering,
Engineering Technology

Committee Members:

Dr. Yuhua Chen, Associate Professor,
Electrical and Computer Engineering

Dr. Zhu Han, Associate Professor,
Electrical and Computer Engineering

Dr. Heidar Malki, Professor and Chair,
Engineering Technology

Dr. Raymond E. Cline, Jr., Professor and Chair,
Information and Logistics Technology

Dr. Suresh K. Khator, Associate Dean,
Cullen College of Engineering

Dr. Badri Roysam, Professor and Chair,
Electrical and Computer Engineering

Acknowledgements

I am very happy to have a great opportunity to express my gratitude to all people that helped, influenced and supported my work directly or indirectly.

I owe my deepest gratitude to my advisor, Dr. Wajiha Shireen, whose encouragement, valuable guidance and support from the initial to the final stage enabled me to develop an understanding of the subject. Her broad knowledge and enthusiasm has greatly influenced my perception of engineering in general. At the same time her intelligence and positive attitude changed my perception of life.

It was an honor for me to have Dr. Yuhua Chen, Dr. Zhu Han, Dr. Heidar Malki, and Dr. Raymond E. Cline, Jr. as my committee members. I am very thankful to them for all the technical discussions, opinions and suggestions which greatly enhanced the quality of this document.

I would like to thank Mr David Owen and the CenterPoint Energy for funding my research. I am also thankful to Dr. Raymond E. Cline, Jr. and the Department of Energy (DOE) for funding very high quality laboratory equipment to carry out my research work.

I am indebted to all my present and past labmates, Radhakrishna Kotti, Sindhukrishna Yarlagadda, Shyam Janakiraman, Adarsh Nagarajan, and Sonal Patel for all their support, guidance and encouragement.

Latly, this thesis would not have been possible without an enormous support, love and understanding from my parents, brother and all my friends.

Design and Controllability of Plug-in Hybrid Electric Vehicle (PHEV) Charging Facilities Integrated with Renewable Energy Resources

An Abstract

of a

Dissertation

Presented to

the Faculty of the Department of Electrical and Computer Engineering

University of Houston

In Partial Fulfillment

of the Requirements for the Degree

Doctor of Philosophy

in Electrical Engineering

by

Preetham Goli

December 2014

Abstract

Electricity generation and transportation account for most of the global primary energy demand. The majority of the world's coal demand is for electricity generation and the majority of the world's oil demand is for transportation. This has triggered an increase in the deployment of renewable energy sources such as photovoltaic (PV) and wind throughout the globe. Likewise, alternative vehicle technologies, such as plug-in hybrid electric vehicles (PHEVs), are being developed to reduce the world's dependence on oil for transportation and to limit transportation-related greenhouse gas emissions. A major barrier for the wide penetration of PHEVs in the market is the underdeveloped charging infrastructure. Another emerging issue is that a large number of PHEVs connected to the grid simultaneously may pose a huge threat to the quality and stability of the overall power system. Since the initial penetration of PHEVs is expected to be confined to a particular neighborhood, charging them simultaneously might cause serious issues to the distribution transformers.

In view of the above issues this dissertation proposes a PHEV charging station architecture for workplace-based parking facilities using renewable energy sources (wind and/or PV) coupled with smart grid technologies. The proposed control algorithm will reduce the stress imposed on the grid at the distribution level during peak load hours. The proposed architecture consists of a DC microgrid that allows three-way interaction between the distributed energy sources, PHEVs and the grid, ensuring optimal usage of available power, charging time and grid stability. It consists of a photovoltaic and/or wind power source, power conditioning unit (PCU) along with an energy storage unit (ESU). The PCU consists of power converters with an intermediate DC-link.

A unique control algorithm, based on the variation in DC link voltage level

and the priority charging levels of PHEVs, facilitates the energy management and scheduling of PHEVs in the charging facility. As the DC link voltage is the only criterion used for switching between various modes, the overall complexity of the system is reduced in comparison to other existing methods.

Table of Contents

List of Figures

List of Tables

Chapter 1 Introduction

1.1 Introduction

The increasing environmental and economic problems coupled with the proliferation in smaller generating units in the form of wind and solar has opened new opportunities to generate power on-site. Along these lines, the so-called microgrid is a widely known and accepted concept that comprises energy storage and generating units in order to get the most from the naturally available renewable energy sources [1]. Although its structure is more complex, and a more expensive one, it provides unparallel flexibility in generating power locally. On the other hand, because of the rising energy costs, concerns about energy security and fossil energy reserves, and growing consumer expectations, plug-in hybrid electric vehicles (PHEVs) are appearing worldwide [2–4] and present a promising, emerging technology. An intelligent synergy of these two concepts combined with advanced control techniques can provide a great platform for developing renewable energy solutions at the lower power level .

Transportation sector has been one of the top contributors of greenhouse gas (GHG) emissions globally. The conventional vehicle operates through internal combustion engine (ICE) which runs on energy derived from fossil fuels (i.e. gasoline or diesel), thus emitting gases such as carbon dioxide, hydrocarbons, carbon monoxide, nitrogen oxides, water etc. From the statistical database of U.S Energy Information Administration (EIA), the world total energy consumption by the end-use sector is shown in Figure 1.1 and the carbon dioxide emissions by the end-use sector is shown in Figure 1.2 [5]. Transportation sector accounted for almost 27% of total energy consumption of the world and 33.7% of the total GHG emissions in 2012 [6].

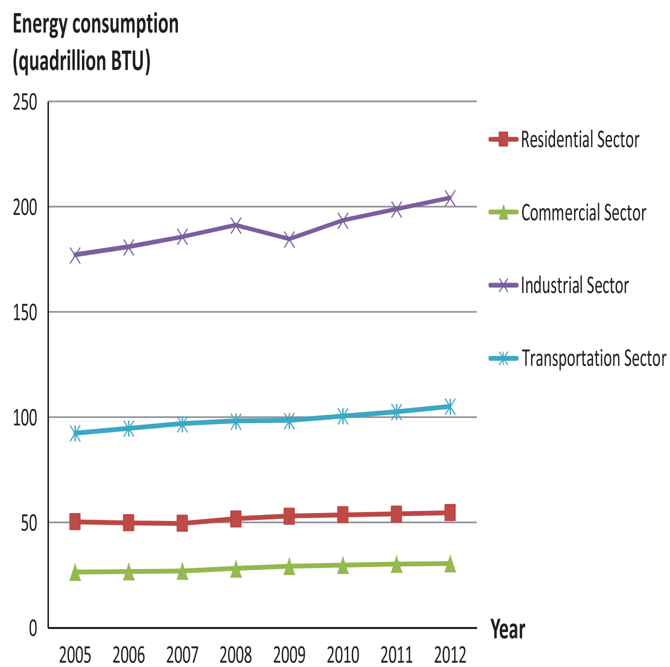

Figure 1.1: The delivered energy consumption (Quadrillion BTU) based on different end-users [5].

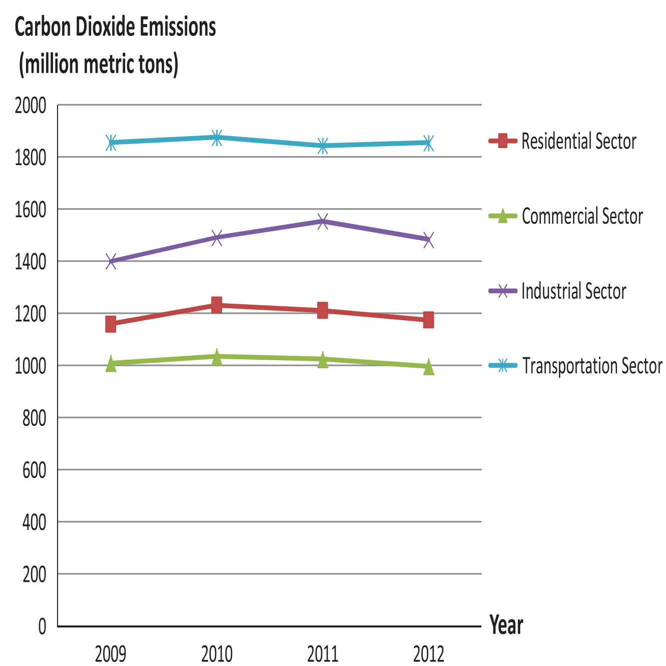

Figure 1.2: The energy-related carbon dioxide emissions (million metric tons CO_2 equivalent) based on different end-users [5].

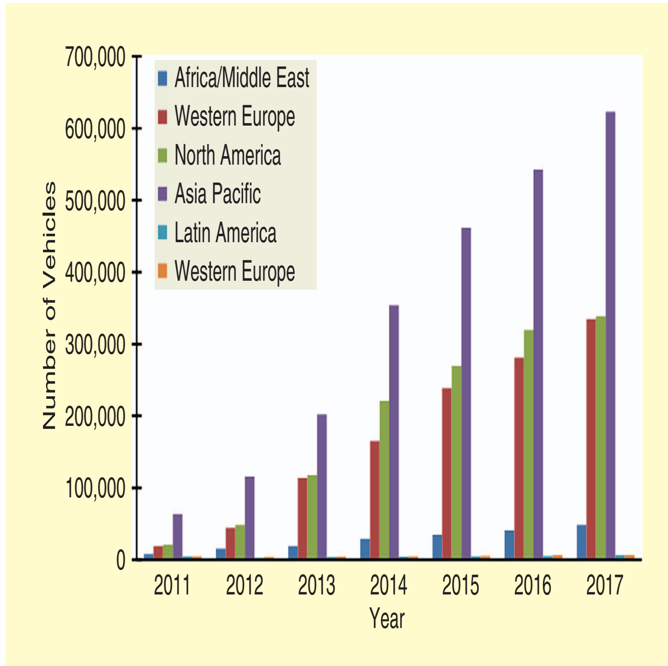

Figure 1.3: Global annual light-duty vehicle sales through 2017, as forecasted by Pike Research [7].

According to Navigant Research, "The average price of fuel for conventional vehicles will continue to rise through the remainder of this decade, driving the demand for electrified (hybrid, plug-in hybrid, and all electric) vehicles" [7]. So far, this prediction is being fulfilled, which is corroborated by Pike Research's findings of increasing electric vehicle (EV) sales and market penetration around the world, as noted in Figure 1.3. The International Energy Agency (IEA) has put forward a positive and ambitious road map to achieve widespread adoption and use of EVs and PHEVs worldwide by 2050. The road map targets a 30% reduction in global CO_2 levels by 2050 relative to 2005. The reduction is to be implemented through efficiency improvements and electrified transportation, with an EV share of at least 50% of the global light-duty vehicle sales.

To meet the expected penetration of PHEVs, it is essential to install charging facilities at appropriate locations for recharging PHEVs. These charging facilities are required to be built at home, neighborhood workplaces and markets/shopping malls in order to keep the PHEVs powered up and running reliably. The proliferation of these charging facilities will add stress to the already overloaded U.S. grid creating new challenges for the distribution network. Since upgrading of transformers en masse is an expensive option, this issue needs close attention with the increasing penetration of PHEVs.

1.2 Research Motivation and Objectives

The typical charging time of PHEVs is 7 to 8 hours, which might make it hard to accommodate these additional loads in the load curve without increasing the peak load [8]. Also, the required additional charging energy would have a possible impact on the utility system. Power transformers are one of the most expensive components in a distribution network. With the increasing penetration of PHEVs, a new load peak may be created, which may exceed the transformer capacity. This requires the utilities to upgrade the local distribution transformer or leads to an early replacement. Reduction in the transformer life expectancy will result in an increase in costs to the utilities and the consumers. Hence, the reduced transformer life becomes a very important impact when extra load is taken into consideration.

Expanding the electric system the conventional way, with large generating plants located far from the load centers, would require upgrading the transmission and distribution systems as well. Besides the high costs, this can take many years before obtaining the right-of-way. Alternatively, smaller and cost effective power plants based on renewable energy, such as wind energy, are being considered by the utilities. Also, solar energy can be installed in a fraction of that time on the distribution system. Photovoltaic (PV) presents a modular characteristic and can be easily deployed on the roof top and facades of residences and buildings. In view of this, this dissertation proposes a new architecture for PHEV charging facilities integrated with PV or wind power source. The proposed charging facility will charge the PHEVs from the photovoltaic/wind turbine system, thus reducing the stress on the grid. When the grid is at peak demand and solar power is insufficient to charge the PHEVs then the charging station would enable vehicle charging to be delayed or temporarily interrupted. The use of on-site power generation from renewable sources will be a key step in ensuring that the electricity used to power PHEVs is clean renewable energy. The design of smart, efficient systems will be vital in maximizing the power delivered to PHEVs.

The proposed architecture shown in Figure 1.4 provides a high level view of the charging facility. The proposed architecture consists of a DC microgrid that allows three-way interaction between the distributed energy sources, PHEVs and the grid, ensuring optimal usage of available power, charging time and grid stability. It consists of a photovoltaic or wind power source, a power conditioning unit (PCU) and an energy storage unit (ESU). The PCU consists of power converters with an intermediate DC link. A simple but unique control strategy based on DC link voltage sensing is proposed in which the DC link voltage level is allowed to change in accordance to the changes in solar irradiation or wind speeds. As the DC link voltage is the only criterion responsible for switching between various modes the overall complexity of the system is reduced in comparison to other existing methods.

The contributions of this dissertation can be summarized as follows :

1. Increasing the penetration of renewable energy sources in transportation and the power industry.
2. Smart charging techniques proposed in this research will help in avoiding major expense to upgrade distribution transformers and other substation equipment with the increase in PHEV loads on the distribution system.

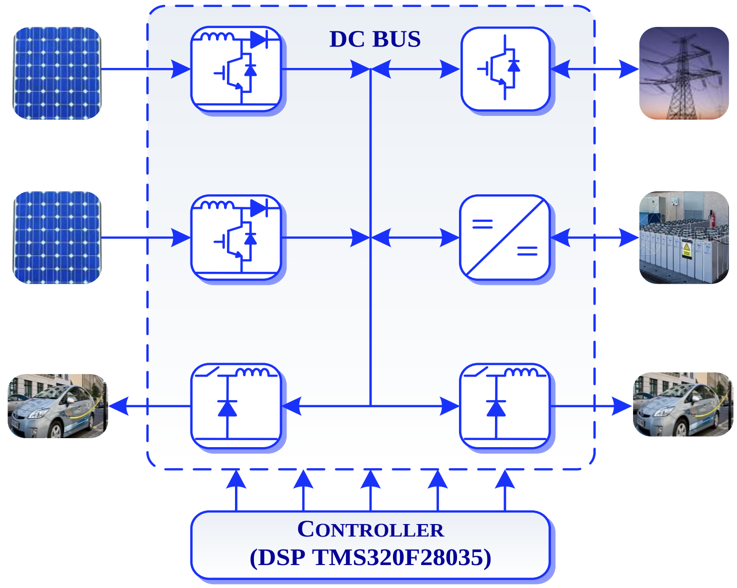

Figure 1.4: Proposed architecture for the charging facility.

3. Improved economic performance of PHEVs could be enabled by the availability of mid-day charging (through the propsoed architecture for charging facilities), increasing the distance traveled using low-cost electricity, and potentially reducing the size of the battery.

4. A more efficient and reliable DC charging infrastructure which offers the additional advantage of fast charging compared to the conventional AC charging methods.

1.3 Dissertation Organization

The contents of this dissertation proposal have been organized in the following manner :

Chapter 1 provides an introduction about the necessity of integrating PHEV charging facilities with renewable energy sources such as wind and solar. The current energy consumption and carbon dioxide emissions from various end user sectors is discussed briefly. The proposed architecture for the charging facility is described vividly and the motivation and contributions of the dissertation are presented.

Chapter 2 covers the detailed literature review on the current state of the knowledge on PHEV charging infrastructure. The existing charging methods and battery technology are discussed. The impact of charging PHEVs on the distribution transformer and the techniques to mitigate this issue are presented. Various power electronic topologies for charging facilities integrated with renewable energy sources are reviewed. Finally the concept of DC link voltage sensing which is a simple but unique control strategy for energy management in the proposed charging facility is explained in detail.

In Chapter 3, the architecture and control of a PV powered workplace-based charging facility is presented. To verify the practical feasibility and effectiveness of the proposed control strategy, laboratory tests have been carried out. Experimental results are presented which support the operation of the charging facility in various modes. This chapter shows how the concept of DC link voltage sensing is contemplated for energy management in a PV integrated charging facility

PHEVs are expected to stay in a workplace-based PV/wind powered charging facility for several hours. On the other hand the power generated by renewable energy sources is highly stochastic in nature. Hence the charging of PHEVs has to be scheduled in order to facilitate the greater use of renewable energy sources for charging them within the stipulated time period. To this end, Chapter 4 presents a real time scheduling algorithm for charging PHEVs in a workplace-based charging facility. The proposed algorithm is based on the DC link voltage level and certain charging priority levels

As small wind turbine research & development continues to reduce capital expense and increase generation efficiency, more homeowners and small businesses will begin to utilize wind as an alternative renewable source of energy. Hence charging PHEVs from small scale wind turbines is also being realized as a viable alternative. In view of this, Chapter 5 proposes a charging station architecture with a small scale wind turbine as the primary source. Coordinated control strategy based on DC link voltage sensing is proposed to facilitate the operation of the charging facility in standalone and grid-connected mode. The proposed architecture and the control algorithm are validated through simulations and experimental results.

Chapter 6 gives some conclusions and directions for the future work on integrating renewable energy sources into the existing power grid though a network of charging facilities powered by PV/wind.

Chapter 2 Review of PHEV Charging Infrastructure

This chapter presents the detailed literature review on the current state of the knowledge on PHEV charging infrastructure. The existing charging methods and battery technology are discussed. The impact of charging PHEVs on the distribution transformer and the techniques to mitigate this issue are presented. Various power electronic topologies and control algorithms for charging facilities integrated with renewable energy sources are reviewed. The concept of DC link voltage sensing which is a simple but unique control strategy for energy management in the proposed charging facility is explained in detail. Issues related to the grid integration of PHEVs and PV systems are addressed. Finally recent trends, advancements, and on going projects on solar based charging stations are presented.

2.1 PHEV Charging Infrastructure

The rate of PHEV adoption will be determined by behavioral considerations concerning charging location (density), the duration of charging time, and the current challenge of range anxiety.

A diagram of a typical PHEV energy transfer system is shown in Figure 2.1. A low-frequency transformer is used to deliver AC power from the grid to the neighborhood where the electric vehicle supply equipment (EVSE) is installed. Typically, the EVSE includes conductors, electric vehicle (EV) connectors, attachment plugs, communication protocols, and all other fittings, devices, and power outlets. The EVSE serves as the energy transfer interface between the premises wirings and the PHEV's on-board or off-board battery chargers.

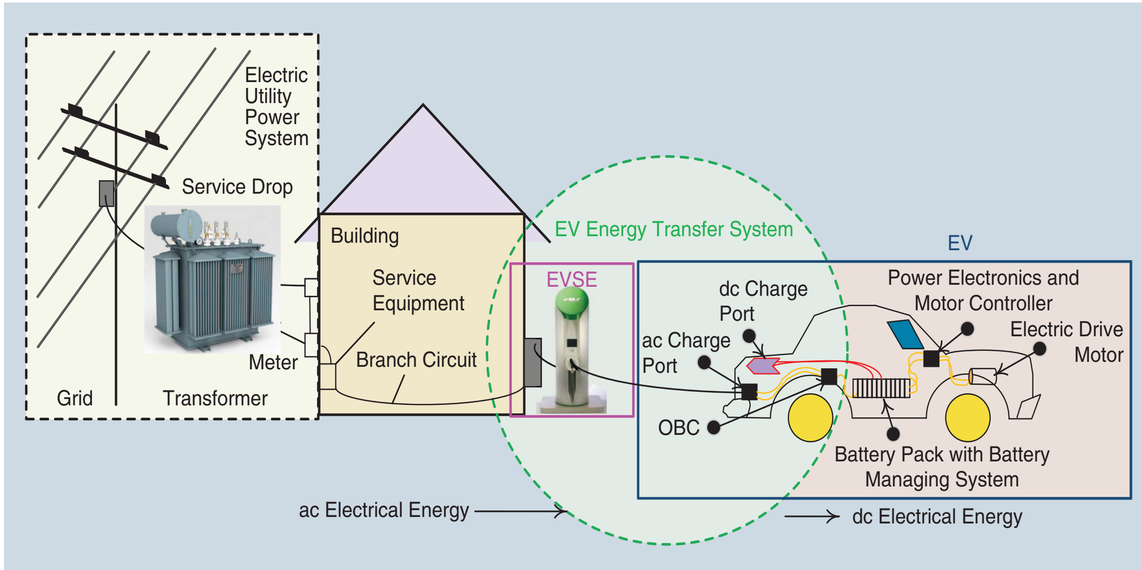

Figure 2.1: A diagram of a PHEV energy transfer system.

There are several charging levels for PHEVs that reflect the power capability and charging duration. These levels have been standardized to reveal the PHEVs low or fast charging scenarios. The slow charging (typically upto 8 hrs - PHEV or 20 hrs - EV) can be experienced at home or office areas whereas the fast charging (typically 15 min to 1h) at dedicated charging stations in commercial or public places. As shown in Table 5.1, the AC Level 1 is practically realized at home environment while the AC Level 2 is suitable for public and commercial areas like workplace, movie theaters, shopping malls etc. However, the DC-fast charging (DC Level 1-3) is envisioned to cover the public, private or commercial charging stations [9,10].

Figures 2.2 and 2.3 illustrate the PHEV charging configurations for the AC Level 1 & 2 requirements (PHEV includes an on-board charger) and DC Level 1 & 2 (electric vehicle supply equipment (EVSE) includes an off-board charger), respectively. The two figures illustrate the setup of the facilities at the charging point and embedded PHEV kits for charging scenarios by considering the AC and DC charging levels as depicted in Table 5.1. With the AC Level 1 and 2 config-

Table 2.1: AC/DC charging levels characteristics as per SAE J1772 standard

Power level type	Voltage level [V]	Current capacity [A]	Power capacity [kW]
AC Level 1	120 VAC	12	1.4
AC Level 2	240 VAC	Up to 80	19.2
Ac Level 3	-	-	>20
DC Level 1	200 - 500 VDC	<80	Up to 40
DC Level 2	200 - 500 VDC	<200	Up to 100
DC Level 3	200 - 600 VDC	< 400	Up to 240

urations in Figure 2.2, the electric vehicle supply equipment (EVSE) is provided at the charging point by supplying the AC power to an on-board charger. However, with the DC Level 1 and 2 configurations in Figure 2.3, the charging point supplies the DC current to the PHEV battery pack.

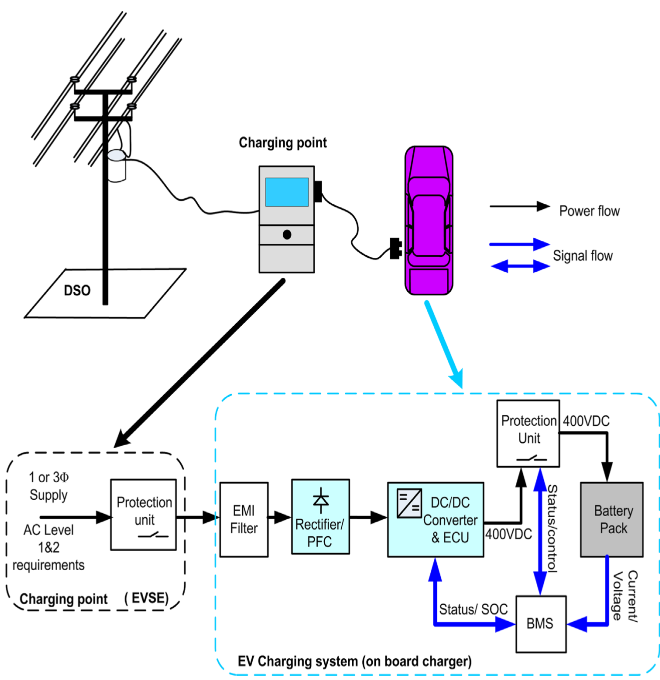

Figure 2.2: PHEV charging configuration for AC level 1 and 2 setup (i.e. on-board charger).

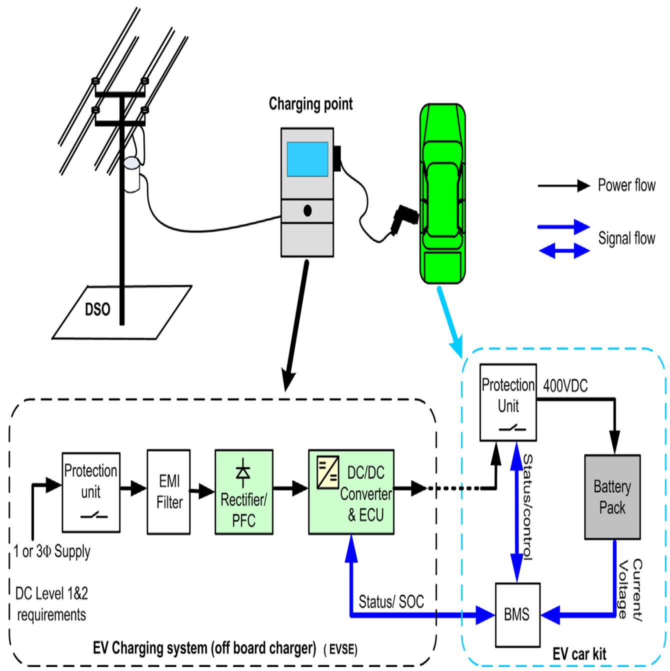

Figure 2.3: PHEV charging configuration for DC level 1 and 2 framework (i.e. off-board charger).

2.2 Battery Technology

Today's battery technology is quite an obstacle for marketability of PHEVs. In order for a PHEV to achieve a substantial all-electric range, it must have much larger battery capacity than HEVs (hybrid electric vehicles). At present, batteries with such high power requirements come at a very high cost. A Li-ion (Lithium-ion) cell has a higher energy density than other battery chemistries such as lead acid cell, nickel cadmium cell, and Ni-metal(Nickel-metal) hydride cell. In PHEVs, the energy density and the weight of the battery are two of the most critical parameters that determine the electric range of the vehicle. Consequently, the Li-ion cell has dominated the market of commercially available PHEVs. This can be observed in Table 2.2, as all the listed PHEVs are equipped with an Li-ion battery pack. Although extended life cycles, increased energy density, and a slight cost reduction have been achieved with the evolution of battery technology, the Li-ion battery pack is still the most expensive and heaviest component of a

PHEV.

Table 2.2: Battery capacity and technologies by various EV/PHEV manufacturers

Vehicle Model/EV type	Battery type/Capacity	Battery Charger (kW)
Nissan Leaf/EV	Li-ion/24 kWh	3.3
BMW ActiveE/EV	Li-ion/32 kWh	7.2
Ford Focus/EV	Li-ion/23 kWh	6.6
Mitsubishi I/EV	Li-ion/16 kWh	3.3
Honda Fit/EV	Li-ion/20 kWh	3.3
Toyota Prius/PHEV	Li-ion/4.4 kWh	3.3
Chevy volt/PHEV	Li-ion/16 kWh	3.3
Cadillac ELR/PHEV	Li-ion/16.5 kWh	3.3
Tesla Model S/EV	Li-ion/85 kWh	10

2.3 Impact of PHEV Charging on the Distribution System

Large-scale penetration of PHEVs can have a detrimental and destabilizing effect on the electric power grid. With the variation in demand, the production of power can vary significantly. Variation in charging time of PHEVs can result in distinct differences in fuels and generating technologies [11]. Figure 2.4 illustrates the impact of charging one million PHEVs on the Virginia - Carolinas electric grid in 2018 on the various generation technologies. As shown in Figure 2.4, at low specific power and late in the evening, coal was the major fuel used, while charging more heavily during peak times led to more use of combustion turbines and combined cycle plants. Since the initial deployment of PHEVs is assumed to be clustered to a particular neighborhood, many authors have focused their research on the study of distribution transformer impacts. Depending upon the time, place of vehicle charging, various charging methods, and the charging power levels, there could be several ramifications on the distribution network. Various analytical techniques and different simulation tools were employed by several authors to estimate the transformers loss-of-life, average lifetime and harmonic losses. The percentage of transformers loss-of-life and average lifetime are important factors to be considered while studying the charging behavior of PHEVs on the future distribution system. High penetration of PHEVs in the future will increase the loss-of-life factor of distribution transformers [12–15].

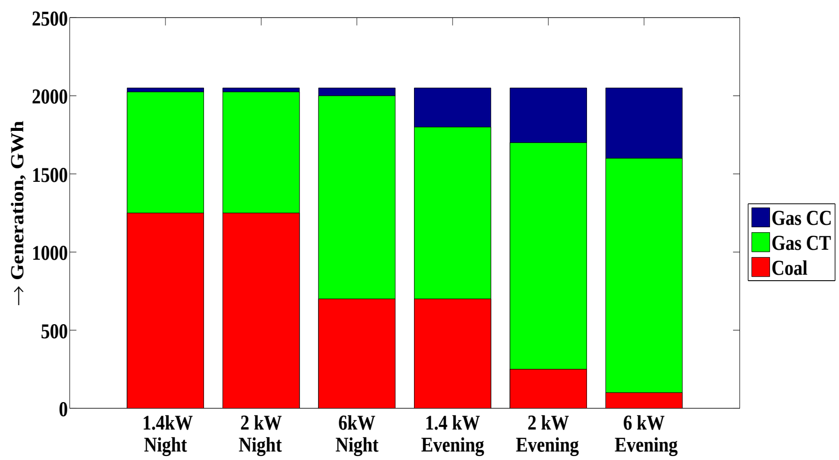

Figure 2.4: Generation shares by plant type for PHEV charging level and timing [11].

The impact of controlled and uncontrolled charging of PHEVs on the average lifetime of a transformer is described in [13] and [15]. As per [13], the average lifetime of a transformer is reduced by 4-20% under uncontrolled charging for a PHEV penetration of 10%. At 50% penetration of PHEVs, the average lifetime is reduced by 200-300% with uncontrolled charging. On the other hand controlled charging increases the lifetime by 100-200% with respect to uncontrolled charging for 50% penetration of PHEVs. Plug-in electric vehicle charging rates can have a significant impact on the lifetime of a transformer [13], [14]. Table 2.3 summarizes the sensitivity of transformer lifetime to different charging rates (3.6 kW and 7.7 kW) under controlled and uncontrolled charging for various levels of PHEV penetration. As expected, transformer life degradation is exacerbated when the charging rate is increased from 3.6 kW to 7.7 kW.

Table 2.3: Impact of charging PHEVs [13]

Charger Rating	**3.6 kW**				**7.7 kW**			
Charger Type	**Uncontrolled**		**Controlled**		**Uncontrolled**		**Controlled**	
PHEV Penetration	**Minimum Lifetime (years)**	**Average Lifetime (years)**	**Minimum Lifetime (years)**	**Average Lifetime (years)**	**Minimum Lifetime (years)**	**Average Lifetime (years)**	**Minimum Lifetime (years)**	**Average Lifetime (years)**
10%	29.2	61.1	32.7	56.3	27	49.8	34.1	59.6
25%	26.8	37.4	25.7	55.5	16.8	36.5	33.3	52.9
50%	12.2	38.9	10.7	45.2	11.2	24.3	29.9	48.4
75%	16	31.4	11.7	49.1	5.8	14.5	42.9	62.2
100%	8.3	18.4	12.8	37.8	2.3	10.5	26.8	38.8

The percentage of transformers loss-of-life can be minimized through distributed charging and controlled off-peak charging which requires coordination among utilities, customers and charging stations. Simulation results in [16] show that distributing the load profile of the battery charging helps to minimize the distribution transformer loss-of-life. Power management of the PHEV battery charge profile can help manage the loss-of-life of the distribution transformer. Controlled off-peak charging can shift PHEVs charging load to an off-peak time. Usually charging PHEVs at night time is proposed as the best way to mitigate the loss-of-life issues of distribution transformers. However, PHEVs can also introduce a new peak or near peak in early off-peak time. Generally, the impact of extra load on transformers in summer is much greater than that in winter. However, some winter mornings with peak load may be an exception. Charging from midnight through early morning in those days may exert strong impact on transformers. Figure 2.5 describes this effect by taking the average residential load for East Texas into consideration. As shown in the figure for a particular day in winter, February 11th, the load consumed in the early morning is higher than that in

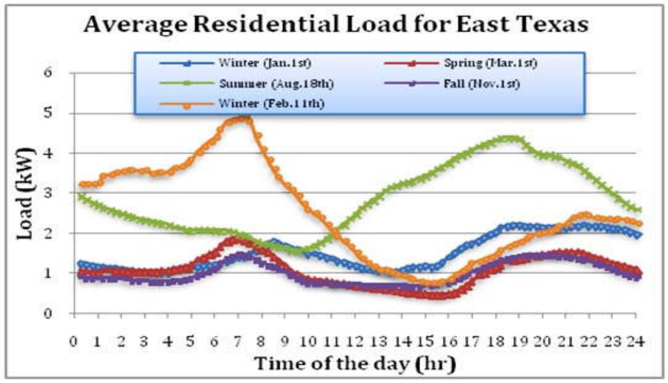

Figure 2.5: 15-minute interval data of average residential individual customer in East Texas [12].

summer days. Therefore, it is not always appropriate to charge electric vehicles at 1 am in those days. The required control strategy should depend on the actual load profile in a particular area for a particular time period.

2.4 Mitigating the Impact of PHEV Charging on the Distribution System

To mitigate the issue of transformer loss-of-life due to PHEV charging, integration of renewables like rooftop PV systems into the existing power grid has been proposed. In [17], a case study for the year 2030 was built based on demand increase, forecasted PHEV and DG units. The results showed that PHEV battery charging would prove onerous for the constraints studied. DG penetration would be able to provide support for PHEV battery charging but PHEV battery charging management would be necessary to minimize the impact in order to reach high levels of PHEV penetration. Reference [18] presents a methodology to quantify the benefits of the distribution transformer life extension brought about by customer-owned DG units. The results show that distribution transformer loss-of-life variation, as a function of the DG penetration level, presenting a monotonically decreasing characteristic which saturates after a certain penetration level. The possibility of smoothing out the load variance in a household microgrid by regulating the charging patterns of family PHEVs is investigated in [19]. The residential PV system was simulated with PHEV charge-discharge control. Several cases with different combinations of PV, PHEV, V2H (Vehicle to Home i.e. discharge of PHEV) and various charging schemes were analyzed. Table 2.4 shows the various scenarios possible. From the information available from the table, Case 1 describes a residential facility without PV and PHEV. Case 2 describes a residential facility integrated with rooftop PV system without PHEV. Therefore, these 2 cases analyze the effects of using PV while using gasoline vehicles instead of PHEVs. Case 3 represents a residential facility with PV and PHEV without V2H capabilities. Cases 4 to 6 have all the facilities (i.e. PV, PHEV, and V2H capabilities) but their charge-discharge schemes are different.

Table 2.4: Possible scenarios for a residential facility with PV and PHEV

Case	**PV**	**PHEV**	**V2H**	**Charging Scheme**
1	×	×	×	n/a
2	✓	×	×	n/a
3	✓	✓	×	Fixed (100 % SOC)
4	✓	✓	✓	Fixed (100 % SOC)
5	✓	✓	✓	Fixed (80 % SOC)
6	✓	✓	✓	Variable value

Simulation results for various cases are shown in Figure 2.6. The local consumption rate of PV output increased by 1.7% when gasoline vehicles (case 2) are replaced with PHEVs (case 3). On the other hand, the rate of PV utilization increased by 8.6% when the charging scheme changed from fixed (fixed target of SOC - case 5) to variable (variable target value of SOC - case 6).

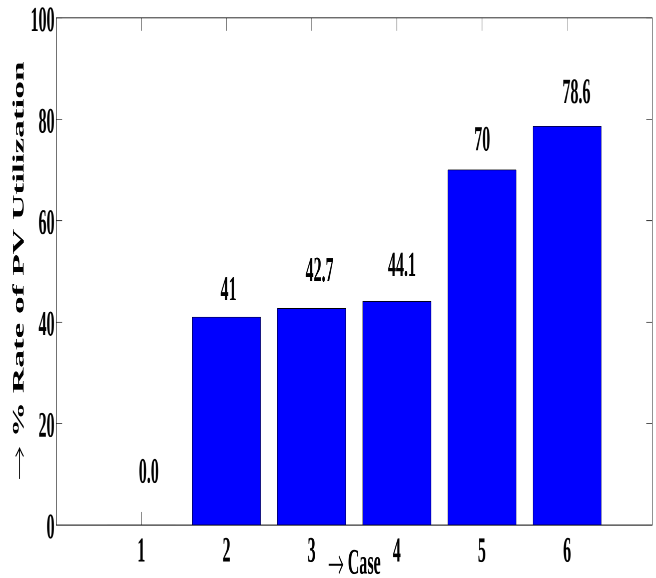

Figure 2.6: The rate of PV utilization.

The investigation on the large penetration of rooftop PV solar and PHEVs is reported in [20]. The study is centered on the impacts of the synergy between PHEV charging and large distributed rooftop PV installations especially with the voltage mitigation support. This mutual relationship works to complement each other; hence the PHEVs can enhance large integration of the PV solar by providing voltage support and can reduce the stresses on the power distribution system through V2G (vehicle-to-grid) services. It is noted that a specific integration of PV solar and PHEVs presented a reduction of about 15% of the voltage fluctuations. The integration of PV rooftop in photovoltaic charging facilities (PCFs) can relieve the burden on the distribution networks, by reducing the effective load seen by the distribution grid during peak charging period, as well as supplying power to grid when excess power is generated by PV rooftops. A PV parking lot for PHEVs

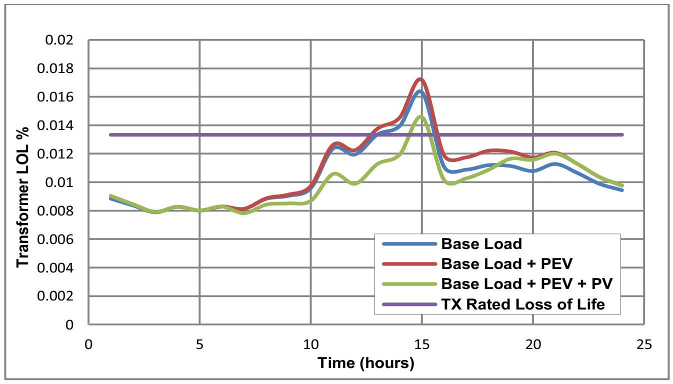

Figure 2.7: Stochastic distribution transformer loss-of-life [22].

is proposed in [21], in which the PHEVs can be charged from the PV source as well as the distribution grid. Mathematical models are developed to estimate the electric power capacity for PV parking lot. An evaluation of the impacts resulting from the expected PHEV scenarios are performed through stochastic sequential simulations of the distribution system with PHEV load and PV generation in [22]. Figure 2.7 shows the LOL (loss-of-life) experienced at a particular distribution transformer, for change in stochastic PHEV load and PV generation units. It is evident from the figure that rooftop PV coupled with PHEVs can reduce LOL of the distribution transformer. Results from [23] indicate that administration of solar PV into the network causes a transformer LOL reduction of 18% when integrated with a PHEV penetration level of 27.27%. Investigation signifies that compilation of solar PV and PHEV coupling throughout the network reduces the transformer power demand and henceforth, reduces the LOL during peak sun hours. These studies have shown that PV generation coupled with PHEV charging can delay and reduce the temperature rise of distribution transformers.

2.5 Proposed Architectures for PV Based PHEV Charging Facilities

Photovoltaic solar energy has a better correlation between generation and load, as the power is generated during the day when demand on the power grid is high. As described in Section 2.4 solar panels on rooftops or free-standing solar carports provide an excellent method of charging PHEVs, while minimizing the impact of daytime charging on the distribution network. Topologies for solar carports or photovoltaic charging facilities (PCFs) vary depending on their location, the expected number of PHEVs and their duration of stay in the parking lot. In view of this, this section reviews the various architectures proposed for PV Based PHEV Charging Facilities.

The charging units for PHEVs can be either on-board or off-board as described in Section 2.1. In case of an off-board charger, the charger is an external unit as shown in Figure 2.3 while in the case of an on-board charger it is a component of the vehicle. On-board chargers are supplied with AC power and they consist of an AC/DC rectifier, DC/DC boost converter for power factor correction and a DC/DC converter to charge the battery as shown in Figure 2.2. Currently AC charging is being employed to charge PHEVs by means of on-board chargers. The major drawback of this technology is that it does not support fast charging as it is required to increase the power capability of the on-board charger thereby increasing the weight and therefore the cost of the PHEV. Hence to support fast charging of PHEVs off-board chargers are proposed which directly supply DC power to the PHEV charging inlet. It is to be noted that in case of an off-board charger the entire power conversion (AC/DC) takes place in an external unit and therefore it is feasible to increase the ratings of the power converters in order to support fast charging.

AC system is being used since years for power distribution and there are well developed infrastructure-standards and technologies. DC system on the other hand has many advantages, starting with the fact that overall efficiency of the system could be higher and it facilitates the integration of renewable energy sources with fewer power converters. Since PV arrays generate DC power, a charging facility featuring PV power facilitates the charging of PHEVs from a DC bus. The DC bus system is expected to be more effective, efficient and economical than an equivalent aggregate of AC-DC battery chargers connected to the AC grid, since it relieves the battery chargers from the need for a bi-directional, front-end, power-factor correction (PFC) stage [24]. Various methods have been proposed for integrating PHEV chargers within a photovoltaic system. Several power electronic topologies for a PCF have been proposed in the literature based on the type and the number of converters which are classified as:

Centralized Architecture

Distributed Architecture

Single Stage Conversion With Z-converter

2.5.1 Centralized Architecture

Detailed block diagram representing the centralized architecture is shown in Figure 2.8. It consists of a central DC/DC boost converter which performs the function of maximum power point tracking. The DC/DC chargers are integrated with the PV charging facility at the DC link. Multiple PHEVs can be charged by increasing the corresponding ratings of PV panels and the associated power converters. Each parking spot must have a dedicated DC/DC buck converter which is connected to the DC link. This configuration is suitable for charging stations in the range of several kilowatts. It is applicable for charging vehicles like

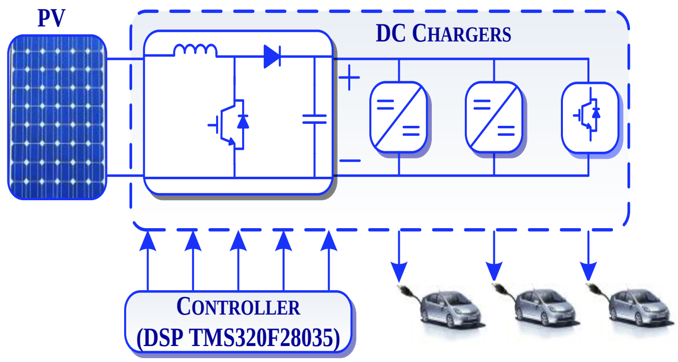

Figure 2.8: Centralized architecture.

golf carts, campus utility vehicles etc which commute for very short distances with low battery capacities. Battery switch station powered by PV is a good candidate for adopting centralized architecture. But this kind of configuration does not support fast charging since installation of a very high power DC/DC converter is very expensive and it is vulnerable to single fault shutdown.

2.5.2 Distributed Architecture

Presence of DC/DC converters with high power ratings is an important criterion for fast charging of PHEVs. This can be achieved economically through distributed architecture as shown in Figure 2.9. The architecture consists of several strings of PV panels and each string of PV panels is interfaced with their own DC/DC converter and shares a common DC bus, which connects to an AC utility grid through a bi-directional DC/AC converter [25, 26]. The DC/DC battery chargers are connected to the DC bus. Each parking spot requires an individual DC/DC converter to charge the PHEVs. The proposed architecture is suitable for installation at places such as workplace, universities, shopping malls etc where the demand of PHEVs and their duration of stay in the parking lots are highly

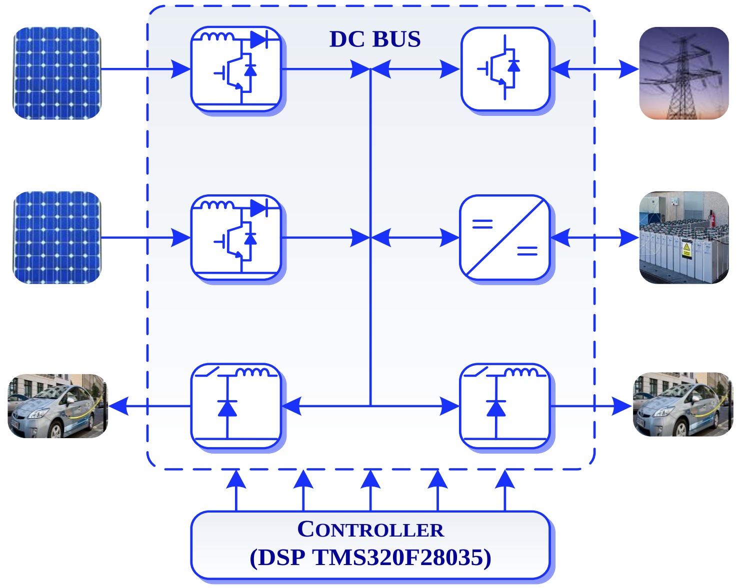

Figure 2.9: Distributed architecture.

probabilistic in nature. It is more reliable since the PHEVs can be charged from the grid during the periods of low insolation or cloudy weather. Also, it is important to note that the extra energy generated by PV can be injected into grid, which can be used to balance the PV costs.

A PCF requires constant power from the PV or the grid to meet the high demand of PHEVs. The reliability of a PCF can be improved by including an energy storage unit such as a battery bank, ultra capacitor, fuel cell etc. For instance in [27] the power generated by roof top photovoltaic system is stored in VRLA (valve-regulated lead-acid battery) batteries and fuel cells in a PHEV docking station. The PHEVs arriving at the docking station can be charged from two separate tracks i.e. using the energy from the VRLA batteries or the fuel cells. The use of storage capacity in PCFs has the following advantages [28]:

- Efficient use of renewable energy sources

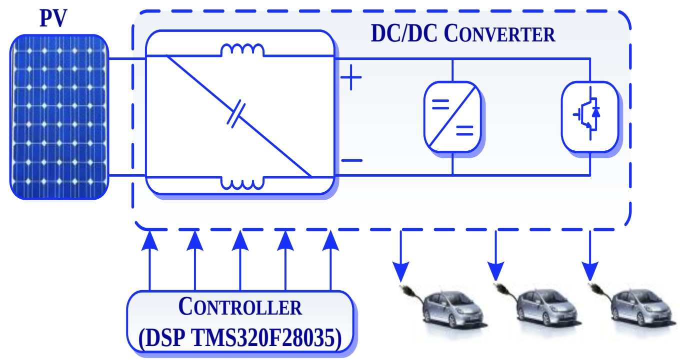

Figure 2.10: Single stage conversion with Z-converter.

- Maximization of renewable energy sources contribution
- Better demand and production match, better auxiliary service supply and improved overall reliability

The core idea of including an ESU is that the power demand by PHEVs can be either supplied by the PV or the utility or through a local energy storage unit. Energy derived from the ESU can charge the PHEVs during certain contingencies such as islanding condition without the availability of PV power. It facilitates the charging of PHEVs using minimum energy from the grid. The charging station appears as a DC microgrid with local generation from the PV system, PHEVs as loads and battery bank representing the storage system.

2.5.3 Single Stage Conversion with Z-converter

The double stage conversion described in the above architectures is replaced by a single stage using a Z-converter [29, 30] as shown in Figure 2.10. It is integrated with a DC/DC converter to provide galvanic isolation. The Z-converter has double modulation capability, and can shape the grid current while simultaneously regulating PHEV battery charging. This ensures close to unity power factor for all operating modes and power flow paths; achieving this with a single conversion stage can be considered a unique advantage of the Z-converter. Furthermore, this topology possesses inherent buck-boost capability, allowing increased voltage range on the PV or grid. Despite the single conversion stage, reliability, rather than efficiency or cost, is the strong point of the Z-topology. Also the single-phase power processed by the Z-converter consists of 120 Hz double line frequency ripple. This ripple can be mitigated by placing an additional decoupling capacitor across the PV source which introduces possible deviation from perfectly constant power extraction at the PV panels. Table 2.5 summarizes the comparisons among various architectures with regards to the power level, applications, and issues.

Table 2.5: Comparison of architectures for PV based charging facilities

Architecture	Charger Type	Power Level	Power Flow	Applications	Issues
Centralized Architecture	DC off-board	DC Level 1	PV to PHEVs with the power conditioned by DC/DC converters	To charge fleet based electric vehicles such as golf carts, campus commute vehicles etc. Charging batteries in battery switch stations	Not suitable for fast charging and Vulnerable to single point fault shutdown
Distributed Architecture	DC off-board	Suitable for DC Level 2 and DC Level 3	PV to PHEVs or grid to PHEVS or both via DC/DC and DC/AC bi-directional converters	Charging stations at places such as universities, workplaces, shopping malls etc	High cost of installation due to the presence of multiple DC/DC converters
Single Stage Conversion with Z-Converter	DC off-board	DC Level 1	PV PHEVs or grid to PHEVs via Z-converter and DC/AC bi-directional converters	Residential charging of PHEVs	Z-converter induces double line frequency ripple at the DC link

2.6 Power Management Algorithms for PV Based Charging Facilities

Workplace based photovoltaic charging facilities and residential PV charging are the two available options for charging PHEVs using solar power. Depending on the solar irradiation, PHEVs can be charged either from the photovoltaic or the distribution grid or both. The solar charging station should distribute the power available at the PV panels to the PHEVs effectively and safely. Typically PHEVs arrive at the charging facility with different state-of-charge (SOC). More than often, the amount of PV power available to charge multiple PHEVs is limited. Furthermore, the PV source is stochastic in nature, its power characteristic is nonlinear and the PHEV batteries to be charged should be within certain voltage and current limits. Therefore, this process necessitates intelligent control of the power conditioning unit to manage the direction of power flow in PV integrated charging stations. Several algorithms have been proposed in the literature which differ significantly based on the type and location of the PCF. The algorithms also differ based on the various control parameters such as PV power, load demand, state-of-charge etc. Accordingly they can be classified as follows:

Residential Photovoltaic Charging

Battery Switch Stations

Workplace Photovoltaic Charging

2.6.1 Residential Photovoltaic Charging

Few authors [31–34] have proposed an architecture for a grid-connected residential photovoltaic system that can be used to charge PHEVs as well as to supply the existing household loads. The control algorithms depend on the power generated by the PV and the SOC of the PHEV battery. Raul et al. [33] proposed a residential load coordination mechanism to charge PHEVs. Depending on the load demand of the distribution transformers, the PHEVs can be charged using renewable energy (PV/Wind) or the power from the grid. Each household is installed with a rooftop PV system and a small scale wind turbine. A residential microgrid composed of rooftop panels and a biodiesel generator to charge PHEVs and supply AC/DC household loads is described in [35]. In order to share the load among the sources, master-slave control method is employed. The operation of the residential microgrid depends on the PV power, load demand, SOC of the battery storage and tariff set by the utility. Most of the PHEVs are not available for charging during daytime at residential facilities. Hence, this process demands for an additional component in the form of an energy storage unit in the form of a battery bank which might not be economically attractive for an individual home owner. Residential charging is advantageous for households with more than one PHEV.

2.6.2 Battery Switch Stations

A PV based battery control strategy for charging multiple batteries in a solar battery charging station (SBCS) is proposed in [36]. The architecture of the SBCS is similar to the one shown in Figure 2.8 but the DC/DC chargers are replaced by bi-directional switches. The proposed control strategy as described in the flowchart shown in Figure 2.11 first charges each individual battery until they reach the same voltage level and then charges the multiple batteries in parallel simultaneously according to the battery charging period and the available solar energy. This control strategy eliminates the use of multiple DC/DC converters per battery connection, making the SBCS less complicated and economical. Though being economical, the proposed architecture does not consider the scenarios when the PV panel is not generating any power or generating power in excess. Hence it cannot be considered for charging PHEVs. A PV-based battery switch station (BSS) is proposed in [37]. The energy exchange strategy depends on the battery swapping demand of the PHEVs and power generated by the PV. An algorithm is proposed to charge EV batteries using the maximum energy from PV.

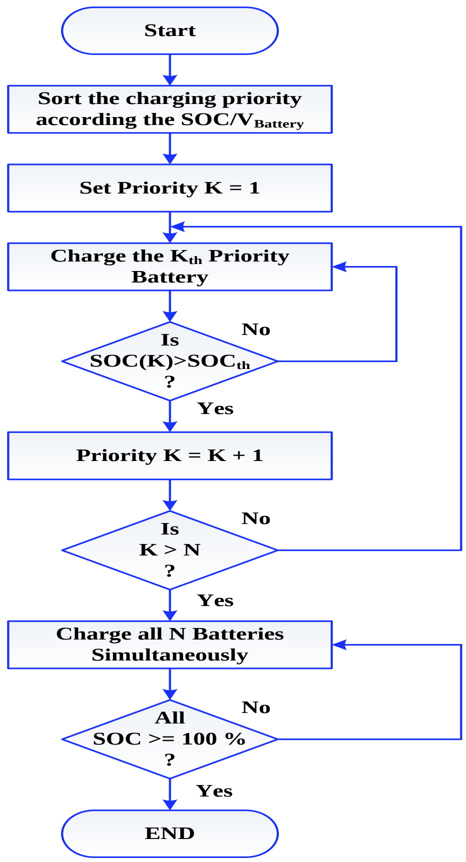

Figure 2.11: Control strategy for the proposed solar battery charging station.

2.6.3 Workplace Charging

In few cases, authors have proposed the idea of inserting a DC/DC battery charger at the DC link of the grid-connected PV system. By measuring the power generated by the PV and the power demand of the PHEV, the control algorithm ensures the charging of the PHEV battery from the appropriate source as described in [38]. Based on the imbalance between the PV power and the load demand, various scenarios are described. In case of [39], the power flow in a PV parking lot is managed through a set of computer controlled relays. PV panels of different ratings are interfaced with EV chargers and the power grid through computer controlled relays. Depending on the irradiation levels, the relays direct the entire PV power to the EVs or the grid or both. Hamilton et al. [25] & [26] proposed an extension to this method for a modular DC PV charging station. Several PV panels are interfaced with the DC bus through a set of DC/DC converters. The DC/DC converter intelligently controls the power flow to the PHEVs based on a certain preset limits of the DC bus voltage. Based on the preset limits the energy conversion unit facilitates three-way energy flow among the power grid, PV modules and PHEVs.

The concept of DC bus signaling has been proposed by several authors to schedule power to DC loads in a microgrid [40–44]. Few of them have extended this concept to charge PHEVs in a microgrid environment [43,44]. A smart charging station architecture integrated with PV power is proposed in [43] and [44]. The smart charging station can operate in standalone mode and grid-connected mode. The switching between various modes is facilitated by the variation in DC link voltage levels induced due to the change in solar insolation. During the period of low solar insolation and peak load on distribution transformer, the controller shifts the charging of PHEVs to non-peak period. The proposed control algorithm is simple as it involves only a single parameter i.e. DC link voltage to manage the direction of power flow in the charging station. It facilitates the charging of PHEVs using minimum energy from the grid without any adverse impacts on the distribution transformer. Flowchart describing the controller logic is shown in Figure 2.12. The following sections explain the concept of DC link voltage sensing and its application for control and management of PV powered charging facilities.

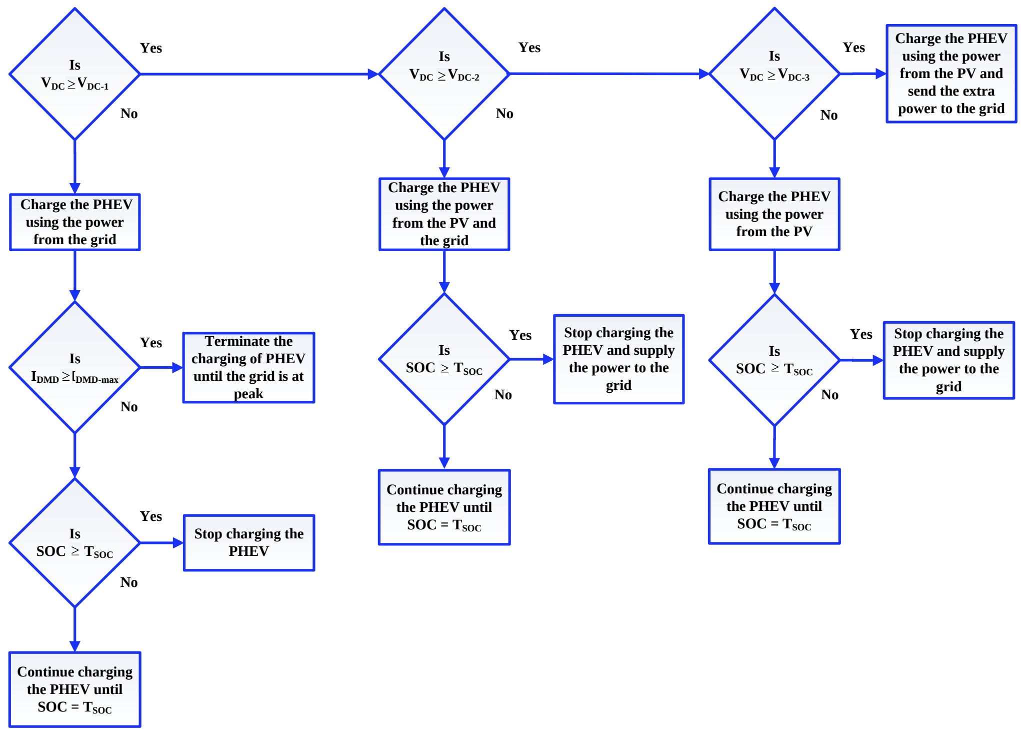

Figure 2.12: Flowchart describing the controller logic based on DC link voltage sensing.

2.7 Concept of DC Link Voltage Sensing

The elements and devices in the proposed architecture shown in Figure 1.4 of Chapter 1 can be summarized into three categories, i.e., an energy generation unit, an energy storage unit, and loads and hence the configuration can be considered as a typical case of DC microgrid with renewable generation and energy storage. The primary requirement for DC microgrid operation is to maintain the common DC bus voltage within an acceptable range. The terminals within a microgrid can be generally categorized into four types: generation, load, energy storage unit (ESU), and grid-connection using voltage-source converters (VSCs). These four types of terminals can be further divided into two groups in terms of their contribution to system control and operation which are the power terminal and the slack terminal [45].

A power terminal is the one which outputs or absorbs power to/from the microgrid on its own and usually does not take the system's need into account. Typical examples would be variable DC loads (PHEVs) and nondispatchable (variable) generation, such as wind turbines and photovoltaic based generations, when operating purely according to environmental conditions. Conversely, a slack terminal is the one which is responsible for balancing the power surplus/deficit caused by power terminals and maintaining stable system operation. Typical examples include a grid-connected VSC terminal (G-VSC) and ESU when they are actively supporting the DC microgrid system.

As previously described, different measures shall be taken by each terminal according to the system operating conditions, thus a fast and reliable scheme for acknowledging system operation status is essential. Apart from using as communication means, DC link voltage is a good indicator of the system's operational status.

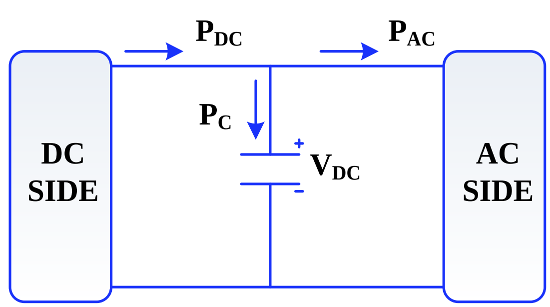

Figure 2.13: Equivalent circuit of the DC bus.

The simplified equivalent circuit of the DC bus is shown in Figure 2.13, where P_{DC} and P_{AC} represent the total power on the DC side and the AC side of the DC bus respectively.

From Figure 2.13, the charging power of the DC capacitor is

$$P_C = P_{DC} - P_{AC} \tag{2.1}$$

and for the DC voltage

$$V_{dc} \frac{dV_{dc}}{dt} = \frac{1}{C}(P_{DC} - P_{AC}), \tag{2.2}$$

where C refers to the total DC capacitance value.

From Equation 2.2, it can be inferred that a constant DC voltage indicates a balanced power flow among all the terminals, and a rising or dropping DC voltage indicates power surplus or deficit, respectively. Since the DC voltage can be used as an effective indicator of power-flow status, the control scheme of the proposed charging facility can be designed according to DC voltage variation. The operational voltage range can be divided into several levels. Based on the voltage level the charging facility has several modes of operation which are subsequently described in detail in Chapters 3 and 4.

2.8 Grid Integration Issues

Although there are many benefits related to the grid integration of PHEVs, increasing the number of PHEVs may impact power distribution system dynamics and performance due to the overloading of transformers, cables, and feeders. As discussed in Section 2.4 these issues can be resolved by charging facilities integrated with PV power. The ability of PHEVs to assist the integration of renewable energy sources into the existing power grid (and vice versa) though is potentially the most transformative impact on the electricity system [46], [47]. Several studies revealed that the integration of PV solar systems into the electric power grid is pretty mature and practically viable [48].

The existing power grid suffers from unpredictable and intermittent supply of electricity from the PV source. The power available from PV can be very high (more than the power demand) or very low (less than the power demand) depending on the available solar insolation. If the energy injected to the grid from PV is too high, centralized power plants must decrease their production to restore balance or the distributed generator units must be curtailed. By utilizing the concept of V2G (vehicle-to-grid) PHEVs can help match consumption and generation by discharging and charging so the utility does not need to decrease the power output. PHEVs can also act as a buffer and store excess power generated by PV source. This stored energy can be used for driving needs or to provide power to the grid at a later time. Thus Grid integration of PHEVs increases the flexibility for the grid to better utilize intermittent renewable sources.

Though the concept of V2G is being promoted as a superior concept in a smart grid environment, there are also some impediments and barriers to V2G transition. Some of the biggest challenges are battery degradation and the implementation of a reliable two- way communication infrastructure for coordinating large number of distributed energy resources and PHEVs [49]. On the other hand the concept of integrating PHEVs within a photovoltaic system can be simpler and easier to deploy. The high voltage DC bus present between the maximum power point tracker and the inverter provides a convenient point for the integration of DC/DC PHEV chargers as shown in Figure 2.9 [50]. This function of integrating the PHEV chargers at the high voltage DC bus can be named as vehicle-to-DC link (V2DC). In addition to providing fast charging a V2DC system is capable of offsetting the sudden fluctuations of the PV power due to clouding conditions, thereby reducing the rate of change of inverter output power to a level below the ramp rate of existing grid resources [51,52]. Thus network of PCFs located at appropriate points on the distribution feeder ensure that PHEVs are being charged from clean, renewable energy. From the perspective of grid operator's, reduced variability of PV output power translates to reduced spinning reserve requirements and greater grid stability, especially on grids with high penetrations of PV source.

2.9 Recent Advancements

Realizing the benefits of charging PHEVs using solar power, several research institutes, government organizations and universities are embarking on initiatives to integrate solar photovoltaic and PHEVs. Companies such as SolarCity, onesuninc and Merit Solar are promoting the installation of PCFs at residential and commercial parking garages [53–55]. Several demonstration projects are underway at many places to setup PV powered charging stations. With the financial assistance from DOE (Department of Energy), ORNL (Oak Ridge National Laboratory) has teamed up with TVA (Tennessee Valley Authority), EPRI (Electric Power Research Institute) and Nissan to install 125 solar-assisted charging stations across the state of Tennessee [56, 57].

Figure 2.14: ORNL solar-assisted EV charging station [56, 57].

Currently ORNL has installed 25 solar powered charging stations in their campus. One such facility is shown in Figure 2.14. Each charging station is equipped with 47 kW array which provides enough energy annually to offset the electricity required to drive 25 Nissan Leafs almost 10,000 miles per vehicle per year. The EVSEs (electric vehicle supply equipment), solar PV inverters, and the battery charger/inverter units are all internet-connected. The data collected is necessary for analysis and interpretation with regard to vehicle performance, maintenance, and operational issues. EPRI has developed a 10 space Smart Modal Area Recharge Terminal Station (SMART) that incorporates a photovoltaic array (PV) with battery storage for PHEV charging [58]. The Results from this development can be used as the basis for continuing efforts to deploy a number of solar powered public charging stations . Understanding how the public will interact with this new infrastructure can allow future deployment of charging hardware in a way that best meets the needs of the driving public-while doing so in a cost-effective manner.

2.10 Summary

To mitigate the loading on distribution transformers due to PHEV charging, smart charging strategies coupled with renewable energy resources are necessary. This chapter presented a detailed review of the integration of PHEVs and PV systems into the existing power grid. It has been observed that charging PHEVs using rooftop PV system would minimize the distribution transformers loss-of-life. Several power electronic topologies for PV based charging stations are presented and compared. Distributed architecture seems to be the best option for installing PCFs at workplaces, shopping malls, universities etc. as it is less vulnerable to faults on the distribution system and also facilitates fast charging. The study of various PV based charging facilities has shown that intelligent control of power conditioning unit is imperative for managing the power flow in PCFs. Several control algorithms are investigated and flowcharts depicting the controller logic are presented. Since the architecture of the PCF appears as a DC microgrid, by employing the concept of DC link voltage sensing its operation can switch between standalone mode and grid-connected mode.

Chapter 3 PV Integrated Smart Charging of PHEVs Based on DC Link Voltage Sensing

This chapter presents the architecture and control of a workplace-based charging facility integrated with a photovoltaic (PV) system. The power needed to charge the plug-in hybrids comes from grid-connected PV generation or the utility or both. A scaled down version of the proposed architecture is implemented in the laboratory environment covering all the modes of operation that are supported with both, theoretical explanations and experimental results. This chapter shows how the concept of DC link voltage sensing is contemplated for energy management in a PV integrated charging facility.

3.1 Introduction

The ongoing research in the field of plug-in hybrid electric vehicles (PHEVs) and the growing global awareness for a pollution free environment, will lead to an increase in the number of PHEVs in the near future. The proliferation of these PHEVs will add stress to the already overloaded U.S. grid creating new challenges for the distribution network. Though it is always advantageous to charge the PHEVs during night time there will be considerable PHEV load during the day and even during the hours of peak demand [59]. Transmission and distribution systems can be upgraded to meet the peak demand but this may result in capacity surplus during normal operating conditions. There is also a potential risk of night-charging challenge as the TOU (time-of-use) pricing is designed to discourage charging during the daytime. This would overload the distribution transformers which are otherwise designed to cool overnight. Though installing transformers with higher power rating would solve the problem, it is a rather expensive option. Hence, it's time to develop charging station infrastructure coupled with smart charging strategies which can reduce the stress imposed on the grid. One way is to use renewable energy resources to charge the PHEVs. Photovoltaic systems would be the best choice among the available options because of the following reasons:

- The PVs can be installed on the roof top of a commercial parking lot for charging PHEVs during peak time as they can be made dispatchable by employing external storage units. This improves the energy efficiency of the utility as the PHEV load during peak time is reduced.

- PV technology is expected to be practical and cost - effective at the kW scale and as a result it is a good candidate for grid-connected photovoltaic charging stations [60], [61].

A review of the literature suggests that research on PHEV charging and their impact felt on the grid is being carried out around the world with keen interest. Many pilot ventures on PV charging stations are also being undertaken [62]. In most of the cases AC charging is employed because AC system has been used for years and there are well developed standards and technologies. DC charging on the other hand increases the overall efficiency by reducing the number of power conversion stages and also offers the advantage of fast charging [25, 63, 64]. As shown in Figure 3.1, PHEVs are directly connected to the DC link by employing a DC/DC buck converter. The proposed architecture is an effective solution for charging PHEVs using a photovoltaic system.

Several DC charging station architectures have been proposed by the researchers [26, 65, 66]. In case of [65] the control of the individual electric vehicle charging processes is decentralized, while a separate central control deals with the power transfer from the AC grid to the DC link. The authors conclude that DC fast charging of multiple EVs is possible but the impact of fast charging on the grid and ways to eliminate or reduce the stress on the grid are not discussed.

An intelligent energy management system (IEMS) is proposed in [67]. The IEMS allocates power to the vehicle battery chargers through real time monitoring, to ensure optimal usage of available power, charging time and grid stability. However, control and architecture of the power electronic interface needed to implement the IEMS is not discussed.

In reference [26] the authors proposed a plug-in hybrid electric vehicle (PHEV) solar carport charging station concept featuring a multi-port power electronic interface connecting photovoltaic modules, PHEVs, and the power grid. Reference [25] proposes a solar carport with direct DC/DC interface to increase the overall efficiency. Though both the above papers deal with energy conversion systems featuring three-way energy flow involving the power grid, PV modules, and plug-in hybrid vehicles, the paper did not implement smart charging techniques to reduce the impact on distribution transformers.

The concept of DC bus signaling (DBS) has been employed to supply power to the DC loads. DBS induces DC bus voltage level changes to realize the communications between different source/storage interface converters [41], [40]. Though DBS is a novel idea it does not take the change in sun's insolation into consideration which in turn impacts the DC bus voltage level. In [43] the DC link voltage level changes due to the change in sun's insolation but the feasibility of the proposed control strategy was not validated experimentally. This dissertation validates the practical feasibility of the proposed control strategy in [43] through experimental results using a laboratory prototype. The change in irradiation of the sun induces changes in the DC link voltage level. Based on the change in

DC link voltage level and the loading condition of the distribution transformer the operation of the charging station can be categorized into four modes: grid-connected rectification, PV charging and grid-connected rectification, PV charging and grid-connected inversion.

3.2 Significance of the Proposed Charging Station

It is predicted that there will be one million plug-in hybrid electric vehicles on the road by the year 2015 [68], [69]. This will add extra load to the already overloaded U.S grid. Extensive research on design and implementation of a smarter grid is going to play an important role in the integration of PHEVs to the existing electric power system [70]. Smart grid technologies may be a solution to manage the charging rates and time scheduling of the PHEVs which have a significant impact on the system load curve. A PHEV with smart or controlled mid-day charging may provide overall improved vehicle performance, increasing the drive time traveled using low cost electricity and potentially reducing the size of the battery [71].

The proposed charging station will charge the PHEVs from the photovoltaic system, thus reducing the stress on the grid. When the grid is at peak demand and solar power is insufficient to charge the PHEVs then the charging station would enable vehicle charging to be delayed or temporarily interrupted. The charging station also includes an energy storage unit (ESU) which consists of a battery bank to store energy during off-peak hours. The control of the charging station is based on the change in DC link voltage level due to the change in irradiation of the sun. The proposed control method is simple and unique.

The goal of the proposed architecture is: to charge the PHEVs using minimum energy from the utility with a kind of demand side management to improve the energy efficiency. Smart charging techniques like the one proposed in this chapter will be required to avoid major expense to upgrade the transformers and other substation equipment [72–74]. Also, according to the data gathered by National Household Travel Survey, 60% of vehicles are parked at the workplace for more than 4 hrs [75]. In view of this, the proposed charging station will be appropriate for parking facilities at a workplace.

3.3 Architecture of the Charging Station

Figure 3.1 shows a detailed block diagram of the proposed charging station architecture. The main components of the charging station are the power conditioning unit (PCU), photovoltaic array, energy storage unit (ESU) and the controller. The PCU consists of a DC/DC boost converter which also performs the function of maximum power point tracking (MPPT), a DC/DC buck converter with battery management system embedded in the controller, an energy storage unit (ESU) and a DC/AC bi-directional grid tied converter. The ESU will support the charging of PHEV when there is no power available either from the grid or the PV system. The battery pack in the ESU can be charged from the grid during off-peak hours.

The block diagram in Figure 3.1 and the following control description is based on charging requirements of a single PHEV. Multiple PHEVs can be charged by increasing the corresponding ratings of the charging station components like the PV panels and the associated power converters. Each PHEV must have a separate buck converter installed for each charge point.

The controller monitors and controls the power flow in the system. As shown in Figure 3.1 the controller operation is based on eight inputs. $V_{DC-link}$, SOC and I_{DTR} are used to determine the direction of power flow. V_{PV} and I_{PV} are used

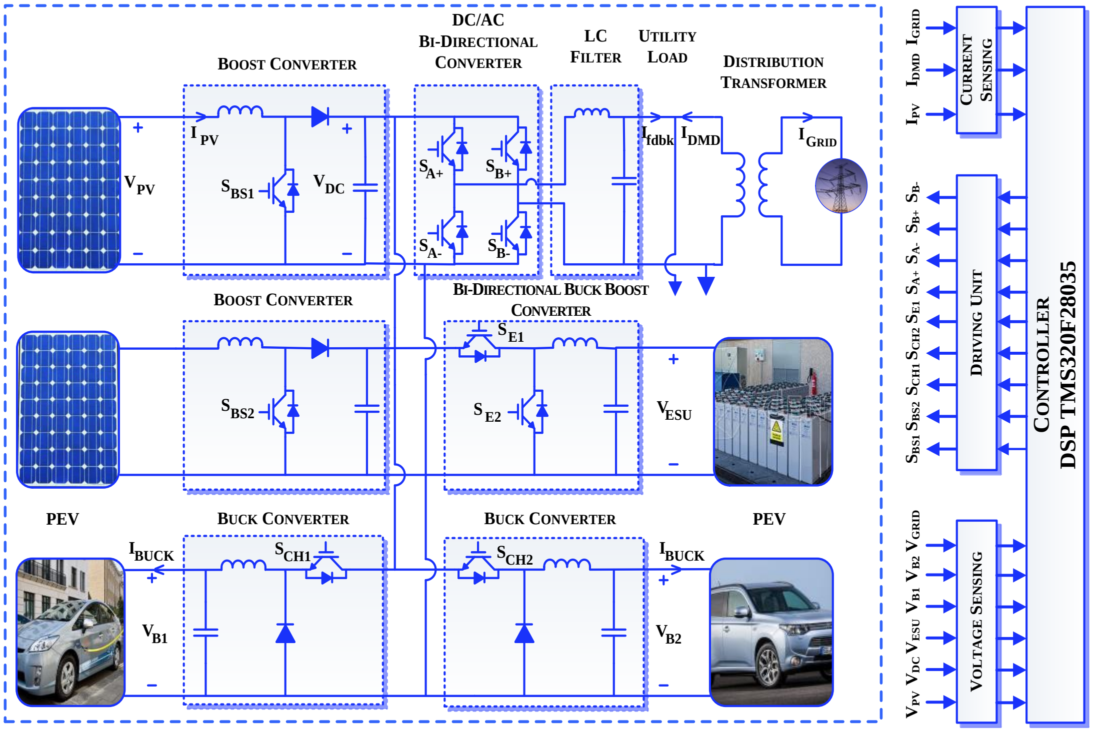

Figure 3.1: Detailed circuit configuration of the proposed architecture.

to implement MPPT by means of incremental conductance algorithm. $V_{DC-link}$ is the magnitude of the voltage at the DC link, V_B is the detected battery voltage of the PHEV which is the measure of state-of-charge (SOC). I_{DTR} is the loading condition of the distribution transformer, $I_{boostsw}$ is the current flowing through the boost switch, I_{fdbk} is the current delivered by the DC/AC converter to the grid, V_{PV} is the voltage across the PV array and I_{PV} is the current flowing from the PV array.

Based on the control signals the controller performs the following tasks:

- Controls the DC/DC boost converter to extract the maximum power from the PV emulator by implementing the incremental conductance algorithm.
- Manages the charging of the PHEV by monitoring its state-of-charge (SOC).

The controller disconnects the buck converter from the PHEV based on the loading of distribution transformer and the state-of-charge (SOC) of the battery.

- Generates PWM signals at 20 kHz to facilitate the switching of the inverter switches. PWM signals at high switching frequency ensures a sinusoidal voltage at the inverter output.

- The controller changes the modes of operation based on the DC link voltage. Based on the change in DC link voltage the converters are controlled to manage the direction of power flow in each mode.

3.4 Control Algorithm and Modes of Operation

The control of the PCU is based on DC link voltage sensing and the switching between various modes of operation occurs due to the change in the voltage level at the DC link. From Figure 3.2, the instantaneous power relationship in a grid-connected PV system is given by

$$p_{dc}(t) = p_{ESU}(t) + p_c(t) + p_{PHEV}(t) + p_{ac}(t), \tag{3.1}$$

where P_{dc} is the output power of the DC/DC converter on the DC side, P_{ESU} is the power delivered to (or by) the ESU, P_c is the power to the DC link capacitor, P_{PHEV} is the power consumed by the plug-in hybrid electric vehicles, and P_{ac} is the power extracted by the inverter on the AC side. The instantaneous AC power (output of the inverter) can be written as

$$\begin{aligned} P_{grid}(t) &= (V_m sin\omega t)(I_m sin\omega t) \ and \\ &= \frac{V_m I_m}{2} - \frac{V_m I_m}{2} cos2\omega t, \end{aligned} \tag{3.2}$$

where P_{grid} is the power injected into the grid, V_m is the amplitude of the phase

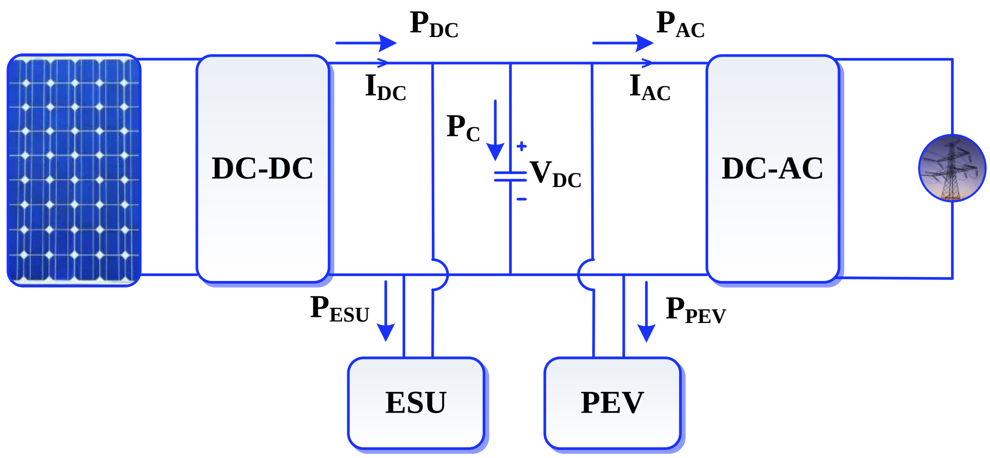

Figure 3.2: Grid-connected PV system.

voltage and I_m is the amplitude of the grid current. The AC power includes a DC term and a second-order ripple in the DC voltage. The average input power to the AC side can be written as

$$P_{AC} = V_{DC} I_{AC}, \tag{3.3}$$

where I_{AC} is the average input current on the DC side of the inverter. Equating the average power on the DC side to the DC term on the AC side

$$\frac{V_m I_m}{2} = \eta V_{dc} I_{AC}, \tag{3.4}$$

where η is the efficiency of the inverter. If V_{dc} and $V_{(dc(ref))}$ are the actual and reference values of DC link voltage, respectively, the change in energy (ΔE_{dc}) stored in the DC link capacitor C_{dc} can be written as

$$\Delta E_{dc} = \frac{C_{dc}}{2}(V_{dc(ref)}^2 - V_{dc}^2). \tag{3.5}$$

To inject the PV power to the grid while maintaining a constant V_{dc}, the following energy balance should be satisfied as

$$\Delta E_{dc} = T(p_{dc} - p_{ESU} - p_{PHEV} - \frac{V_m I_m}{2\eta}), \tag{3.6}$$

where T is the time period of AC supply.

Combining Equation 3.5 and Equation 3.6

$$V_{dc}^2 = V_{dc(ref)}^2 - \frac{2T}{C_{dc}}(p_{dc} - p_{PHEV}) + \frac{2T}{C_{dc}}p_{dc} + \frac{2T}{C_{dc}\eta}V_m I_m, \tag{3.7}$$

$$V_{dc} = \sqrt{V_{dc(ref)}^2 - \frac{2T}{C_{dc}}(p_{dc} - p_{PHEV}) + \frac{2T}{C_{dc}}p_{dc} + \frac{2T}{C_{dc}\eta}V_m I_m}, \; and \tag{3.8}$$

$$V_{dc} = \sqrt{V_{dc(ref)}^2 - \frac{2T}{C_{dc}}(\eta_{boost} p_{pv} - p_{PHEV}) + \frac{2T}{C_{dc}}p_{dc} + \frac{2T}{C_{dc}\eta}V_m I_m}, \tag{3.9}$$

where η_{boost} is the efficiency of the DC/DC converter on the DC side.

From Equation 3.9, it is clear that the fluctuations in PV power due to the change in solar irradiance causes variations in the DC link voltage. For a workplace-based charging facility PHEVs can be assumed to stay in the parking lot from morning till evening. Hence the variation in PHEV load is not considered.

Also from Equation 3.6, the charging power of the DC capacitor can be written as

$$p_c = p_{dc} - p_{ESU} - p_{PHEV} - \frac{V_m I_m}{2\eta}, \tag{3.10}$$

$$\frac{1}{2}CV_{dc}^2 = p_{dc} - p_{ESU} - p_{PHEV} - \frac{V_m I_m}{2\eta}, and \tag{3.11}$$

$$CV_{dc}\frac{dV_{dc}}{dt} = p_{dc} - p_{ESU} - p_{PHEV} - \frac{V_m I_m}{2\eta}. \tag{3.12}$$

From Equation 3.12, it can be inferred that a constant DC voltage indicates a balanced power flow among all the terminals, and a rising or dropping DC voltage indicates power surplus or deficit, respectively. Since the DC voltage can be used as an effective indicator of power-flow status, the control scheme of the proposed charging facility can be designed according to DC link voltage variation. Assuming the PHEV demand to be constant over a period of time, the variation in DC link voltage occurs only due to the fluctuation in solar insolation. The operational voltage range can be divided into several levels. Based on the voltage level the charging facility has several modes of operation.

Figure 3.3 shows the variation in the DC link voltage and the power from the PV array with step changes in irradiation. A PV panel of rating 5.5kW was modeled in Matlab taking the battery capacity of a single PHEV into consideration. The reference voltage levels have been chosen based on the relation between DC voltage and output AC voltage of a single-phase pulsewidth modulation (PWM) inverter which is given by

$$V_M = kV_{dc}, \tag{3.13}$$

where

V_M = Peak value of the fundamental voltage on the AC side;

k = Modulation index of the PWM inverter;

V_{dc} = the nominal DC link voltage.

As per the above equation the nominal DC link voltage ($V_{DC-Link}$) is chosen as 400 V considering the RMS output voltage to be 208 V and a modulation index of 0.8. The reference voltage levels vary based on the nominal voltage and operation requirements of the charging facility. So far, the standardizations of DC grid requirements such as the optimal voltage level and the tolerance band of DC-bus voltage have not been commonly established in spite of its well-recognized operations with higher efficiency and better compatibility. Different DC voltage tolerances are defined in [40, 41] for low and medium voltage DC microgrids, respectively. Based on the above references, the threshold voltage levels have been chosen as V_{DC-1} = 360 V, $V_{DC-Link}$ = 400 V and V_{DC-2} = 440V as shown in Figure 3.3. The modes of operation of the charging station are classified depending on the change in the DC link voltage. As the DC link voltage is the only criteria for switching between various modes the overall complexity of the system is reduced.

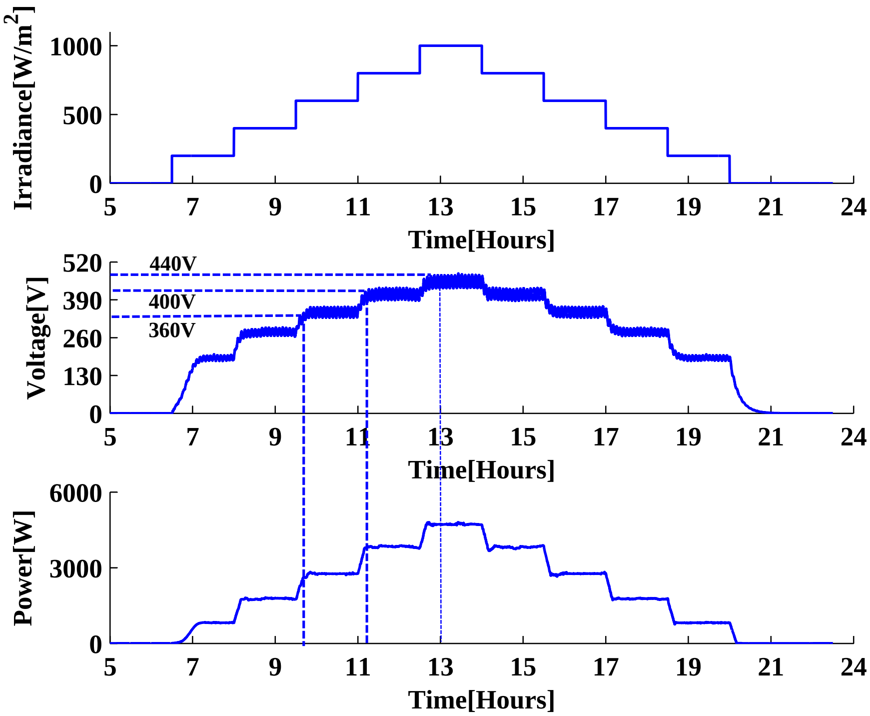

Figure 3.3: Change in the DC link voltage and Power generated by the PV with the change in sun condition.

3.4.1 Modes of Operation

Based on the threshold values defined in the previous section the operation of the charging station can be categorized into three modes: Mode - 1 (grid-connected rectification), Mode - 2 (PV charging with grid-connection), and Mode - 3 (grid-connected inversion). A set of variables I_{DTR}, $I_{DTR-max}$, V_{DC-1}, $V_{DC-Link}$, V_{DC-2}, V_B and V_{BH} are used to describe the modes of operation.

I_{DTR} represents the distribution transformer load and $I_{DTR-max}$ represents the peak load condition of the transformer. $V_{DC-link}$ is the voltage at the DC link. V_{DC-1} and V_{DC-2} are the chosen reference voltage levels of the DC link. V_B is the detected battery voltage of the PHEV. V_{BH} is the battery voltage corresponding to the threshold value of the state-of-charge. The charging of PHEV should be terminated once the battery voltage V_B is equal to V_{BH}. Figure 3.4 shows the direction of power flow during various modes of operation of the charging station.

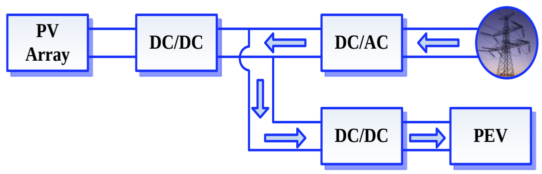

(a) Grid-rectification

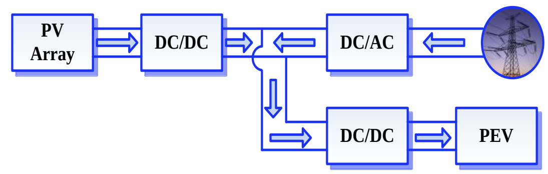

(b) PV charging and grid-rectification

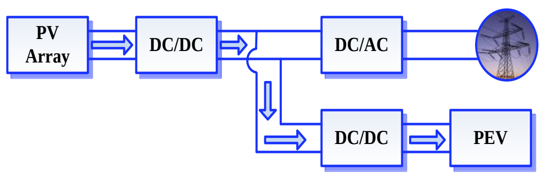

(c) PV charging

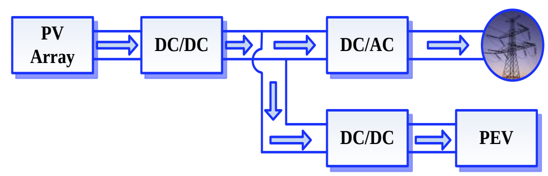

(d) Grid-inversion

Figure 3.4: Direction of power flow during the operation modes.

The four modes of operation are described as follows:

Mode 1 : $V_{DC-link} < V_{DC-1}$ *: Grid-connected rectification*

Case-1 : $V_{DC-link} < V_{DC-1}$ *and* $I_{DTR} < I_{DTR-max}$

In this mode the power generated by the photovoltaic system is less than the PHEV load demand either due to low radiation or bad weather conditions. As the grid is at off-peak, it continues to supply power till the vehicle is completely charged. The controller terminates the charging of PHEV by disabling the DC/DC buck converter when V_B exceeds V_{BH} and the grid supplies power to charge the battery pack in the ESU. Figures 3.4 (a) and (b) represent the direction of power flow in the charging facility during this mode.

Case-2 : $V_{DC-link} < V_{DC-1}$ *and* $I_{DTR} \geq I_{DTR-max}$

This mode is similar to Case-1 but with an increase in local demand on the distribution transformer. In order to reduce the stress on the grid, the charging of PHEV is terminated temporarily by de-activating the grid-connected bi-directional DC/AC converter. As the distribution transformer is relieved from the additional burden of charging the PHEV, it can continue supplying power to the local loads during the peak time. During this period the PHEV can be charged by the ESU if the stored energy is sufficient to cater the needs of PHEV charging. Once the grid is back to off-peak condition (i.e. $I_{DTR} < I_{DTR-max}$) the charging of the PHEV is restored and the controller monitors its charging.

Mode-2 : $V_{DC-1} \leq V_{DC-link} \leq V_{DC-2}$ *: PV charging with grid-connection*

In this mode the charging facility operates either as a grid-connected (rectification or inversion) or a standalone system. The charging facility shifts its operation between different modes based on the current command generated by the inverter control which is explained in the next section. A negative reference current command indicates the operation of the charging facility in rectification mode while a positive reference current command shifts the operation to grid-inversion mode.

The charging facility operates as a standalone system when the reference current command is zero. If at any point I_{DTR} exceeds $I_{DTR-max}$ the bi-directional DC/AC converter is isolated from the grid. The PV system continues charging the PHEV where as the grid caters to the peak load demand. It is also possible to halt the charging of the PHEVs temporarily so that the charging facility can operate as a normal grid-connected PV system and support the grid during the peak load demand period. Figures 3.4 (b), (c) and (d) represent various directions of power flow possible during this mode.

Mode-3 : $V_{DC-link} > V_{DC-2}$ *: Grid inversion mode*

The PV array generates excess power once the DC link voltage exceeds V_{DC-2} (= 440V) as shown in Figure 3.3. This additional power generated by the PV array is sent to the grid via the bi-directional DC/AC converter. Once the PHEVs are charged, all the power from the PV source is sent to the grid. The direction of power flow during this mode is shown in Figure 3.4 (d).

3.5 Stability Analysis and Controller Design

3.5.1 Small Signal Modeling of DC/DC Boost Converter

The boost converter is intended to control the PV voltage in order to track the maximum power point (MPP). In order to design a controller to obtain the required steady-state and transient response, the power stage of the DC/DC converter can be linearized using state-space averaging method [76]. The boost converter can be described by nonlinear state-space-averaged equations as

$$L\frac{d\hat{i}_L}{dt} = \hat{v}_{in}(t) - (1-D)\hat{v}_o(t) + V_o\hat{d}(t) \; and \tag{3.14}$$

$$C\frac{d\hat{v}_o}{dt} = (1-D)\hat{i}_L(t) - I_L\hat{d}(t) - \frac{\hat{v}_o(t)}{R}. \tag{3.15}$$

From the above equations the control to output transfer function is obtained in Laplace domain as

$$\frac{\hat{v}_o(s)}{\hat{d}(s)} = \frac{(1-D)V_o - (LI_L)s}{(LC)s^2 + \frac{L}{R}s + (1-D)^2}, \tag{3.16}$$

where $\hat{v}_{in}$, $\hat{v}_o$, $\hat{i}_L$ and $\hat{d}$ denote the average values of the input voltage, the output voltage, the inductor current and the duty cycle of the switching for the boost converter, respectively.

The DC link voltage is kept constant at 400 V by the DC/AC grid-side voltage source converter (G-VSC). The inductor ripple current (ΔI_L) is considered to be 10% of the maximum output current and the output voltage ripple (ΔV_o) is considered to be smaller than 0.5% of the maximum output voltage. Based on the above requirements the values of inductance (L) and capacitance (C) are chosen as 12.5 mH and 0.75 mF for a switching frequency of 10 kHz. Substituting the values of L and C in Equation 3.16 the transfer function is obtained as

$$\frac{\hat{v}_o(s)}{\hat{d}(s)} = \frac{200 - 1.2s}{(9.375 \times 10^{-6})s^2 + 0.48s + 0.25}. \tag{3.17}$$

Figure 3.5 shows the bode plot representation for the uncompensated boost converter.

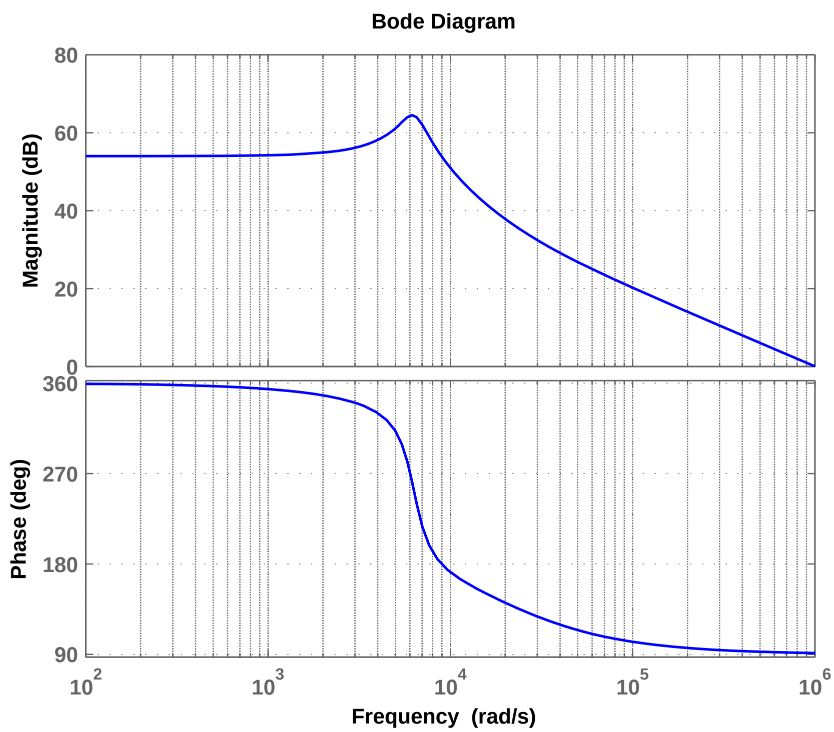

Figure 3.5: Bode plot for uncompensated boost converter.

3.5.2 Small Signal Modeling of DC/DC Buck Converter

The DC/DC buck converter functions as the charging circuit and controls the charging rate of the PHEVs. The inductor current and the capacitor voltage of the small signal AC model of the buck converter are given as

$$L\frac{d\hat{i}_L}{dt} = D\hat{v}_{in}(t) - \hat{d}(t)V_{in} \; and \tag{3.18}$$

$$C\frac{d\hat{v}_o}{dt} = -\frac{\hat{v}_o(t)}{R}D. \tag{3.19}$$

The output voltage variation $\hat{v}_o(t)$ can be expressed in laplace domain as

$$\hat{v}_o(s) = G_{vd}(s)\hat{d}(s) + G_{vd}(s)\hat{v}_{in}(s). \tag{3.20}$$

The first term represents the control to output transfer function while the second term represents the line to output transfer function. The transfer function of $G_{vd}(s)$ and $G_{vg}(s)$ can be defined as

$$G_{vd}(s) = \frac{\hat{v}_o(s)}{\hat{d}(s)} \tag{3.21}$$

and

$$G_{vg}(s) = \frac{\hat{v}_o(s)}{\hat{v}_{in}(s)}. \tag{3.22}$$

The control to output transfer function required for the stability analysis of DC/DC buck converter is represented as follows:

$$\begin{aligned} G_{vd}(s) &= \frac{V_{in}}{LCs^2 + \frac{L}{R}s + 1} \; and \\ &= \frac{V_o}{D(LCs^2 + \frac{L}{R}s + 1)}. \end{aligned} \tag{3.23}$$

Since the buck converter is connected across the DC link the input voltage is constant at 400 V. The inductor ripple current (ΔI_L) is considered to be 10% of the maximum output current and the output voltage ripple (ΔV_o) is considered to be smaller than 0.5% of the maximum output voltage. Based on the above requirements the values of inductance (L) and capacitance (C) are chosen as 5 mH and 0.5 mF for a switching frequency of 10 kHz. Substituting the values of L and C in Equation 3.23 the transfer function is obtained as

$$\frac{\hat{v}_o(s)}{\hat{d}(s)} = \frac{400}{(2.5 \times 10^{-6})s^2 + (5.5 \times 10^{-5})s + 1}. \tag{3.24}$$

Figure 3.6 shows the bode plot representation for the uncompensated buck converter.

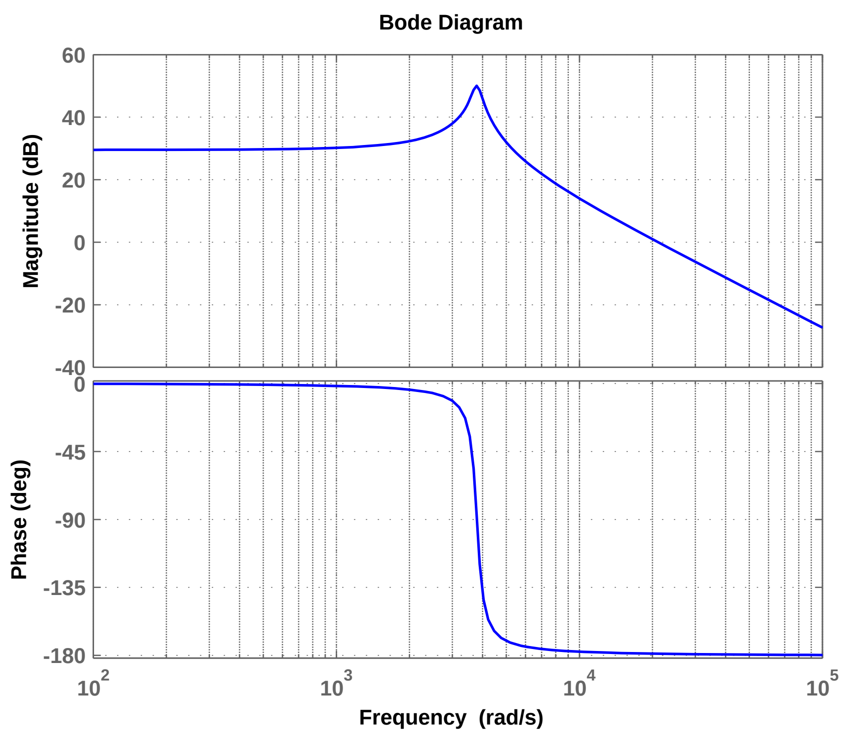

Figure 3.6: Bode plot for uncompensated buck converter.

3.5.3 Small Signal Modeling of DC/DC Buck-Boost Converter

Since the battery has a relatively large time constant, it can be modeled as a constant voltage source in small signal analysis. The average state-space model of the battery converter could be defined by the following equations

$$\frac{d\hat{i}_{batt}(t)}{dt} = (\frac{1-D}{L})\hat{v}_o(t) + \frac{D}{L}V_{batt} \; and \tag{3.25}$$

$$\frac{d\hat{v}_o(t)}{dt} = (\frac{1-D}{C})\hat{i}_{batt}(t) - \frac{1}{C}\hat{i}_o(t). \tag{3.26}$$

The control to output transfer function of the converter can be expressed by

$$\frac{\hat{v}_o(s)}{\hat{d}(s)} = \frac{V_o(1-D)}{LCs^2 + (1-D)^2}. \tag{3.27}$$

The ESU supports the charging of PHEVs during extreme conditions such as low solar insolation and peak demand on the distribution transformer. Using a bi-directional buck-boost converter, the battery voltage can be kept lower as compared to nominal DC link voltage (400 V) and hence fewer batteries need to be connected in series. In the proposed system a 100 Ahr battery with a nominal voltage of 100 V is selected as the ESU. Following the similar requirements as specified for the DC/DC converters as modeled above the values of L and C are obtained as 7.5 mH and 0.5 mH. Substituting these values in Equation 3.27 gives

$$\frac{\hat{v}_o(s)}{\hat{d}(s)} = \frac{200}{(3.75 \times 10^{-6})s^2 + 0.25}. \tag{3.28}$$

Figure 3.7 shows the bode plot representation for the uncompensated buck converter.

3.5.4 Control Description

A. DC/DC Boost Converter

The control method for DC/DC boost converter is summarized in Figure 3.8. A single phase boost stage is used to boost the PV voltage and track the MPP of the panel. To track the MPP, input voltage (V_{PV}) and input current (I_{PV}) are sensed. The two values are then used by the MPPT algorithm. The MPPT is realized using an outer voltage loop that regulates the input

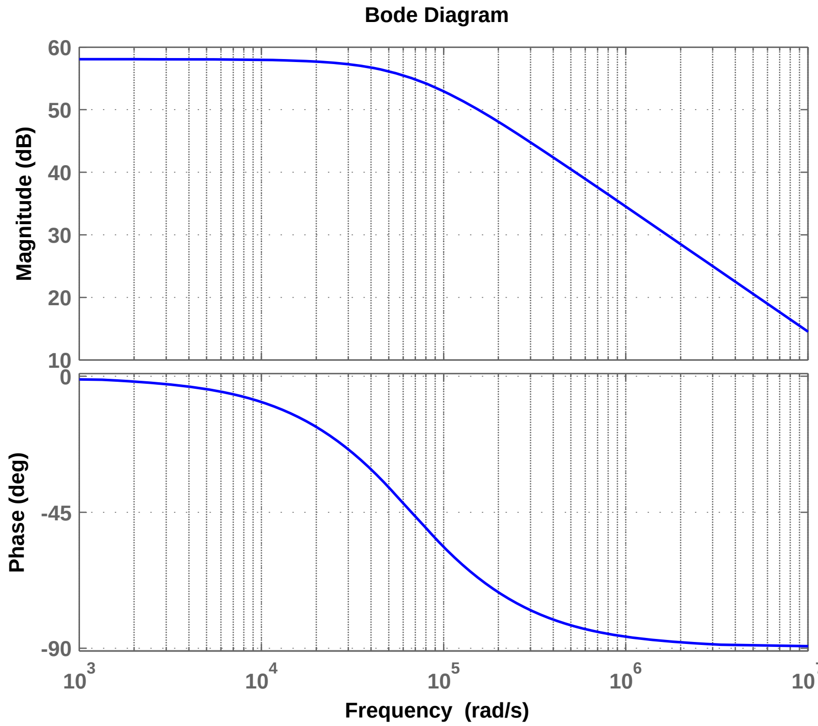

Figure 3.7: Bode plot for uncompensated buck-boost converter.

voltage i.e. panel voltage by modulating the current reference for the inner current loop of the boost stage.

Two 2-pole 2-zero controllers, G_V(S) and G_I(S) are used to close the inner DC/DC boost current loop and the outer input voltage loop. MPPT algorithm provides reference input voltage, V_{MPPT} to the boost stage to enable

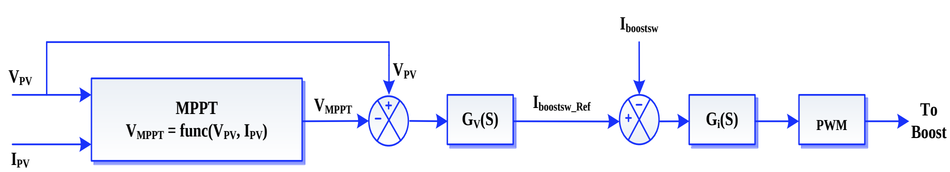

Figure 3.8: Control diagram of DC/DC boost converter.

panel operation at maximum power point. The sensed input voltage is compared with the voltage command (V_{MPPT}), generated by MPPT controller, in the voltage control loop. The voltage controller output, $I_{boostsw\_Ref}$ is then compared with the output current ($I_{boostsw}$) feedback in the current controller. The current loop controller output determines the PWM duty cycle so as to regulate the input voltage indirectly.

B. DC/AC Inverter

The control method for grid-connected DC/AC converter is shown in Figure 3.9. This stage uses two nested control loops – an outer voltage loop and an inner current loop. V_{DC} is the reference voltage for the DC link, $V_{DC-link}$ is the detected DC link voltage, V_{grid} is the voltage at the secondary of the distribution transformer, θ is the grid phase angle, I_{Ref} is the reference current for the DC/AC converter generated by the voltage loop and I_{fdbk} is the current fed into the grid by the DC/AC converter.

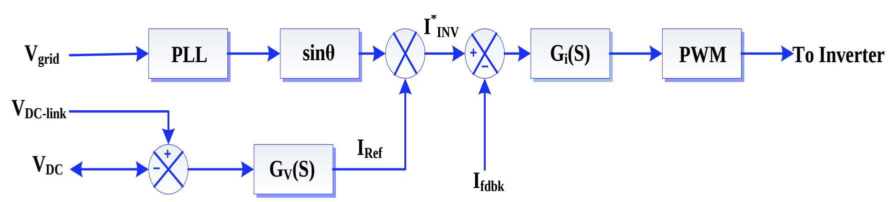

Figure 3.9: Control diagram of DC/AC Inverter.

Two PID controllers, G_V(S) and G_i(S) are used to close the outer voltage loop and the inner current loop. The voltage loop generates the reference command (I_{Ref}) for the current loop as increasing the current command will load the stage and hence cause a drop in the DC link voltage. The sign for reference and the feedback are reversed. The current command is then multiplied by the AC angle to get the instantaneous current reference. Since the inverter is grid-connected the grid angle is provided by the phase locked loop (PLL). The instantaneous current reference is then used by the current compensator along with the feedback current (I_{fdbk}) to provide duty cycle for the full bridge inverter.

C. DC-DC Buck Converter

The control method for DC-DC buck converter for PHEV charging is based on V_B,V_{BH}, I_{DTR} and $I_{DTR-max}$ as shown in Figure 3.10 . V_B is the detected battery voltage, V_{BH} is the battery voltage corresponding to 95% SOC. I_{DTR} is the load on the distribution transformer and $I_{DTR-max}$ represents the peak load condition. The control mode is determined by the detected battery voltage of the PHEV and the loading condition of the distribution transformer. The charging of the PHEV is turned off once the battery voltage reaches V_{BH} or the distribution transformer reaches the peak load condition.

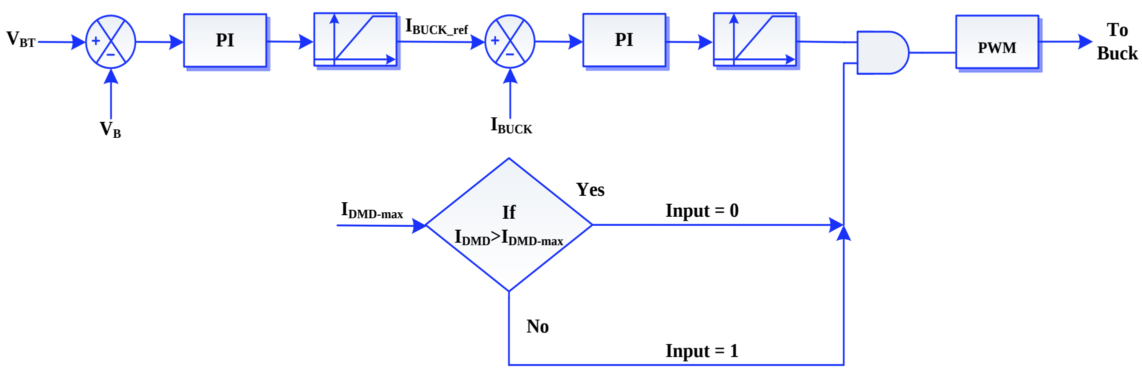

Figure 3.10: Control diagram of DC/DC buck converter.

3.6 Simulation Studies

In order to validate the proposed control algorithm simulations were done in Matlab Simulink using the simpowersystems toolbox. The reference DC bus voltages i.e. V_{DC-1}, $V_{DC-Link}$ and V_{DC-2} are set at 360 V, 400 V and 440 V. The reference DC link voltage levels are selected based on a training mode wherein the PHEV load is kept constant and the solar irradiation is allowed to vary in steps. The values of $I_{DMD-max}$ and T_{soc} are set at 80A (peak-to-peak) and 95%. Toyota Prius plug-in hybrid has been chosen as the PHEV which has a total battery capacity equal to 4.5 kWh and nominal voltage equal to 48 V. The RMS value of AC grid voltage is 208 V. A PV panel of rating 5.5 kW has been modeled taking the battery capacity of the PHEV into consideration.

Figure 3.11 shows the transition of the grid from off-peak to on-peak when the charging station is operating in Mode-1. The loading condition is accessed by measuring the current (I_{DMD}) on the secondary side of the distribution transformer. Initially the grid is at off-peak and hence the AC grid delivers the power required to charge the PHEV and other local loads. As shown in Figure 3.11, from 1.5 s - 2.0 s the current flowing in the secondary side of the distribution transformer is less than 80A. With the increase in utility load at 2.0 s, I_{DMD} exceeds 80A ($I_{DMD-max}$). The charging of the PHEV is terminated when the current flowing from the distribution transformer, I_{DMD} exceeds $I_{DMD-max}$. This is done to reduce the stress being imposed on the AC grid during the peak time. Hence the power consumed by the PHEV reduces to zero during the peak time as shown in the figure.

The simulation results for the transition from grid - rectification to PV charging during Mode-2 are shown in Figure 3.12. During the initial stages the DC bus voltage is around 360 V and the grid continues to supply the deficit power to charge the PHEV. Once the DC bus voltage exceeds 400 V, the PV system alone caters the charging of PHEV. The power flowing from the PV and the Power Grid is shown in Figure 3.12. As shown in the figure, the deficit power of 1000W to charge the PHEV is supplied by the grid during rectification and it does not supply any power during PV charging mode as the PV alone caters to the demand of the PHEV.

The transition from PV charging to grid-inversion mode is shown in Figure 3.13. With the DC bus voltage exceeding 400V there is an increase in power flowing from the PV. The PV system feeds this excess power to the grid in addition to

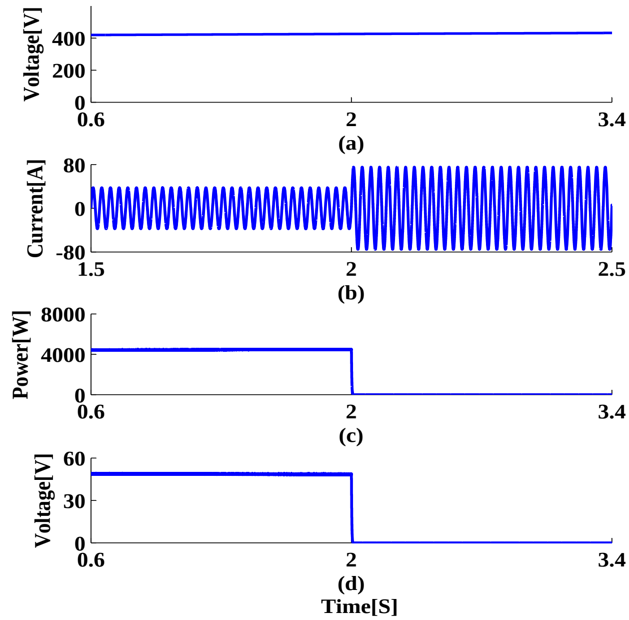

Figure 3.11: Matlab Simulink outputs for transition from Mode-1 Case-1 to Case-2. (a) DC bus voltage. (b) distribution transformer current. (c) Power delivered to the PHEV. (d) Output voltage of the buck converter.

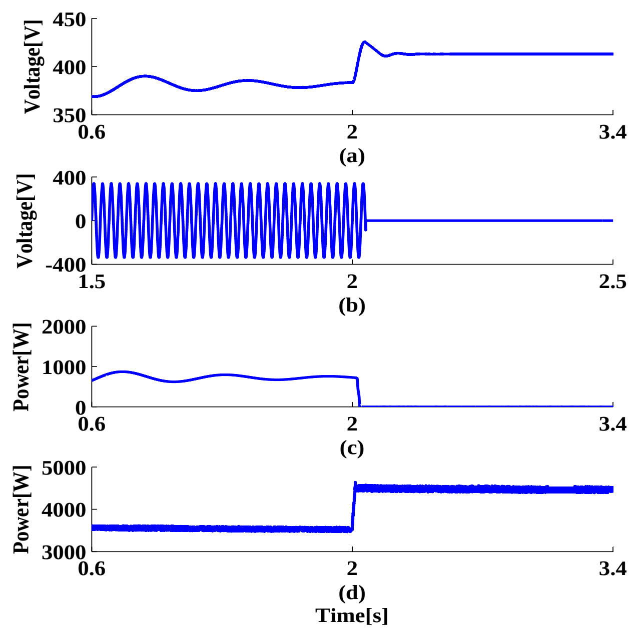

Figure 3.12: Matlab Simulink outputs for transition from from grid-rectification to PV charging. (a) DC bus voltage. (b) Voltage of the grid. (c) Power delivered by the grid. (d) Power delivered by the PV array.

charging the PHEV. The sinusoidal output of the DC/AC bi-directional converter shows that it acts as an inverter in this case. In order to maintain the energy balance the DC link voltage is kept constant at 440V. Finally Figure 3.14 shows the termination of the vehicle charging when SOC = T_{soc}.

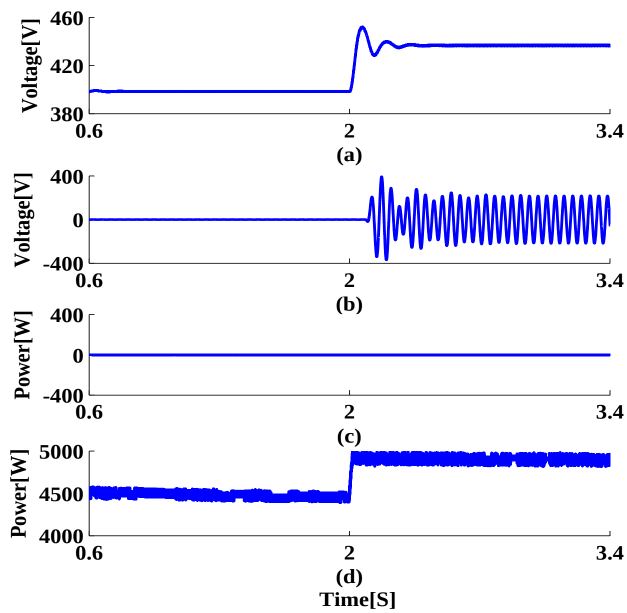

Figure 3.13: Matlab Simulink outputs for transition from PV charging to grid-inversion. (a) DC bus voltage. (b) Voltage of the grid. (c) Power delivered by the grid. (d) Power delivered by the PV array.

3.7 Experimental Verification

To verify the practical feasibility and effectiveness of the proposed control strategies experimental tests have been carried out in the laboratory. TMS320F28035 piccolo card is used to generate all the required control signals.

Figure 3.15 shows the experimental setup of the system. The components include the Solar Explorer Kit by TI (Texas Instruments), power pole board in buck configuration by Hirel, an isolation transformer and a battery. The DC/DC boost converter for the PV stage and the inverter is a part of the solar explorer

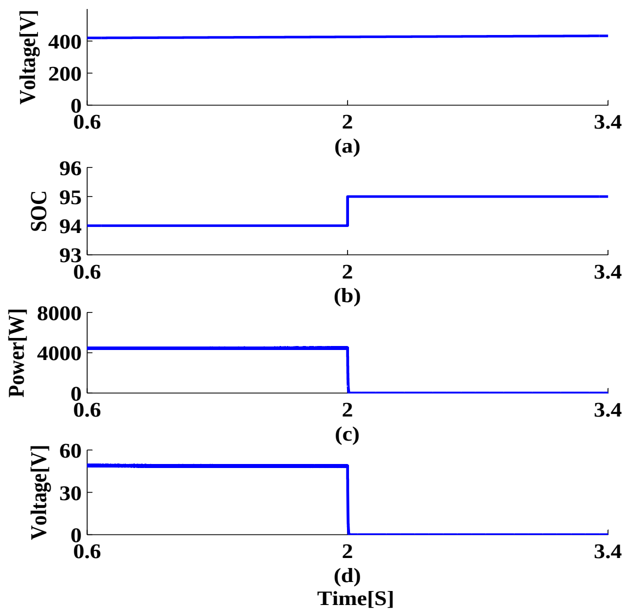

Figure 3.14: Matlab simulink outputs for transition in state-of-the-charge. (a) DC bus voltage. (b) State-of-charge of the PHEV battery. (c) Power delivered to the PHEV. (d) Output voltage of the buck converter.

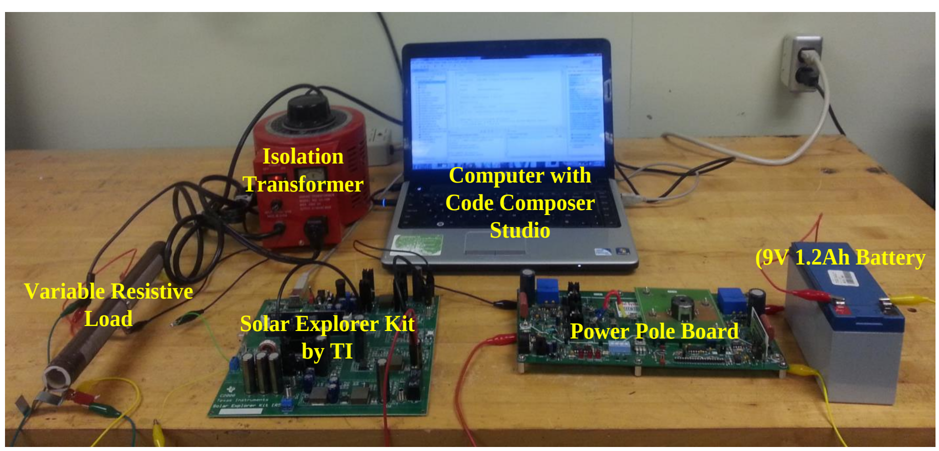

Figure 3.15: Experimental setup.

kit; and the DC/DC buck converter for PHEV charging is the Power-Pole board from Hirel. A synchronous buck-boost stage which is integrated on the board (solar explorer kit) is used to emulate the PV panel. In the place of a PHEV a 9V 1200mAh battery is used. By changing the value of irradiation different modes of operation are emulated. Since this is a scaled down version the DC link reference voltage levels are chosen as V_{DC-1}= 25 V, V_{DC-2} = 35 V and the nominal voltage V_{DC} = 30 V. The value of $I_{DTR-max}$ is chosen as 1.5A. Depending on the reference voltage levels the different modes of operation are classified as follows:

$$V_{dc-Link} < 25\text{ V} – \text{Mode - 1},$$

$$25\text{V} < V_{dc-Link} < 35\text{V} – \text{Mode - 2, and}$$

$$V_{dc-Link} > 35\text{V} – \text{Mode - 3}.$$

Experimental tests have been carried out in terms of steady-state performance and transient-performance between different modes and the results are provided below. Figures 3.16 through 3.26 explain the experimental results for the various modes of operation.

A. *Experimental Results for Mode-1*

Experimental results for Mode-1 are shown in Figure 3.16. With the increase in the loading of distribution transformer, I_{DTR} increases from 1 A to 1.5 A as shown in Figure 3.16 and accordingly the PHEV is turned off so that the grid can cater to other loads without overloading the distribution transformer (assuming that $I_{DTR-max}$ = 1.5A). The turning-off of the PHEV is illustrated by the fact that V_B and I_B go to zero with the increase in distribution transformer loading. This is done by generating a duty cycle of zero for the buck converter switch. It can be seen from Figure 3.16 that the DC link voltage is maintained at 24.7 V ($\approxeq$ 25 V).

B. *Experimental Results for Mode-2*

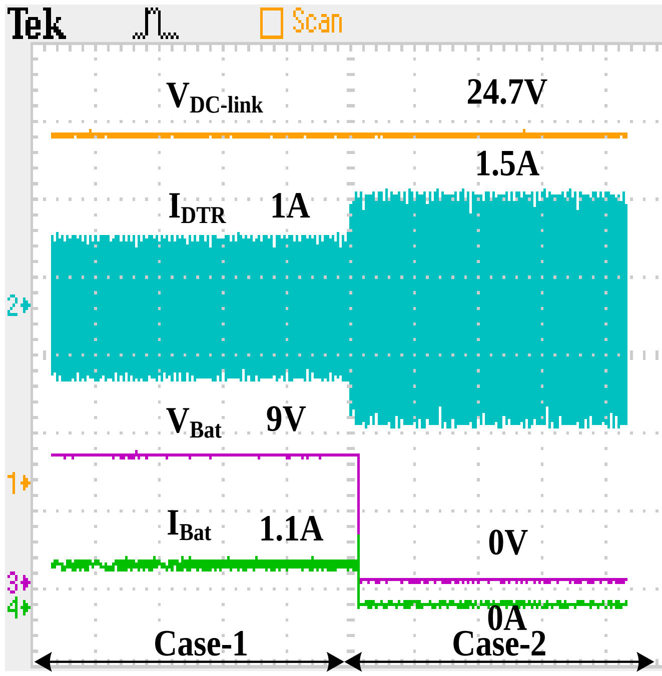

Figure 3.16: Experimental outputs describing the loading of distribution transformer in Mode-1.

Figure 3.17 shows the steady-state experimental results of Mode-2. The DC link voltage is 29.7 V and power is drawn from both the grid as well as PV. Current flowing from the PV, I_{PV} (0.88A) and current flowing from the grid, I_{grid} (0.3A RMS) are shown in Figure 3.17.

Experimental results for the transition between grid-rectification to PV charging during Mode-2 are shown in Figure 3.18. In the initial state, the DC link voltage is around 25.7 V and current flows from both the PV as well as the grid to charge the PHEV. Once the DC link voltage increases to 35.4V (Mode-3) no power is drawn from the grid.

Figure 3.19 shows the steady-state experimental results of PV charging during Mode-2. The DC link voltage is 29.9 V ($\approxeq$ 30 V) and the power is delivered by the PV alone which is 10.7 W.

Figure 3.21 represents the condition when the distribution transformer gets overloaded in Mode-2. With the overloading of distribution transformer, the

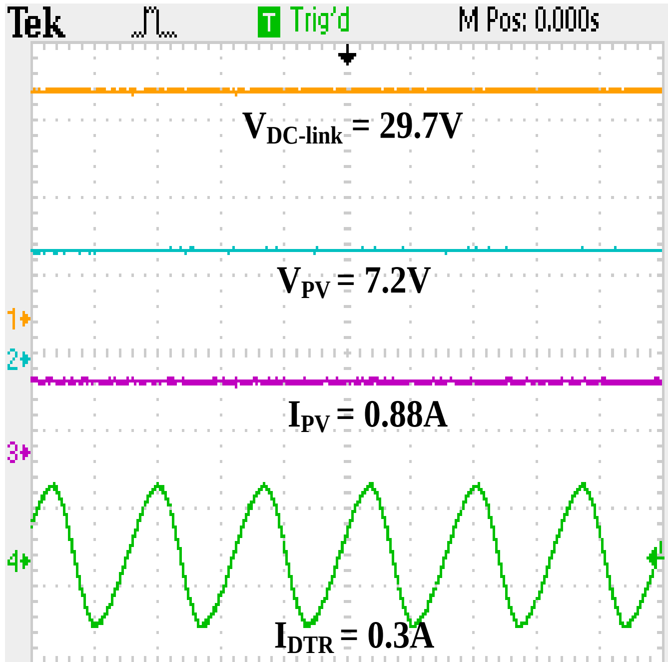

Figure 3.17: Experimental outputs for Mode-2.

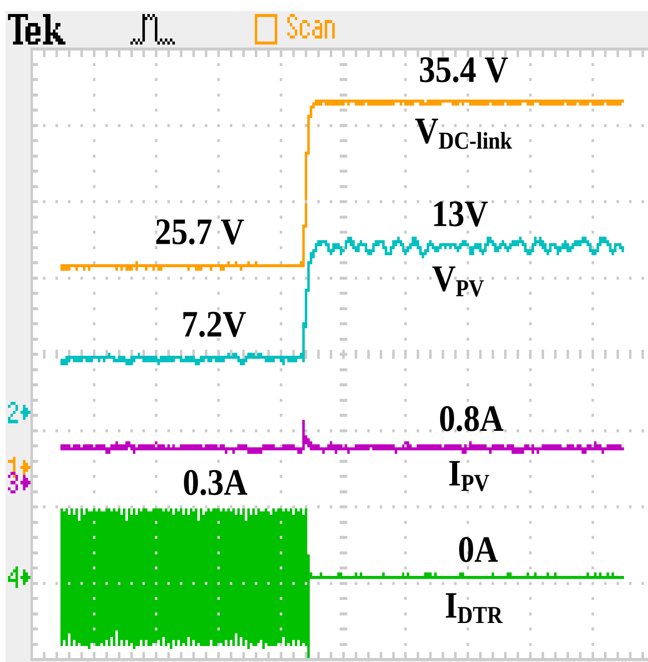

Figure 3.18: Experimental outputs for transition from grid-rectification to PV charging.

buck converter is turned off (to halt the charging of PHEV) and the inverter starts operating.

Transition from PV charging to grid-inversion during Mode-2 is shown in Figure 3.20. With the change in DC link voltage from 28.4V to 35.4V the bi-directional converter goes from off-state to on-state. Figure 3.22 shows

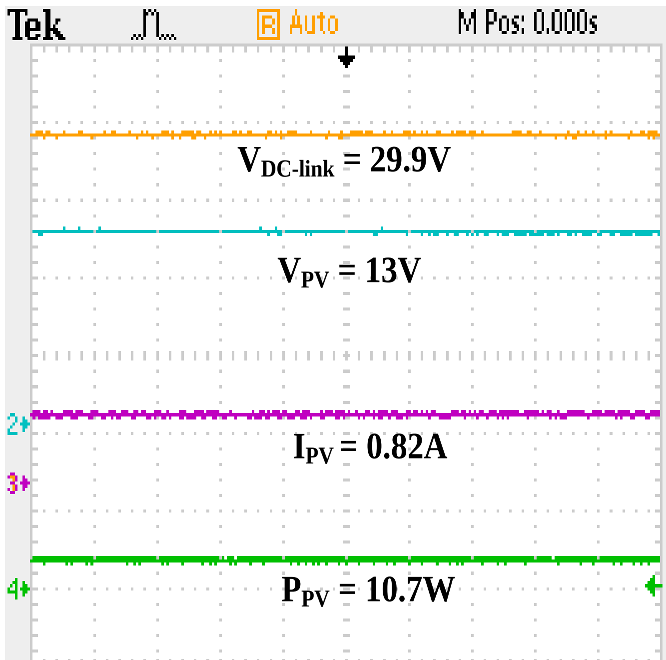

Figure 3.19: Steady-State experimental outputs for PV charging.

the turning-off of the PHEV charging when the state-of-charge reaches the threshold value. To turn off the PHEV, the duty cycle of the buck converter is made zero and hence V_B and I_B become zero as shown in Figure 3.22.

C. *Experimental Results for Mode-3*

Mode-3 resembles the normal operation of a grid-connected PV system. In this case the battery has been completely charged and hence the entire power generated by the PV is delivered to the grid.

Figure 3.23 shows the steady-state experimental results of Mode-3. The DC link voltage is 34.9 V ($\approxeq$ 35 V) and the output voltage of the inverter is a sine

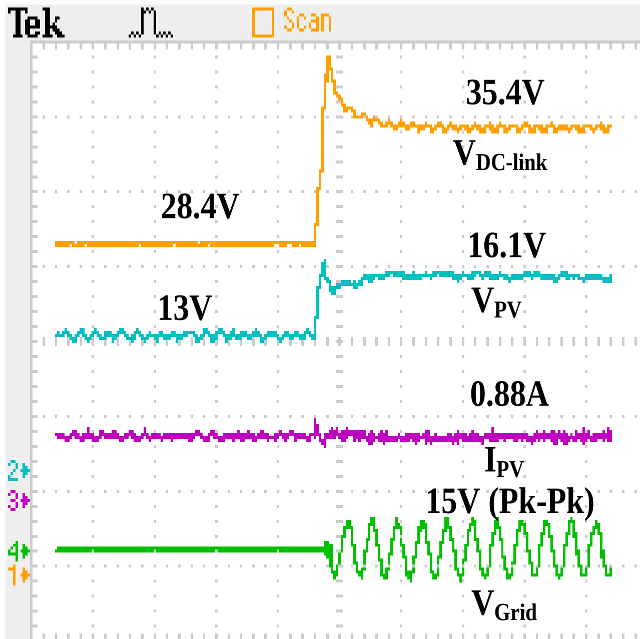

Figure 3.20: Experimental outputs for transition from PV charging to grid-inversion.

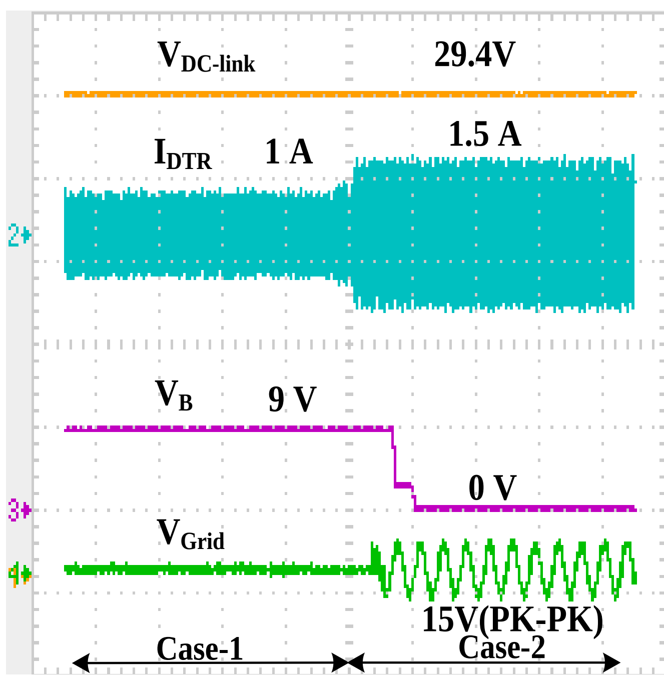

Figure 3.21: Experimental outputs describing the loading of distribution transformer in Mode-2.

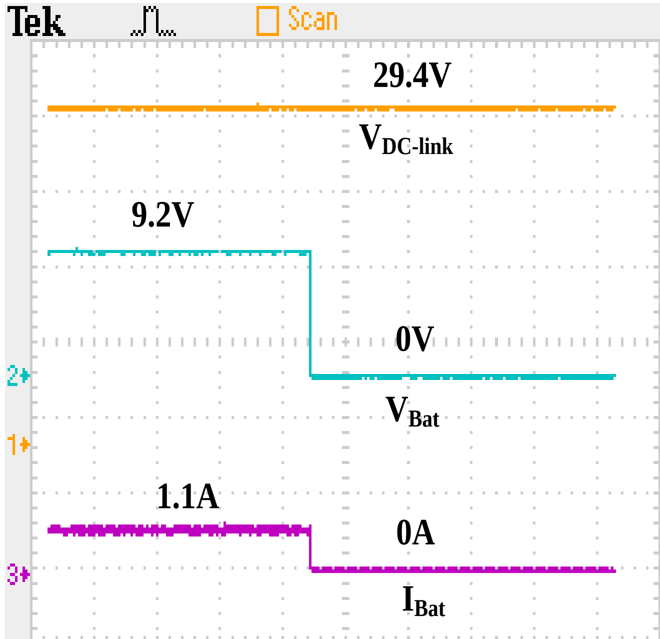

Figure 3.22: Experimental outputs describing the transition in state-of-charge.

wave. The peak-to-peak value of the inverter output voltage is maintained at 15V irrespective of the variation in DC link voltage from 25V to 35V. This is ensured by controlling the modulation index of the inverter. Figure 3.24 shows the experimental results of Mode-3 when the DC link voltage is 28.9V. The sinusoidal output voltage is maintained at 15V peak-to-peak just as in Figure 3.23 when the DC link voltage is approximately 35V.

Figure 3.25 shows the synchronization of the sinusoidal phase locked loop (SPLL) with the AC grid voltage. A high switching frequency along with LCL filter meets the total harmonic distortion (THD) requirements. Unipolar switching strategy was followed for inverter switching and the switching takes place at 20 kHz. The inverter switching at 20 kHz together with the LCL filter generates a filtered single phase AC output. The total harmonic distortion (THD) of the inverter output voltage is calculated to be 5.4% obtained from the Fast Fourier Transform (FFT) shown in Figure 3.26.

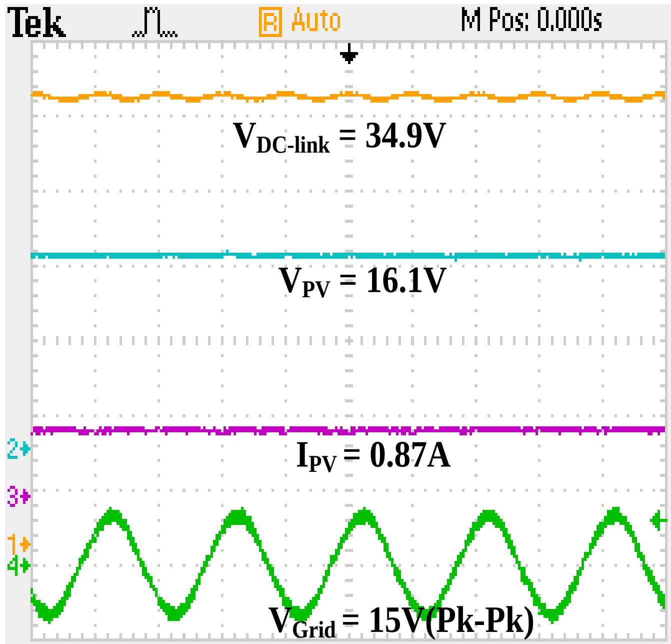

Figure 3.23: Steady state experimental outputs for Mode-3.

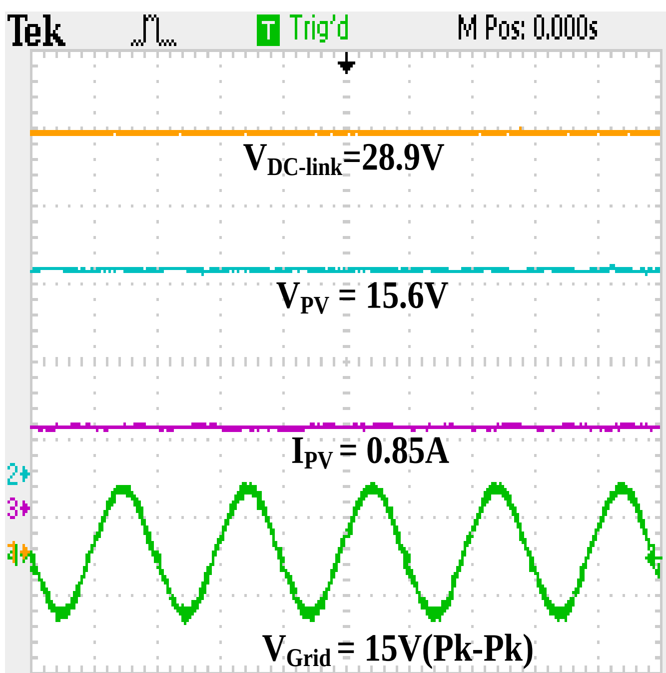

Figure 3.24: Experimental outputs for Mode-3 with a change in DC link voltage.

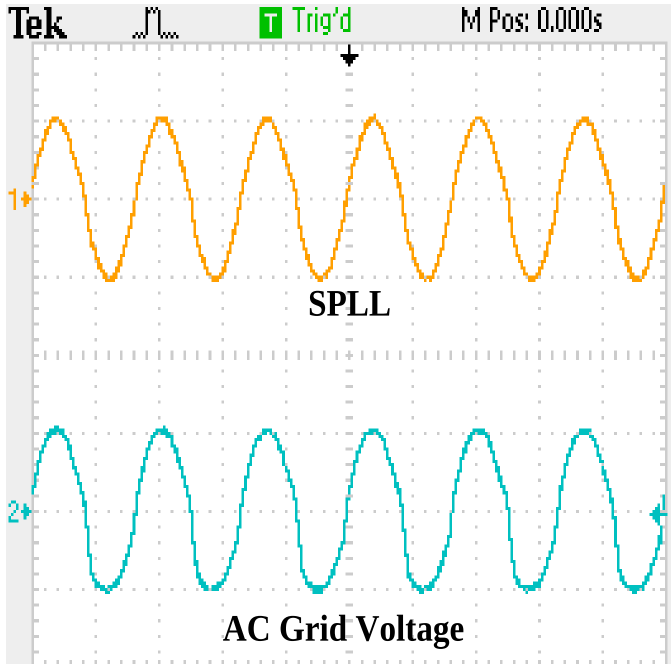

Figure 3.25: Grid synchronization.

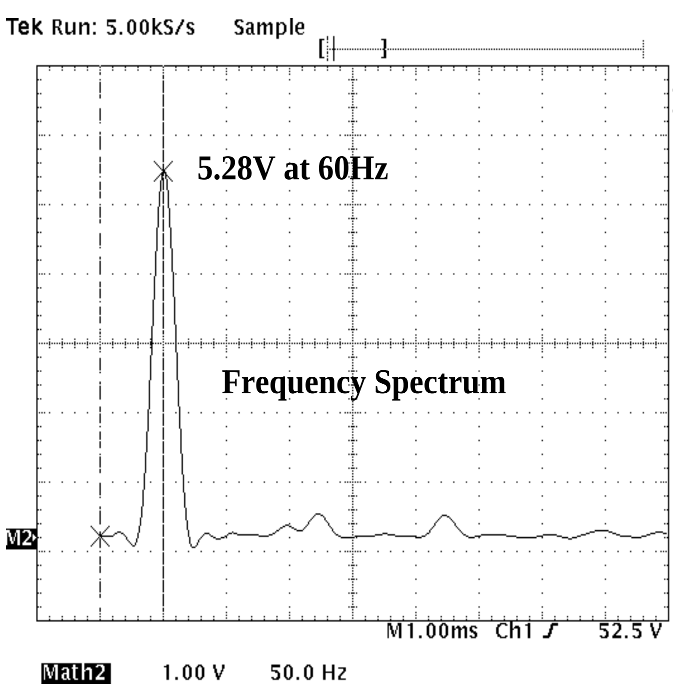

Figure 3.26: FFT of inverter output voltage.

3.8 Summary

This chapter presents a charging station architecture by using a combination of photovoltaic system and smart charging strategies. A unique control strategy based on DC link voltage sensing, which decides the direction of power flow is presented and the various modes of operation has been described. The practical feasibility and effectiveness of the proposed control strategy has been validated by experimental results from a laboratory prototype. The proposed control method based on the change in DC link voltage level due to the change in irradiation of the sun, is simple and unique. The charging algorithm facilitates charging of the PHEVs using minimum energy from the utility with a kind of demand management to improve the energy efficiency. Smart charging techniques like the one proposed in this chapter will help in avoiding major expense to upgrade distribution transformers and other substation equipment with the increase in PHEV loads on the distribution system.

Chapter 4 Smart Scheduling of PHEV Charging in Parking Facilities Powered by Renewable Energy Resources

This chapter presents a real-time smart scheduling algorithm (SSA) that uses a set of priority levels and the change in DC link voltage level to schedule the charging of plug-in hybrid electric vehicles (PHEVs) in a photovoltaic (PV) based charging facility. The priority levels are defined based on the arrival time, departure time, the initial state-of-charge and the battery capacity of the PHEVs. The developed SSA is aimed at reducing the overall cost of charging the PHEVs, mitigating their impact on the distribution network and also contributes to peak shaving. In order to validate the proposed SSA simulations are carried out using the MATLAB/SIMULINK toolbox.

4.1 Introduction

Recharging PHEVs poses a challenge to utilities due to their increase in electricity demand. One of the most important challenge is that the distribution system of the electric grid may be severely stressed as the PHEV penetration level increases as described in Section 2.3 of Chapter 3. To this end Chapter 2 has proposed a new architecture for charging facilities powered by PV in order to mitigate the impact on the distribution transformer. In the proposed architecture it has been assumed that the PHEV load demand is constant from morning till evening. But unlike this scenario the charging demand in such locations is highly variable depending on the customer arrival process. Hence it is imperative to coordinate the charging of PHEVs.

Coordination of charging in public infrastructure presents both unique opportunities and challenges [77]. PHEVs arrive between 8-9 AM and leave between 4-5 PM and the charging process takes approximately 2-5 hours. The problem is that the PHEVs arrive in a narrow time band and if the charging starts soon after the arrival, the charging energy need will produce a sudden load peak in the local consumption. An uncoordinated charging strategy might lead to a sizable amount of power being drawn from the grid which imposes a strict peak power constraint. This may further lead to many vehicle charging deadlines not being met. To overcome these issues smart scheduling of PHEV charging is necessary.

Smart scheduling is crucial for the utilities since it spreads the charging load over the time the vehicles are parked at the installation as opposed to placing the full load on the utility at once. PCFs coupled with smart scheduling techniques ensures maximum utilization of solar generation to meet the demand of PHEVs. As shown in Figure 4.1 the individual charging process of PHEVs is scheduled to fill the daily PV production curve so as to minimize the consumption from external network [78].

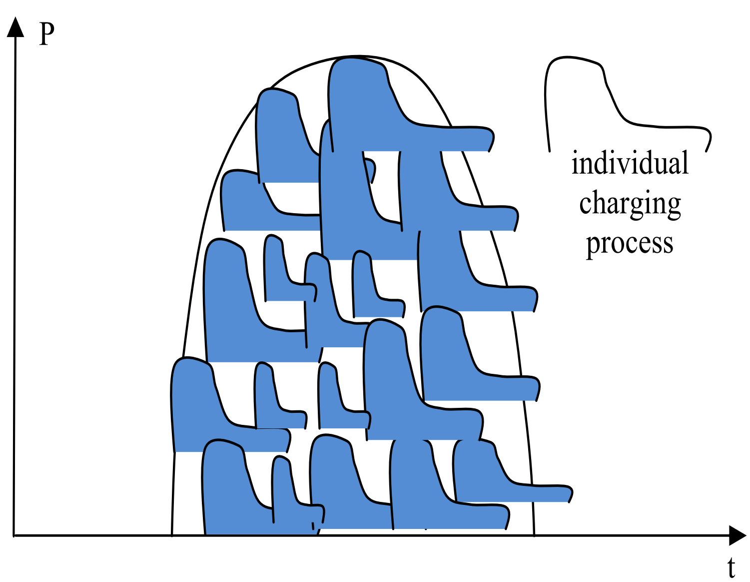

Figure 4.1: Daily PV production and the individual charging processes.

Several scheduling methods involving PHEVs and solar generation are described in the literature. A rule based priority scheduling method is presented in [79–81]. Priorities are defined based on the availability time of the PHEVs in the PCF and the power generated by the PV source. PHEVs with lesser availability time are given the first priority. Accordingly the charging of the PHEVs can be initiated immediately or shifted to a later time. A real-time energy management algorithm (RTEMA) is proposed for a PV based grid-connected charging park [82,83]. The algorithm is based on a set of priority charging levels of PHEVs which are defined based on their state-of-charge (SOC) and the time remaining for their departure. One of the drawbacks of the above methods is that the power available from the PV system is predicted based on online forecasting methods such as Grey Model, Markov Chain model or several prediction algorithms using solar insolation, humidity, and temperature.

This chapter presents a new method independent of online forecasting methods to schedule the charging of PHEVs in PV based charging facilities. The SSA in this paper is based on a set of priority charging levels which are defined based on the power requirement of the PHEV and its duration of stay in the parking lot entered via a Human Machine Interface (HMI). Since the PHEVs enter the charging facility at different time intervals the priority levels are updated whenever a change in DC link voltage is detected.

4.2 Charging Facility Architecture

The detailed architecture of the charging facility is similar to the one already presented in Chapter 2. As shown in Figure 4.2 each charging point is equipped with a charging meter that the customers can plug their PHEVs into. Additionally, the consumers can enter information such as the departure deadline, initial state-

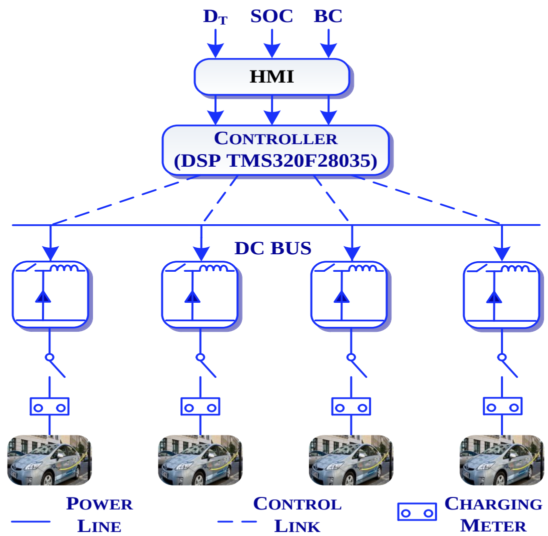

Figure 4.2: System architecture.

of-the-charge (SOC), and the preferred charging rate via a HMI port when they arrive at the parking lot. The data entered by the customers is fed into the DSP based control unit which sorts the PHEVs in a priority order as per the SSA. The controller schedules the charging of PHEVs such that their demand is distributed throughout the day based on their departure time as shown in Figure 4.1. PHEVs with minimum departure time will be charged at higher charging rate and hence the cost of charging will be higher. From Figure 4.2 the inputs to the HMI are defined as follows:

> SOC_i is the intial state-of-the-charge of the i_{th} PHEV at the time of the entering the charging facility.
>
> BC_i is the battery capacity of the i_{th} PHEV.
>
> D_{Ti} is the departure time of the i_{th} PHEV.

The controller should ensure that all the PHEVs should leave the charging facility with as close to a full charge as possible for the period of time the vehicle has been parked. As shown in Figure 4.1 the charging load is spread over the time the vehicles are parked at the installation as opposed to placing the full load on the utility at once. In addition to benefiting the utility through load shifting, the solar generation can now be better utilized to meet the demand of the electric vehicles.

From Figure 4.1,

$$E_{PV} \approx E_{charge} \; and \tag{4.1}$$

$$\int_{t_1}^{t_2} P_{PV}(t)dt \approx \sum_{i=1}^{n} \int_{t_1}^{t_2} C_i dt, \tag{4.2}$$

where

E_{PV} = the energy produced by the PV during the period t_1 - t_2

E_{charge} = the energy consumed by the PHEVs during the period t_1 - t_2

P_{PV} = the actual power of the PV cells

C_i = the actual power of the i-th charger

4.3 Smart Scheduling Algorithm (SSA)

As mentioned earlier the goal of the SSA is to prioritize the charging of PHEVs during the peak load period. The priority order is determined based on the departure time or the power demanded by the PHEVs. The criterion to sort the PHEVs in a priority order is as follows :

- For PHEVs entering the charging facility at different times, the PHEV with the least departure time is given the higher priority.
- If the PHEVs enter and leave the charging facility at the same time, the PHEV with the higher power demand is given the higher priority.

Assuming that each PHEV will be charged from its initial SOC when it arrives at the PCF to the maximum SOC, the power demanded by the ith PHEV ($P_{PHEV,i}$) is

Table 4.1: Charging rate for different charging levels

Priority Level	Power Requirement	Maximum charging rate [kW]	Minimum charging rate [kW]
Level - 1	$P_{PHEV,n} \geq 15$ kW	15	12
Level - 2	10kW $\leq P_{PHEV,n} <$ 15kW	11	8
Level - 3	5kW $\leq P_{PHEV,n} <$ 10kW	7	4
Level - 4	2kW $\leq P_{PHEV,n} <$ 5kW	4	0

calculated as follows:

$$P_{PHEV,i} = \frac{BC \times (SOC_U - SOC_i)}{D_t - A_t} \; and \tag{4.3}$$

$$P_{PHEV} = \sum_{i=1}^{N} P_{PHEV,i} \tag{4.4}$$

where BC is the battery capacity, SOC_U is the upper limit of the state-of-charge, SOC_i is the initial state of the charge, D_t is the departure time, A_t is the arrival time and P_{PHEV} is the total power demanded by the PHEVs. Table 4.1 shows the maximum and minimum charging rates for different priority levels.

Once the PHEV load demand has been calculated and priority levels defined the SSA can be envisaged as described in the flowchart shown in Figure 4.3 :

- The priority levels are updated in real-time as and when the PHEVs enter the parking lot which is indicated by a change in DC link voltage level. Charging of each PHEV begins once it connects to the charger.

- If the total power demanded by the PHEVs, P_{PHEV} exceeds the power delivered by the PV array, P_{PV} then the additional power is delivered by the

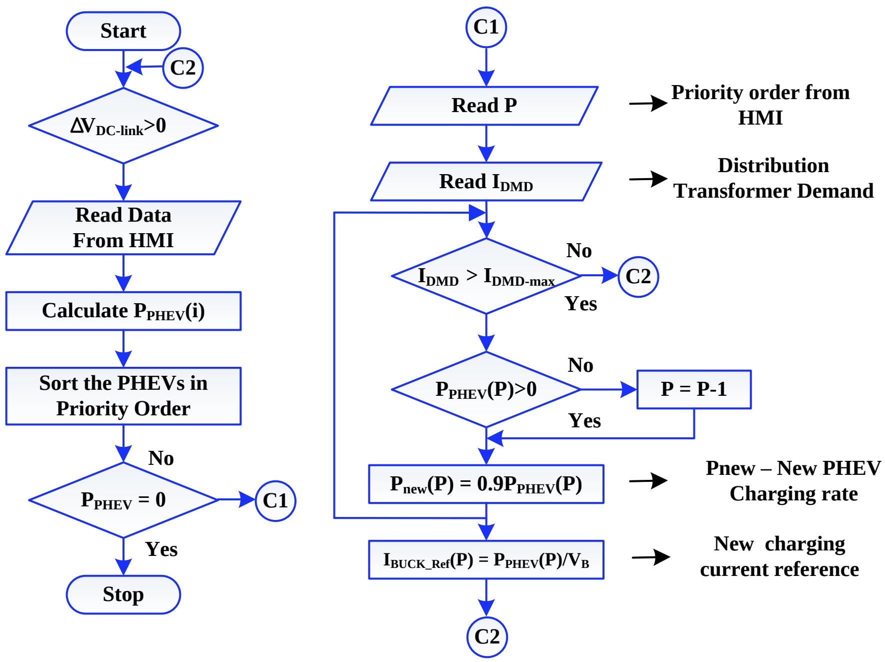

Figure 4.3: Flowchart depicting the smart scheduling algorithm.

grid. The associated controller action based on DC bus has been explained in detail in chapter 3 and therefore it is not dealt here.

- The PHEV charging is rescheduled (starting from the PHEVs in the lower priority level) when the total current delivered by the distribution transformer, I_{DMD} exceeds the threshold value, $I_{DMD-max}$.

- The charging rates of the PHEVs is decremented in steps of 0.1 kW until the load demand on the distribution transformer is equal to the threshold level (i.e., $I_{DMD} = I_{DMD-max}$).

- If there is an increase in PV power (indicated by the change in DC link voltage level) or a decrease in distribution transformer load demand the charging rates of the PHEVs are incremented. They might as well be promoted to higher priority levels to meet their departure deadlines.

- The SSA is terminated once all the PHEVs are completely charged or they leave the charging facility i.e. $P_{PHEV} = 0$.

4.4 Case Studies and Simulation Results

In order to validate the proposed control algorithm for the PV powered smart charging facility, simulations have been carried out using the Sim-Power Systems toolbox of MATLAB/SIMULINK. Table 4.2 shows the detailed ratings of the various components. As mentioned in the table, a PV panel rated at 10 kW is considered. The grid-connected voltage source converter (G-VSC) is rated at 10 kW and the nominal DC link voltage is maintained at 400 V.

The developed smart charging facility is a small parking garage in a workplace, university campus or a shopping mall which contains 4 parking spaces. The distribution transformer is rated at 15 kVA and therefore the maximum load demand before it gets overloaded is 12 kW at 0.8 pf. The connection and disconnection time and the initial and final SOC of PHEVs is represented under the respective case studies. Simulation studies are carried out for the following cases:

Case 1) PHEVs enter and leave the charging facility at the same time. Therefore the priority levels are classified based on their load demand.

Case 2) PHEVs enter and leave the facility at different times. Hence the priority levels are classified based on the departure times.

4.4.1 Case 1

This case corresponds to the situation when the PHEVs enter and leave the facility at the same time. It represents the typical environment in a workplace based charging facility. The connection and disconnection time and the initial and

Table 4.2: Ratings of the simulation system

DC link	Nominal Voltage	400 V
PV Panel	Power Rating	10 kW, PMSG
GS-VSC	Power Rating	10 kW
Transformer	Nominal Voltage	0.208/0.460 kV (L-L)
	Power Rating	15 kVA
DC/DC Converters	Boost Converter	f = 100 kHz, L = 7 mH, c = 0.8 mF
	Buck Converter	f = 100 kHz, L = 5.375 mH, C = 20 μF

Table 4.3: PHEV arrival and departure data for Case 1

Priority Order	**PHEV Model**	**Battery Capacity**	**Arrival Time**	**Departure Time**	**Initial SOC**	**Final SOC**	**Duration of Stay**	**PHEV Load Demand**
4	Toyota Prius	4.4 kWh	10 AM	4 PM	20%	100%	6 hr	0.52 kW
3	Nissan Leaf	24 kWh	10 AM	4 PM	40%	90%	6 hr	1.87 kW
1	Tesla Model S	85 kWh	10 AM	4 PM	50%	90%	6 hr	5.67 kW
2	Chevy Volt	16 kWh	10 AM	4 PM	20%	90%	6 hr	2 kW

final SOC of PHEVs is represented in Table 4.3. Figure 4.4 shows the simulation results for case 1.

As mentioned in Table 4.3 all the four PHEVs enter the charging facility at 10:00 AM and leave at 4:00 PM. From Figure 4.4 (a) it can be seen that the initiation of PHEV charging results in a change in DC link level which triggers the SSA. Since the PHEVs enter and leave the charging facility at the same time, the priority orders are defined based on their load demand as shown in Table 4.3.

The PHEV load demand from 10:00 AM - 4:00 PM is 10.06 kW as shown in Figure 4.4. The charging prority levels are updated each and every time a change in DC link voltage level is detected. At 2:00 PM the current delivered by the distribution transformer, I_{DMD} exceeds the threshold value, $I_{DMD-max}$. Hence the rate of charge of the PHEVs is decremented starting from the PHEVs in the lower priority level.

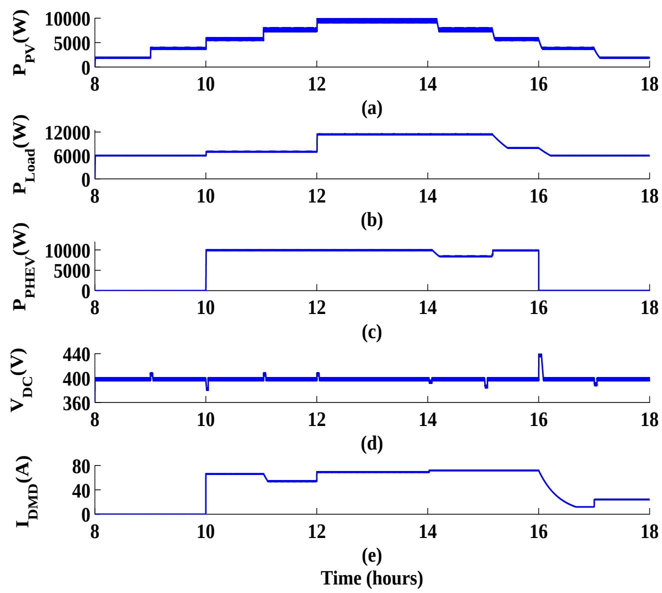

Figure 4.4: Simulation results for Case 1.

Table 4.4: PHEV arrival and departure data for Case 2

Priority Order	PHEV Model	Battery Capacity	Arrival Time	Departure Time	Initial SOC	Final SOC	Duration of Stay	PHEV Load Demand
1	Toyota Prius	4.4 kWh	8 AM	9 AM	20%	100%	1 hr	3.08 kW
2	Chevy Volt	16 kWh	9 AM	1 PM	20%	90%	4 hr	2.8 kW
3	Tesla Model S	85 kWh	10 AM	3 PM	50%	90%	5 hr	6.8 kW
4	Nissan Leaf	24 kWh	10 AM	4 PM	40%	90%	6 hr	2 kW

The charging rates of PHEV-3 and PHEV-4 are updated at 3:00 when a change in DC link voltage level is detected. The controller terminates once all the PHEVs leave the charging facility at 4:00 PM which is indicated by the drop in PHEV load demand, P_{PHEV} to zero. Figure shows the charging profiles of each PHEV. It can be seen from Figures 4.5 (a) and (b) that the charging rates of PHEV-4 and PHEV-2 are reduced at 2:00 PM when I_{DMD} exceeds $I_{DMD-max}$.

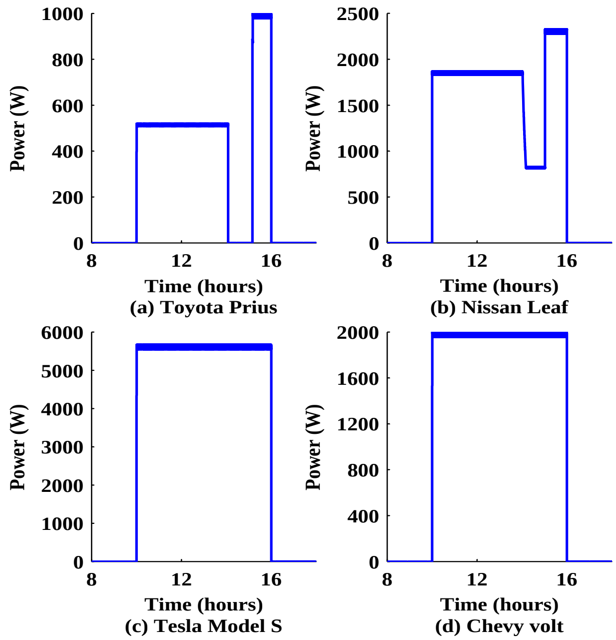

Figure 4.5: PHEV charging profiles for Case 1.

4.4.2 Case 2

This case corresponds to the situation when the PHEVs enter and leave the facility at different times. This type of situation can be considered in places such as shopping malls where the PHEVs present a random demand profile. The connection and disconnection time and the initial and final SOC of PHEVs is represented in Table 4.4. Figure 4.6 shows the simulation results for case 2.

As shown in Table 4.4 since the PHEVs enter at different times the priority order of charging changes dynamically. The priority order shown in the table is used as an initial reference to designate each PHEV.

At 8:00 AM PHEV-1 enters the charging facility and triggers the SSA. Since there are no other PHEVs in the facility it is given a priority order of 1. It is completely charged by 9:00 AM and leaves the facility. PHEV-2 starts charging at 9:00 AM and it is given a priority order of 1. Similarly PHEV-3 and PHEV-4 entering the charging facility and trigger the SSA. Subsequently they are assigned

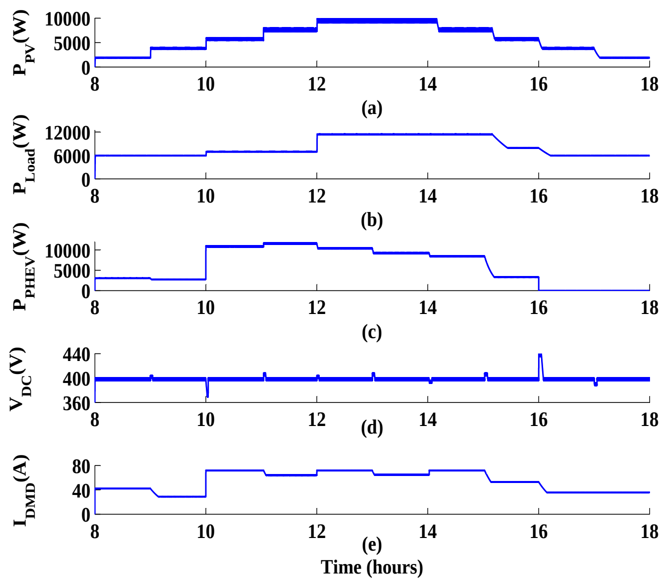

Figure 4.6: Simulation results for Case 2.

priority orders of 2 and 3 respectively.

The total PHEV load at 10:00 AM results in the increase in I_{DMD} beyond the threshold level of $I_{DMD-max}$. Therefore the charging rate of PHEV-4 which has a priority order of 3 is reduced until I_{DMD} is equal to $I_{DMD-max}$. As shown in Figure 4.6 I_{DMD} is maintained at its threshold limit of 41.5 A. This control action occurs at t = 10 AM, t = 12 PM, and t = 2 PM as shown in Figure 4.6 (d).

It has to be noted that the charging rates of each PHEV are continuously updated whenever a change in DC link voltage level is detected. Figure 4.7 shows the charging profiles of each PHEV. As shown in Figure 4.7 (b) the charging rate of PHEV-4 which has the lowest priority varies continuously from 10:00 AM - 4:00 PM. The charging rate is reduced whenever I_{DMD} exceeds $I_{DMD-max}$ and it is increased or maintained during the other periods.

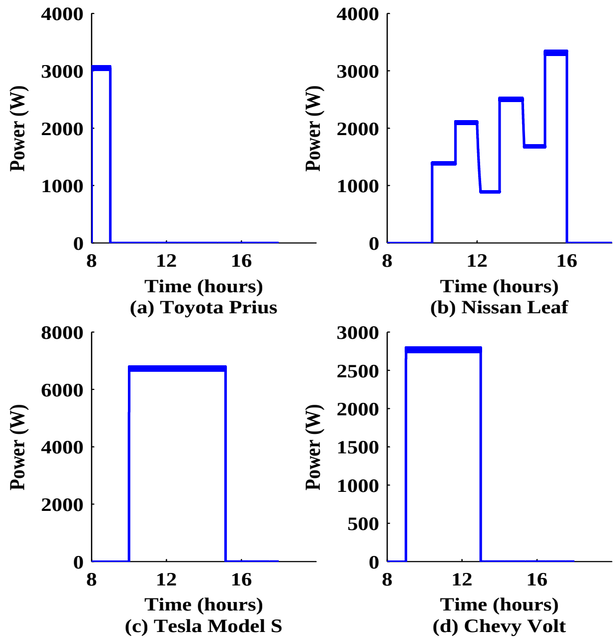

Figure 4.7: PHEV charging profiles for Case 2.

4.5 Summary

A real-time smart scheduling algorithm (SSA) for a workplace based charging facility is presented in this paper. An advantage of the developed algorithm is that the charging rates of the PHEVs during their parking period are varying according to their state-of-charge. The algorithm is simple and easy to develop since it is not based on any online forecasting methods.

Chapter 5 Wind Powered Smart Charging Facility for PHEVs

This chapter proposes a charging station architecture with a small scale wind turbine as the primary source. Coordinated control strategy based on DC link voltage sensing is proposed to facilitate the operation of the charging facility in standalone and grid-connected modes. The proposed architecture and the control algorithm are validated through simulations using MATLAB/SIMULINK toolbox. A scaled down version of the proposed architecture has been implemented in the laboratory and the experimental results are presented.

5.1 Introduction

Plug-in hybrid electric vehicles have already entered the consumer automotive market and they are going to be an integral part of the electric power system. The expected high penetration of PHEVs would have a serious impact on the life of a distribution transformer since they are not designed to deal with the increased demand and new patterns of consumption. In order to minimize the loading on distribution transformers smart charging techniques coupled with renewable energy resources are the need of the hour. Several charging station architectures based on photovoltaic systems are described in the literature [25, 26, 43]. Solar photovoltaic charging is widely being touted as an alternative for charging low to mid-range PHEVs. Another very popular renewable energy resource is power from the wind turbines. Charging PHEVs from small scale wind turbines (1 kW – 15 kW) is also being realized as a viable alternative [84] because of the following reasons:

- Huge improvement in power converter technology for small wind turbines (SWTs) [85]
- High efficiency of the system for capturing energy at lighter winds which are very frequent.

A review of literature suggests that number of studies examined the large-scale, long term impact of PHEVs on the ability of the electric grids to integrate wind energy. The effect of large-scale adoption of PHEVs on the integration of wind energy into the US electricity mix is described in [86]. As per [87], PHEVs (Plug-in Hybrid Electric Vehicles) have the potential to increase the amount of wind energy capacity installed in a regional or national electricity system. More specifically, PHEVs can absorb the excess wind energy production that would otherwise be wasted or curtailed, which improves the economics of wind energy generation.

To mitigate the volatile behavior of wind power, demand response algorithms using PHEVs are proposed [88]. According to [89] proliferation of PHEVs can cause system wide voltage variations beyond recommended limits. It further states that smart charging using the surplus energy from wind production appears to solve the issue of voltage drop. On the whole, these studies indicate that the penetration of PHEVs has the potential to increase the amount of wind energy capacity installed in a regional or national electricity system. But not much emphasis has been laid in the literature regarding the synergy between PHEVs and wind power through smart charging facilities at distribution level. This chapter proposes a smart DC charging facility featuring small scale wind turbine that can be installed in a workplace environment (the concept can be extended to places like universities, shopping malls and other commercial places). The proposed block diagram is shown in Figure 5.1. As shown in the figure, PHEVs are charged using DC power since it has advantages like increased efficiency and reduction in power conversion stages.

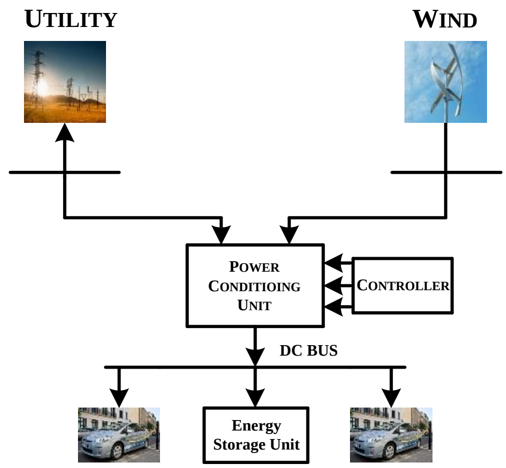

Figure 5.1: Proposed smart charging facility.

The concept of DC bus signaling (DBS) has been proposed by many researchers for proper power management in a DC microgrid [40–42, 44]. In DBS, DC bus voltage is employed as an information carrier to determine the operation modes of various converters according to predefined voltage levels. Though [41] has done extensive work on controlling a grid-connected DC microgrid using DBS, the change in the voltage levels due to the change in suns insolation is not considered. [42] Proposed an improved version of DBS but does not consider the operation of DC microgrid in grid-connected mode. This chapter extends on the similar concept proposed in Chapter 3 and [44] but the PV source in this case is replaced by a small scale wind turbine.

5.2 System Architecture

The circuit configuration of the proposed smart charging facility for PHEVs is shown in Figure 5.2. The system consists of a small scale wind turbine (SWT) using permanent magnet synchronous generator (PMSG), energy storage unit

(ESU), PHEV load and the controlling unit. The SWT is connected to the DC link via an AC/DC diode rectifier and DC/DC boost converter. The DC/DC boost converter performs the function of maximum power point tracking (MPPT) to facilitate the operation of wind turbine at the maximum power point. Energy storage unit (ESU) is connected to the DC bus via a bi-directional DC/DC buck-boost converter. The ESU will support the charging of PHEVs when there is no power available either from the grid or the wind turbine. The battery pack in the ESU can be charged from the grid during off peak hours or from the wind turbine after all the PHEVs have been charged in the charging facility. A DC/DC buck converter controls the charging of the PHEV. The charging facility is connected to the power distribution network through a bi-directional grid-tied converter.

The control description for the charging facility shown in Figure 5.2 is based on the charging requirements of a single PHEV. Multiple PHEVs can be charged by increasing the corresponding ratings of the charging station components like the wind turbine and the associated power converters. Each PHEV must have a separate buck converter installed for each charge point. Since the charging station can be located at public places such as shopping malls, adjacent to freeways, universities etc. the PHEVs enter and leave the parking lot at different time intervals. Hence the PHEVs present a random variation in load demand over a time period. Under this scenario, the variation in DC link voltage occurs due to the fluctuation in wind speed and PHEV load demand.

The control unit monitors and controls the power flow between the source and PHEV based on the change in DC link voltage. As shown in Figure 5.2, the operation of the control unit is based on twelve inputs which determine the direction of power flow in the charging facility and generate the required switching signals for various converters.

$V_{DC-link}$ is the magnitude of the voltage at the DC link which determines

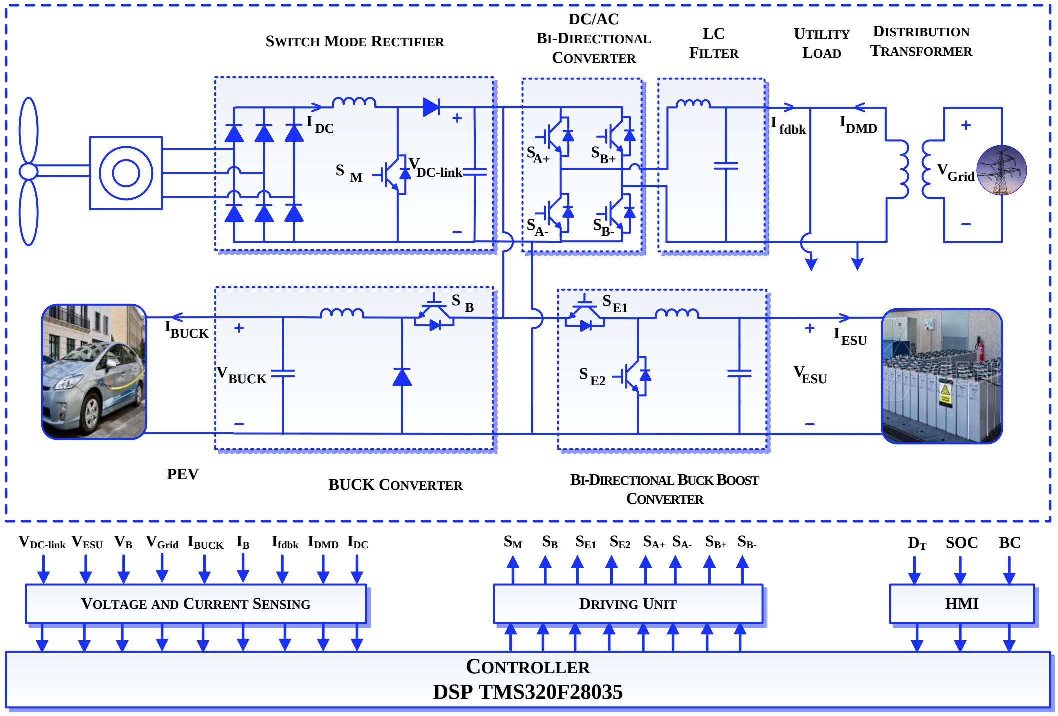

Figure 5.2: Detailed circuit configuration of the proposed architecture.

the various modes of operation.

I_{DMD} is the current delivered by the distribution transformer which determines the peak load condition.

I_{DC} is the inductor current required for the control of boost converter.

V_{BUCK} and I_{BUCK} are the inputs for the buck converter control. V_{BUCK} is the detected battery voltage across the PHEV and I_{BUCK} is the output current of the buck converter.

V_{ESU} and I_{ESU} determine the controller action of the bi-directional buck-boost converter. V_{ESU} is the detected battery voltage across the ESU which is the measure of its SOC and I_{ESU} is the current drawn or injected by the ESU.

V_{Grid} and I_{fdbk} are the inputs for the inverter control. V_{Grid} is the grid side voltage. I_{fdbk} is the current fed into the grid by the DC/AC converter.

D_T, SOC and BC are the data entered by the customers via the HMI port at the time of entering the charging facility. D_T is the departure time, SOC is the state-of-charge of the PHEV batteries and BC is the battery capacity.

5.3 Modeling of the System

This section models the wind turbine and power electronic converters in order to mathematically derive the relationship between wind speed, load and the DC link voltage.

5.3.1 Wind Turbine Model

The power as a function of wind speed V_W can be calculated from the equation of the wind turbine power as

$$P_T = \frac{1}{2} C_P(\lambda) A \rho V_W^3, \tag{5.1}$$

where ρ is the density of the air $[kg/m^3]$ and A is the area $[m^2]$ swept by the turbine. C_P is the power coefficient defining the aerodynamic efficiency of the wind turbine rotor, and is a function of the tip speed ratio λ . The tip speed is defined as the ratio between the peripheral speed of the blades and the wind speed as

$$\lambda = \frac{\Omega \times R}{V_W}, \tag{5.2}$$

where Ω is the rotational speed of the blades (the rotational speed of the low-speed shaft) and R is the blade length.

The wind turbine torque on the shaft can be calculated from the shaft power as

$$T_T = \frac{P_T}{\Omega} = \frac{C_P(\lambda) \times \rho \times R^2 \times H \times V_W^2}{\lambda}. \tag{5.3}$$

The shaft rotational speed optimal control solution using a set point from the wind speed information can be applied if the optimal value of the tip speed ratio, λ_{opt}, is known. The turbine operates on the 'Optimal Regimes Characteristic' (ORC) shown in Figure 5.3 if $\lambda = \lambda_{opt}$, which supposes that the shaft rotational speed is controlled by a closed-loop control system so as to reach its optimal value

$$\Omega_{opt} = \frac{\lambda_{opt}}{R} V_W. \tag{5.4}$$

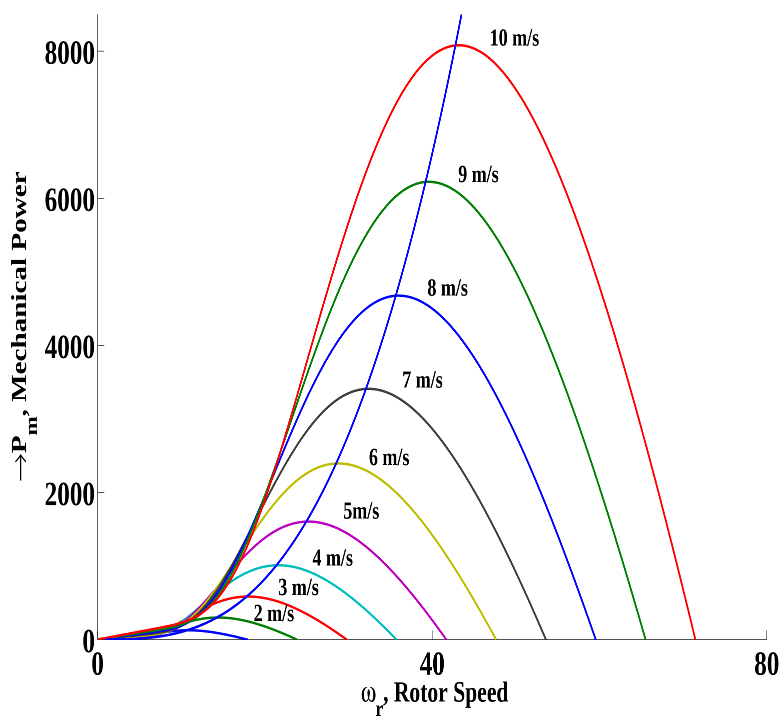

Figure 5.3: The optimal regime characteristics.

5.3.2 Permanent Magnet Synchronous Generator Model

Permanent Magnet Synchronous Generator (PMSG) is preferred over other generators mainly due to its high efficiency. The EMF induced in PMSG is proportional to rotational speed . The equivalent circuit for one phase is shown in Figure 5.4. The constant of the generator is defined as k, and a field magnetic flux

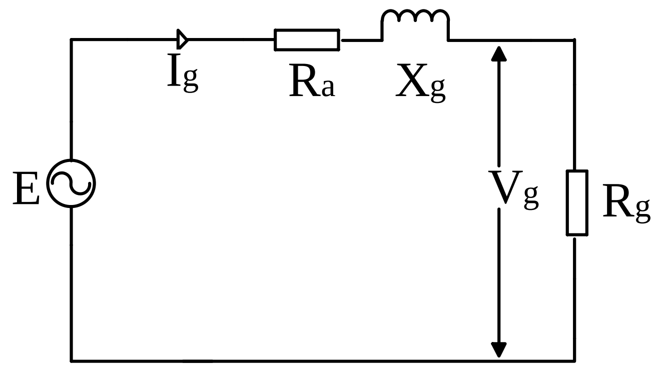

Figure 5.4: Equivalent circuit of PMSG per phase.

ϕ and mechanical angular velocity ω_g. The induced EMF is given by

$$E = k\phi\omega_g. \tag{5.5}$$

Terminal voltage V_g of the generator is

$$V_g = E - R_a I_g - jX_g I_g, \tag{5.6}$$

where I_g is the line current of the generator, R_a is the winding resistance per phase and X_s is the synchronous reactance per phase.
From Equation 5.6 we can deduce the line current as

$$I_g = \frac{E_g}{(R_g + R_a) + jX_s}. \tag{5.7}$$

The amplitude of the line current is expressed as

$$|I_g| = \frac{|E_g|}{\sqrt{(R_a + R_g)^2 + X_s^2}}. \tag{5.8}$$

The generated output power is

$$P = 3|I_g||V_g|cos\phi = 3R_g|I_g|^2 \ and \tag{5.9}$$

$$P = 3R_g \times \frac{E_g^2}{(R_g + R_a)^2 + X_s^2}. \tag{5.10}$$

5.3.3 Design of Three-Phase Diode Bridge Rectifier

The generator is connected with the rectifier circuit as shown in Figure 5.5. It is assumed that the AC power generated by the PMSG is converted into DC power through the diode bridge rectifier circuit. Therefore

$$3V_gI_g = V_{dc1}I_{dc1}, \tag{5.11}$$

where, V_{dc1} and I_{dc1} are the DC side voltage and current, respectively. The value of resistance for one phase of rectifier circuits from the view point of AC side is defined as R_g, and the maximum value of line-to-line voltage is defined as V_{LLPeak}.

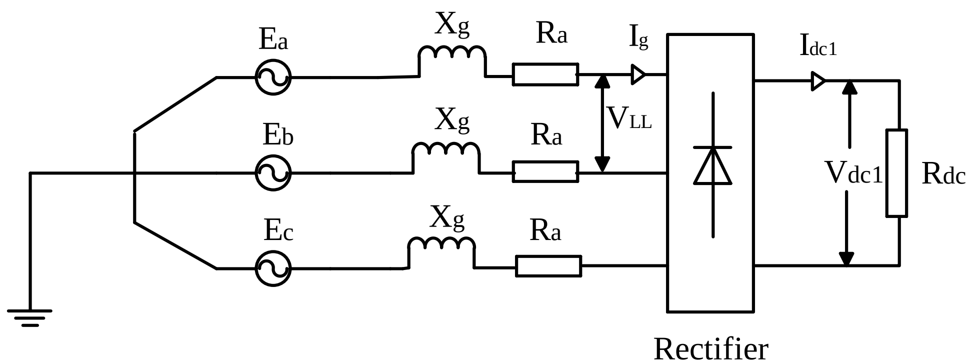

Figure 5.5: PMSG connected to a diode rectifier.

The mean value of DC voltage is obtained as

$$\begin{aligned} V_{dc1} &= \frac{3}{\pi}\int_{\frac{-\pi}{6}}^{\frac{\pi}{6}} V_{LLPeak}cos\theta d\theta \ and \\ &= \frac{3}{\pi}V_{LLPeak}. \end{aligned} \tag{5.12}$$

From the above equations, the relationship between V_{dc1}, line to line voltage V_{LL} and phase voltage V_g is obtained as

$$\begin{aligned} V_{dc1} &= \frac{3\sqrt{2}}{\pi} V_{LL}, \\ &= \frac{3\sqrt{6}}{\pi} V_g, \ and \\ &= \frac{3\sqrt{6}}{\pi} R_g I_g. \end{aligned} \tag{5.13}$$

From Equation 5.13 and Equation 5.11, the following relation between I_{dc1} and I_g is obtained as

$$I_{dc1} = \frac{\pi}{\sqrt{6}} I_g. \tag{5.14}$$

If R_{dc1} is the resistance on the DC side of the bridge rectifier and I_{dc1} is the output current then

$$V_{dc1} = \frac{3\sqrt{6}}{\pi} R_g I_g = R_{dc1} I_{dc1}, \tag{5.15}$$

$$\frac{3\sqrt{6}}{\pi} R_g I_g = R_{dc1} \frac{\pi}{\sqrt{6}} I_g, \ and \tag{5.16}$$

$$R_g = \frac{\pi^2}{18} R_{dc1}. \tag{5.17}$$

5.3.4 DC/DC Boost Converter

The SC output voltage from the generator is converted into DC voltage by the 3-phase diode bridge rectifier and it is boosted by the DC/DC boost converter. In this section, the operation of the boost circuit is theoretically analyzed. The generator and the rectifier circuit are together represented by a DC voltage source for the ease of analysis. The inverter and the power grid are together modeled as a load resistance connected with the DC link. The circuit configuration of the boost converter is shown in Figure 5.6. The inductance and capacitance of the boost circuit are assumed to be sufficiently large in order to reduce the ripple in

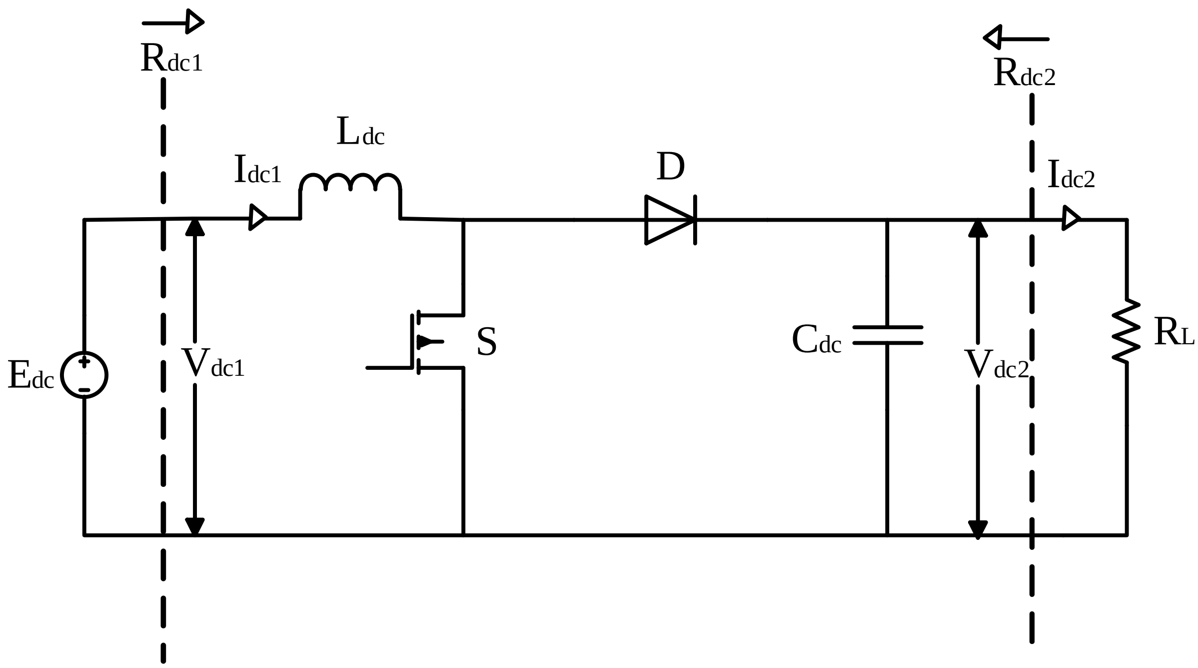

Figure 5.6: Boost converter circuit.

inductor current and the DC output voltage. The following equations express the relation between the input and output voltages and currents

$$V_{dc2} = \frac{1}{(1-D)} V_{dc1} \; and \tag{5.18}$$

$$I_{dc2} = (1-D) I_{dc1}, \tag{5.19}$$

where D is the duty ratio given by

$$D = \frac{t_{on}}{t_{on} + t_{off}}, \tag{5.20}$$

where t_{on} is the turn on period of the switch $'S'$ and t_{off} is the turn off period of the switch.

It is possible that the boost converter circuit along with the load resistance R_L are considered a kind of variable resistance changed by the duty ratio from the viewpoint of the DC voltage source. This variable resistance R_{dc1} is defined as

$$R_{dc1} = \frac{V_{dc1}}{I_{dc1}}. \tag{5.21}$$

Similarly it can be derived that

$$R_{dc2} = \frac{V_{dc2}}{I_{dc2}}. \tag{5.22}$$

Dividing Equation 5.18 by 5.19 we get

$$\frac{V_{dc2}}{I_{dc2}} = \frac{1}{(1-D)^2}\frac{V_{dc1}}{I_{dc1}}. \tag{5.23}$$

The above equation can also be written as

$$R_{dc1} = (1-D)^2 R_L. \tag{5.24}$$

From Equations 5.17 and 5.24 it can be deduced that

$$R_g = \frac{\pi^2}{18}(1-D)^2 R_L. \tag{5.25}$$

From Equations 5.5, 5.10 and 5.25 the output power of the generator can be deduced as

$$P_g = \frac{\pi^2}{6}(1-D)^2 R_L \frac{(k\phi\omega_g)^2}{[\frac{\pi^2}{18}(1-D)^2 R_L + R_a]^2 + X_g^2}. \tag{5.26}$$

As shown in Equation 5.26 the output power of the PMSG is dependent on the generator speed ω_g and the duty ratio D. There exists one duty ratio, D_{max}, for which the electrical power generated by the PMSG becomes maximum. This is obtained by

$$\frac{dP_g}{dD} = 0, \tag{5.27}$$

From the above equation D_{max} is derived as

$$D_{max} = 1 - \left[\frac{R_a^2 + X_s^2}{R_L^2}\right]^{\frac{1}{4}} \frac{3\sqrt{2}}{\pi}. \tag{5.28}$$

5.3.5 DC Link Voltage as a Function of Wind Speed and Load

From Equations 5.5, 5.13 and 5.18, the DC link voltage V_{dc2} can be deduced as

$$\begin{aligned} V_{dc2} &= \frac{1}{1-D}\frac{3\sqrt{6}}{\pi}V_g \ and \\ &= \frac{1}{1-D}\frac{3\sqrt{6}}{\pi}k\phi\Omega. \end{aligned} \tag{5.29}$$

Substituting the expression for D_{max} in Equation 5.29 results in

$$V_{dc2} = \sqrt{3}k\phi\Omega \left[\frac{R_L^2}{R_a^2 + X_s^2} \right]^{\frac{1}{4}}. \tag{5.30}$$

And from Equation 5.2 we get

$$\Omega = \frac{\lambda V_W}{R}. \tag{5.31}$$

Substituting Equation 5.31 in Equation 5.30 gives

$$V_{dc2} = \frac{\sqrt{3}k\phi\lambda}{R} \left[\frac{R_L^2}{R_a^2 + X_s^2} \right]^{\frac{1}{4}} V_{wind}. \tag{5.32}$$

From Equation 5.32, it is clear that the fluctuations in wind speed and the load resistance cause variations in the DC link voltage.

5.4 Control Strategy and Modes of Operation

A fast and reliable scheme for acknowledging the system operation status is essential for WPCF (wind powered charging facility). Apart from using as a communication means, DC link voltage is a good indicator of the operational status of WPCF. In a grid-connected WPCF shown in Figure 5.2, the charging power of the DC capacitor is given by

$$P_C = P_{DC} - P_{AC}, \tag{5.33}$$

where P_{DC} and P_{AC} represent the total power on the DC side and the AC side of the DC bus. Since a WPCF consists of source (wind turbine) and loads (PHEVs) which are stochastic in nature, a decrease/increase in voltage amplitude occurs due to the resultant transients generated by the variation in source or PHEV load demand. The DC voltage dynamics can be formulated based on the principle of power balance as

$$\frac{d}{dt}(\frac{1}{2}CV_{DC}^2) = P_{DC} - P_{AC}. \tag{5.34}$$

Therefore,

$$CV_{DC}\frac{d_{V_{DC}}}{dt} = P_{wind} + P_{ESU} - P_{PHEV} - P_{Grid}, \tag{5.35}$$

where P_{Wind} is the power generated by the wind turbine, P_{ESU} is the power delivered or absorbed by the energy storage unit, P_{PHEV} represents the demand of the PHEVs and P_{Grid} is the power on the grid side. According to the above equation a change in P_{Wind} or P_{PHEV} results in a variation in the DC link voltage. This change in the DC link voltage level is utilized to recognize different operating modes according to the voltage levels defined in Section 5.5. The direction of power flow in the charging facility is based on the pre-defined DC link voltage levels which determine the various modes of operation. The switching between various modes of operation is facilitated by the change in the voltage level at the DC link.

Figure 5.7 shows the variation in the DC link voltage and the power from the wind turbine for various values of wind speed. The reference DC link voltages are chosen by taking into consideration the variation in wind speed within the cut-in and cut-out values. The voltage variation between neighboring thresholds should be carefully selected so that it's neither too small to avoid malfunction during mode switching nor too big to avoid significant voltage variations which may affect the charging of PHEVs [41,42,44]. The nominal DC link voltage, V_{dc}, is chosen as 400 V following the criterion mentioned in Chapter 3. By considering a threshold limit of $\pm$ 10% the reference DC link voltage levels are set at V_{S-1} = 360 V and V_{S-1} = 400 V.

5.4.1 System Operating Modes

For the satisfactory operation of the WPCF during the variations of wind generation, load, and grid-connection conditions, there are a number of differ-

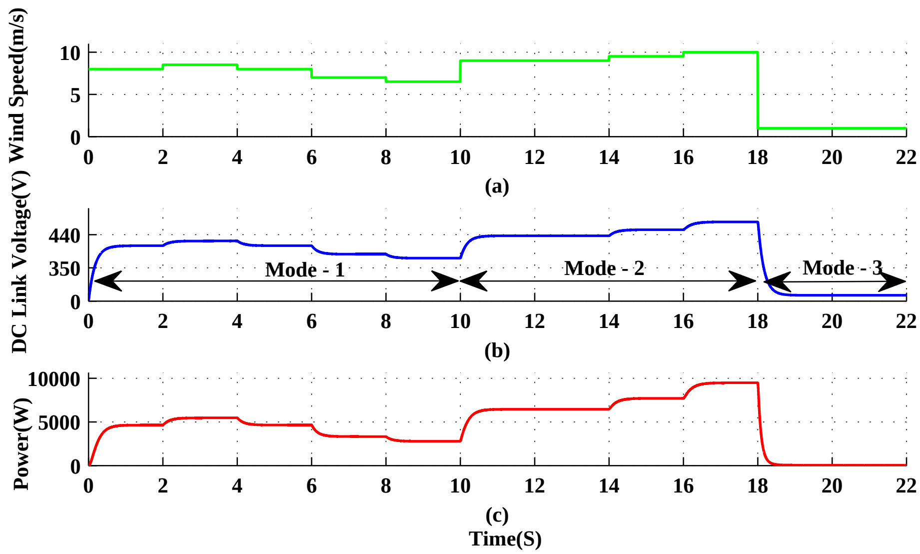

Figure 5.7: Power generated Vs DC link voltage at various wind speeds.

ent operation modes that need to be considered in order to ensure a secure and reliable operation of the charging facility.

Accordingly, the operation of the charging station can be categorized into three modes: Mode-1 (Wind powered charging with grid-connection), Mode-2 (grid-connected inversion) and Mode-3 (grid-connected rectification). A set of variables $V_{DC-link}$, V_{dc}, V_{S-1}, V_{S-2}, I_{DMD} and $I_{DMD-max}$ are used to describe the various modes of operation.

$V_{DC-link}$ is the detected voltage at the DC link. V_{dc} is the nominal DC link voltage.

V_{S-1} and V_{S-2} are the chosen reference voltage levels based on the allowable DC link voltage variation.

I_{DMD} represents the load demand on the distribution transformer and $I_{DMD-max}$ represents the peak load condition of the transformer.

The charging of the PHEV and the ESU should be terminated once the respective battery voltages reach the threshold levels. The following three modes are envisaged.

Mode-1 : $V_{S-1} < V_{DC-link} < V_{S-2}$ ***: Wind powered charging with grid-connection***

When the DC link voltage varies between the allowable voltage band ($V_{S-1} - V_{S-2}$) several scenarios are possible as mentioned below.

Case-1 : $V_{DC-link} < V_{dc}$ ***: Wind powered charging with grid-connected rectification***

This case corresponds to the situation when the power supplied by the wind turbine is not sufficient to meet the PHEV load demand. Hence the DC link voltage drops below the reference voltage level V_{dc}. Two possible scenarios can be considered i.e., a reduction in wind power (P_{Wind}) or an increase in PHEV load demand (P_{PHEV}). One such scenario is showed in Figure 5.8 (a) where the available maximum power from the wind turbine is less than the PHEV load demand. The deficit power within the charging facility is balanced by the grid-side voltage source converter (G-VSC). Neglecting the power losses,

$$P_{Grid} = P_{PHEV} - P_{Wind} - P_{ESU}. \tag{5.36}$$

During the peak load period when the demand on the distribution transformer exceeds the threshold limits ($I_{DMD} > I_{DMDMAX}$), the rate of charging of the PHEVs in the lower priority level is reduced or their charging is terminated temporarily which in-turn reduces the power demanded by the charging facility from the grid. If the peak load condition still persists then the G-VSC is disconnected which completely deactivates the power flow from the grid to the charging facility. During this scenario the ESU switches its control from stand-by mode to discharging mode and supplies the supplementary power to charge the PHEVs in the higher priority level. The required power from the ESU is

$$P_{ESU} = P_{PHEV} - P_{Wind}. \tag{5.37}$$

Once the demand on the distribution transformer is reduced, the G-VSC is turned on to charge the PHEVs.

Case-2 : $V_{DC-link} > V_{dc}$ ***: Wind powered charging with grid-connected inversion***

The DC link voltage exceeds the reference voltage level V_{dc} when there is an increase in the generated wind power (P_{Wind}) or a decrease in the PHEV load demand (P_{PHEV}). Figure 5.8 (b) shows this case in which the available maximum power of the wind turbine is greater than the PHEV demand. The surplus power from the wind turbine is utilized to charge the ESU if its state-of-the-charge (SOC) is less than the threshold limit (SOC_{Max} = 90%). Once the ESU is completely charged the additional power generated by the wind turbine is delivered to the grid via the G-VSC. Neglecting the power losses the power delivered to the grid is represented as,

$$P_{Grid} = P_{Wind} - P_{PHEV} - P_{ESU}. \tag{5.38}$$

Mode-2 : $V_{DC-link} > V_{S-3}$ ***: Grid-connected inversion***

The DC link voltage increases significantly when all the PHEVs are completely charged (light load condition) or when there is a sudden increase in wind speed. In this mode the power generated by the wind turbine charges the ESU and the excess power is delivered to the grid as shown in Figure 5.8 (c) . Assuming all the PHEVs in the charging facility have been completely charged the power delivered to the grid is represented as,

$$P_{Grid} = P_{Wind} - P_{ESU}. \tag{5.39}$$

During this operation of the charging facility in grid-connected mode the DC link voltage is maintained constant at the reference voltage level V_{dc}. Once the PHEVs enter the charging facility and the charging process is initiated, the power delivered to the grid decreases. If a point is reached wherein the wind power is not able to meet the PHEV load demand, the G-VSC control shifts the inversion operation to grid-rectification.

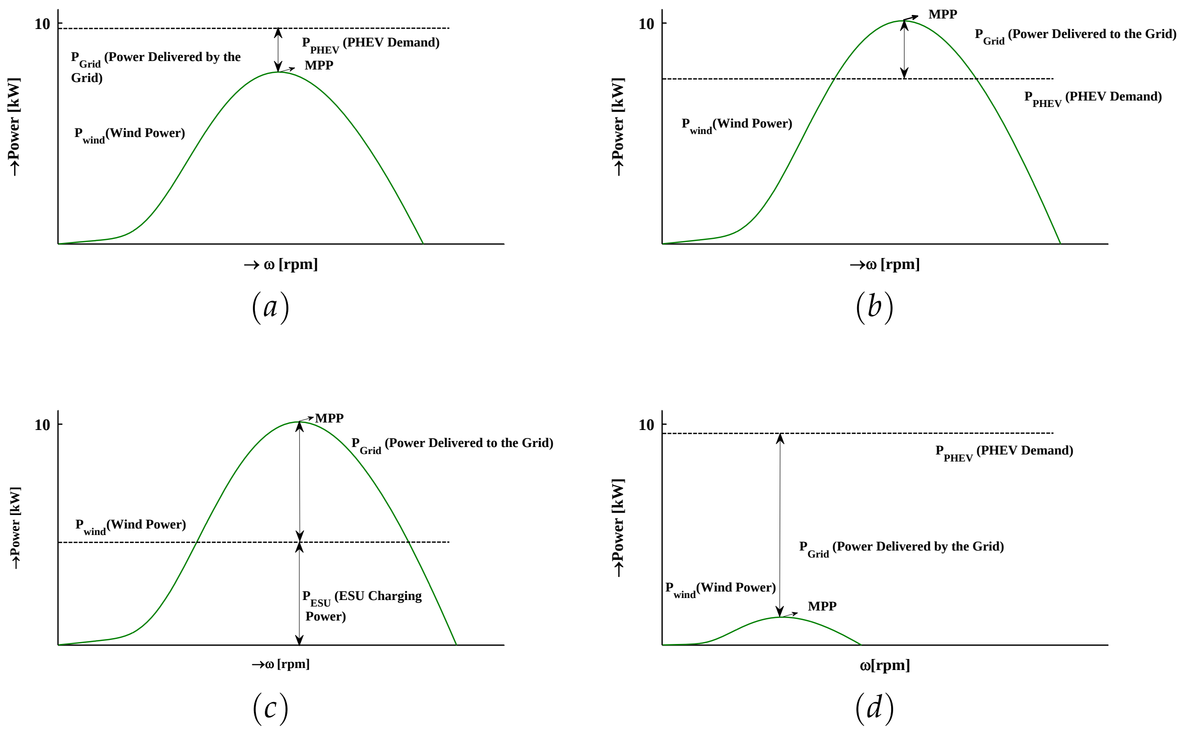

Figure 5.8: Wind power and PHEV load demand during various modes.

Mode-3 : $V_{DC-link} < V_{S-1}$ ***: Grid-connected rectification***

This mode represents extreme conditions such as low wind speeds or very high PHEV load demand. Hence the power demanded by the WPCF from the grid increases appreciably as shown in Figure 5.8 (d). If the grid-side voltage source converter (G-VSC) is not able to provide the required power exchange, the energy storage unit (ESU) switches its control from stand-by mode to discharging mode. An increase in the load demand (PHEV and other utility load) on the distribution transformer ($I_{DMD} > I_{DMD-MAX}$) during the peak load period requires the charging rates of the PHEVs to be lowered or G-VSC to be disconnected. This reduces/deactivates the power flow from the grid to the PHEV in order to satisfy the utility peak load. It should be noted that the distribution transformers are not designed to meet the future PHEV demand and their priority is to satisfy the utility peak load. During this period (which might last for few hours), the ESU is the only source to supply power to the PHEVs. The required power from the ESU is

$$P_{ESU} = P_{PHEV} - P_{Wind}. \tag{5.40}$$

However, during the conditions of low wind (thus small P_{wind}) and heavy PHEV demand, the required P_{ESU} may exceed the power ratings of the battery ES (energy storage) system. Thus, appropriate load shedding is carried out by temporarily terminating the charging of PHEVs at lower priority level. Once the demand on the distribution transformer is reduced, the grid-connected converter is turned on to charge the PHEVs.

5.4.2 System Control

This section outlines the detailed system controls for the three different operation modes previously described.

A) Control Method for DC/DC Bi-Directional Buck-Boost Converter

In the proposed charging facility architecture, the ESU is connected by a bi-directional Buck-Boost converter to the DC bus as shown in Figure 5.2. Under different operating conditions of the WPCF, the ESU operates in charging, discharging or floating modes and the modes are managed according to the DC bus voltage level and the load demand on the distribution transformer. If the battery has not been fully charged, which means that its SOC is less than 95%, the battery will be charged in Mode-1 and Mode-2.

Considering the aforementioned conditions, the control method for the ESU converter is summarized in Figure 5.9. In the Figure, V_{ESU} is the detected battery voltage of the ESU, V_{ESU-H} is the battery voltage corresponding to 95% SOC, V_{ESU-L} is the battery voltage corresponding to 40% SOC, $I_{BC-limit}$ is the maximum current limit for battery charging, $I_{BD-limit}$ is the maximum current limit for battery discharging, I^*_{ESU} is the reference current for the Buck-Boost converter, I_{ESU} is the detected battery current, and D_{ESU1} and D_{ESU2} are the duty ratios for the switches S_{E1} and S_{E2}. As shown in Figure 5.9 the charging/discharging of the ESU is determined by I^*_{ESU}, which is the sum of the charging controller output and discharging controller output

$$I^*_{ESU} = I_{r1} + I_{r2}. \tag{5.41}$$

When I^*_{ESU}>0, the battery converter is used for discharging. when I^*_{ESU}<0, the battery converter is used for charging. Hence, the seamless switching between two modes is realized and the hysterisis is not necessary.

As shown in Figure 5.9, the overcharging protection and overdischarging protection have been taken into account by introducing V_{ESU-H} and V_{ESU-L}.

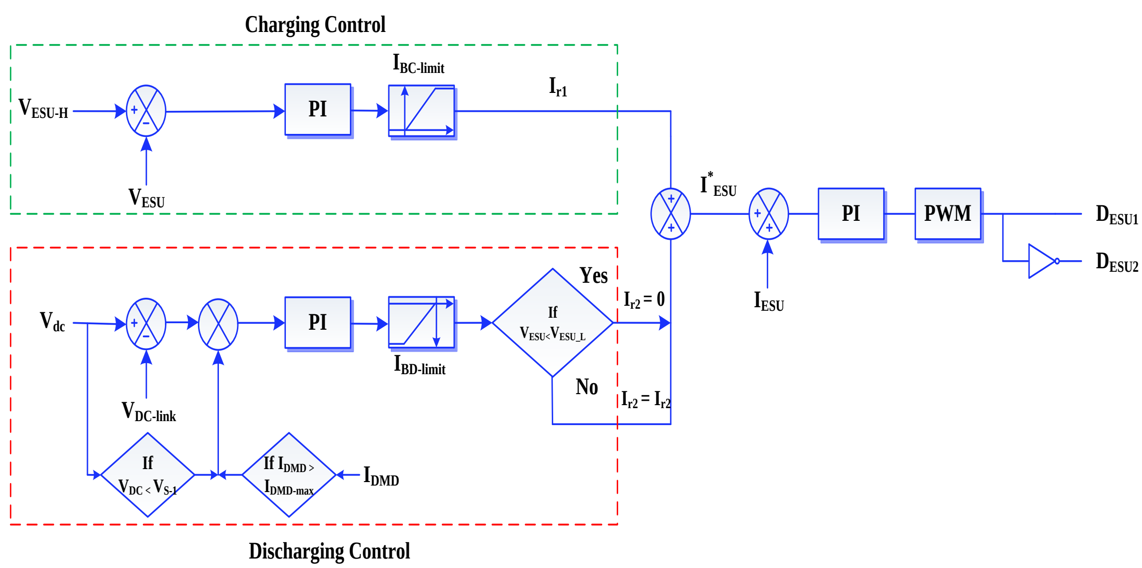

Figure 5.9: Control diagram of DC/DC buck-boost converter.

B) Control Method for DC/DC Buck Converter

The control method for DC/DC buck converter for PHEV charging is based on V_B, V_{BT}, I_{DMD} and $I_{DMD-max}$ as shown in Figure 5.10 . V_B is the detected battery voltage, V_{BT} is the battery voltage corresponding to 95% SOC. I_{DMD} is the load on the distribution transformer and $I_{DMD-max}$ represents the peak load condition. The control mode is determined by the detected battery voltage of the PHEV and the loading condition of the distribution transformer. The charging of the PHEV is terminated once the battery voltage reaches V_{BT}.

As mentioned in Section 5.4.1 during the period when the transformer is subjected to peak load demand the rate of charging of the PHEVs is reduced until the demand is within the allowable limits (i.e., $< I_{DMD-max}$). This is accomplished by classifying the PHEVs in the charging facility in a priority order. Each PHEV is assigned a priority level based on its duration of stay in the charging facility. The power demanded by a PHEV is calculated from the departure time, arrival time, initial SOC and battery capacity of the PHEV. This data is entered by the customers via a HMI port when they arrive at the parking lot. Assuming that each PHEV will be charged from its initial SOC when it arrives at the WPCF to the maximum SOC (95%), the power demanded by the nth PHEV ($P_{PHEV,n}$) is calculated as

$$P_{PHEV,n} = \frac{BC \times (SOC_U - SOC)}{D_t - A_t} \; and \tag{5.42}$$

$$P_{PHEV} = \sum_{n=1}^{N} P_{PHEV,n}, \tag{5.43}$$

where BC is the battery capacity, SOC_U is the upper limit of the state of charge, SOC is the measured state of charge, D_t is the departure time and A_t is the arrival time and P_{PHEV} is the total power demanded by the PHEVs. Table 5.1 shows the maximum and minimum charging rates for various charging levels based on the power demand. The data entered by the customers for four different PHEVs is shown in Table 5.3 wherein the priority order is assigned for each PHEV based on the duration of stay in the parking lot.

Table 5.1: Charging rate for different charging levels

Charging Level	Power Requirement	Maximum charging rate [kW]	Minimum charging rate [kW]
Level - 1	$P_{PHEV,n} \geq 15$ kW	15	12
Level - 2	$10\text{kW} \leq P_{PHEV,n} < 15\text{kW}$	12	6
Level - 3	$5\text{kW} \leq P_{PHEV,n} < 10\text{kW}$	8	4
Level - 4	$2\text{kW} \leq P_{PHEV,n} < 5\text{kW}$	6	2

During the peak demand period the rate of charge is reduced in steps of 0.1 kW for the PHEV which is last in the priority order. If the rate of charge of the current PHEV becomes zero then the process is repeated for the PHEV whcih is next in the priority order. This process continues iteratively until the demand on the transformer is within the allowable limits (i.e., $< I_{DMD-max}$). The flowchart for the iterative process is shown in Figure 5.11. As shown in the figure, the updated reference charging current is obtained in the final step and it is updated in the control loop of buck converter.

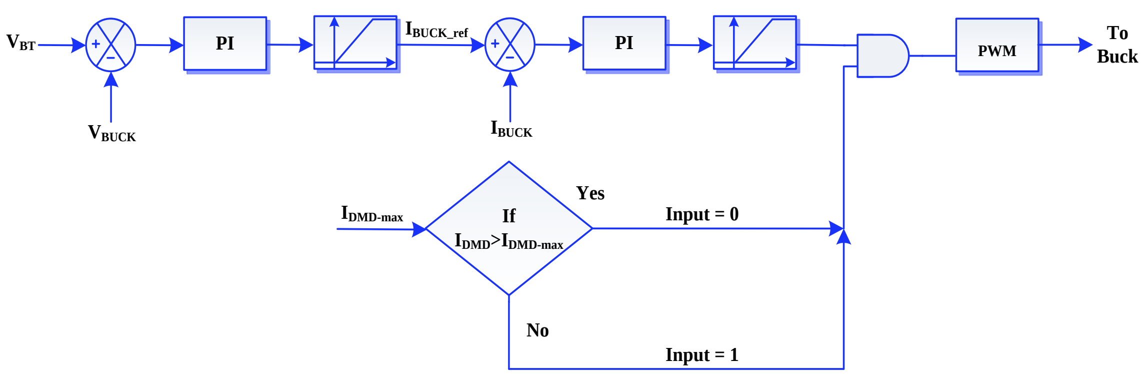

Figure 5.10: Control diagram of DC/DC buck converter.

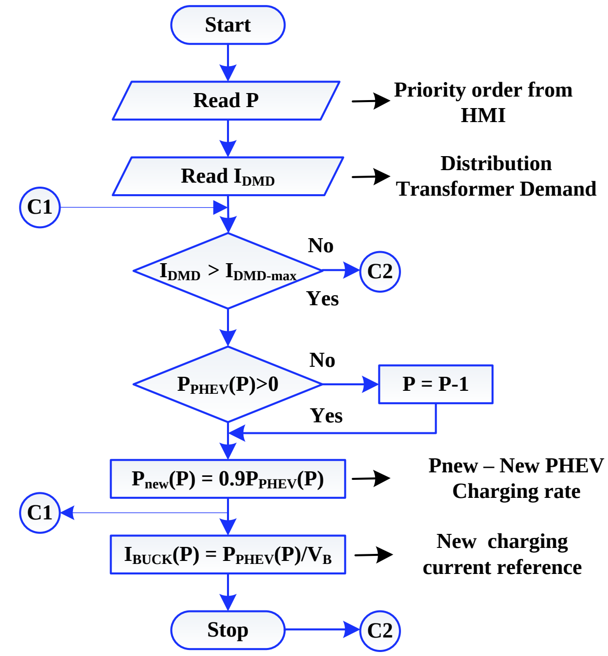

Figure 5.11: Flowchart for PHEV charging control.

B) DC/DC Boost Converter Control

The main aim of variable speed wind energy conversion system is to extract maximum power at all available wind velocities. In a variable speed WECS, the maximum power at different wind velocities is almost a cubic function of generator speed as shown in Figure 5.3. Therefore the generator speed is controlled in order to follow the Power-speed characteristic.

In this regard, the duty cycle of the DC/DC boost converter is generated based on the control scheme shown in Figure 5.12. The outer loop compares the actual wind power P_{Wind} with the reference of the optimum power $(P_{Wind})_{Opt}$ which is obtained as

$$(P_{Wind})_{Opt} = k_{opt}[\Omega_{opt}]^3. \tag{5.44}$$

The above equation is used to estimate the reference DC current (i.e., $(i_{DC})_{ref}$) through inductor of the boost converter. The PI controllers associated with the control scheme shown in Figure 5.12 are tuned using the method discussed in [90].

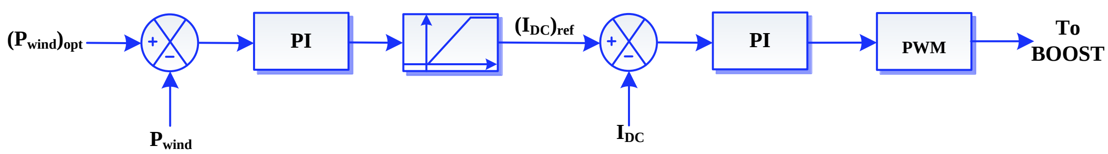

Figure 5.12: Control diagram of DC/DC boost converter.

B) DC/AC G-VSC Control

The control method for grid-connected DC/AC converter is shown in Figure 5.13. This stage uses two nested control loops - an outer voltage loop and an inner current loop. In Figure 5.13, V_{dc} is the reference voltage for the DC bus, $V_{DC-link}$ is the detected DC bus voltage, V_{Grid} is the AC grid voltage, θ is the AC grid phase angle, I_{INV}^* is the reference output current for the DC/AC converter, I_{fdbk} is the output current of the DC/AC converter.

Two Proportional-Integrative (PI) controllers, $G_V(S)$ and $G_i(S)$ are used to close the outer voltage loop and the inner current loop. The voltage loop generates the reference command (I_{Ref}) for the current loop. The current command is then multiplied by the AC angle to get the instantaneous current reference (I_{INV}^*). Since the inverter is grid-connected the grid angle is provided by the phase locked loop (PLL). The instantaneous current reference is then used by the current compensator along with the output current of the DC/AC converter (I_{fdbk}) to provide duty cycle for the full bridge inverter.

The operation of the DC/AC converter in rectifier Mode/inverter Mode during Mode-1 depends on the sign of (I_{Ref}). When the PHEV load demand (P_{PHEV}) exceeds the wind power (P_{Wind}) the deficit power must be supplied by the grid. Hence I_{ref} changes its sign and thereby (I_{fdbk}) flows in the opposite direction i.e., into the charging facility. Similarly when P_{wind} exceeds P_{PHEV} and V_{ESU} is greater than V_{ESU-H} (implies that the ESU is completely charged), I_{fdbk} changes its sign to deliver power to the grid.

The transition from Mode-1 to Mode-2 or Mode-1 to Mode-3 is facilitated by the variation in DC link voltage level. When $V_{DC-link}$ falls below V_{S-1} the sign of I_{Ref} changes immediately such that I_{fdbk} flows towards the charging facility. On the other hand I_{fdbk} flows towards the grid when $V_{DC-link}$ exceeds V_{S-2}.

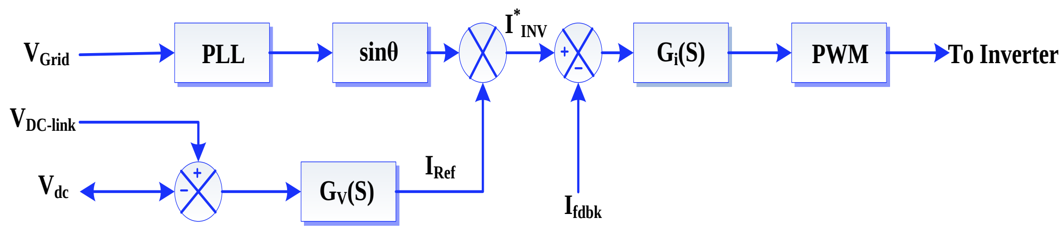

Figure 5.13: Control diagram of DC/AC converter.

5.5 Case Studies

In order to validate the proposed control algorithm for the wind powered smart charging facility, system simulations have been carried out using the SimPowerSystems toolbox of MATLAB/SIMULINK. The detailed ratings of the system elements are listed in Table 5.2. As mentioned in the table, the wind turbine is rated at 10 kW. A 10 kW grid-connected voltage source converter (G-VSC) and a 5 kW Energy Storage Unit (ESU) are used. The initial SOC of the ESU is considered as 90 % and the minimum SOC is fixed at 20 %. The developed smart charging facility is a small parking garage in a workplace, possibly a university campus, which contains four parking spaces. The connection and disconnection time and the initial and final SOC of PHEVs is represented in Table 5.3.

The DC-link reference voltage (V_{dc}) is set at 400 V. In the case of a DC microgrid system such as the architecture of the charging facility described in this chapter, a DC voltage tolerance of $\pm$ 10% is generally allowed. Considering that the PHEV batteries employ front end DC/DC buck converters, from the control

Table 5.2: Ratings of the simulation system

DC link	Nominal Voltage	400 V
Wind Turbine	Power Rating	10 kW, PMSG
GS-VSC	Power Rating	10 kW
Transformer	Nominal Voltage	0.208/0.460 kV (L-L)
	Power Rating	15 kVA
ESU	Nominal Voltage	100 V
	Battery Capacity	50 Ah, Lithium-ion type
DC/DC Converters	Boost Converter	f = 100 kHz, L = 7 mH, c = 0.8 mF
	Buck Converter	f = 100 kHz, L = 5.375 mH, C = 20 μF

point of view, the variations in the DC bus voltage can be viewed as the input voltage disturbance for the front end converters. Therefore, voltage variations in the specified range ($\pm$ 10%) can be acceptable for the PHEV batteries. Based on this, V_{S-1} and V_{S-2} are configured at 360 V (10% below V_{dc}) and 440 V (10% above V_{dc}) respectively. The switching frequencies for all of the DC/DC converters is 100 kHz while the switching frequency of G-VSC is 10kHz. The threshold value of the demand on the distribution transformer is set at 41.5 A. A 100 V/50 Ah battery is modeled by using the state of charge according to the following equations [91]:

$$E = E_0 - k\frac{Q}{Q - \int idt} + Ae^{-B.\int idt} \; and \tag{5.45}$$

$$V = E - R.i, \tag{5.46}$$

where E_0, E, and V are the battery constant voltage, no-load voltage, and terminal voltage respectively. Q is the battery capacity, I is the battery current, and R is the battery internal resistance. K, A and B are the polarization voltage, exponential zone amplitude, and inverse time constant, respectively.

During the simulation, the charging and discharging rate of the battery are set at 1200 times the actual rate (the time constant in the integral term of $\int idt$ is set at 3 s instead of the actual value of 1 hr, that is, 3600 s) in order to simulate the conditions of high/low battery capacity.

Table 5.3: PHEV charging profile

Priority Order	PHEV Model	Battery Capacity	Initial SOC	Final SOC	Duration of Stay	PHEV Load Demand
1	Toyota Prius	4.4 kWh	0%	100%	1 hr	4.4 kW
4	Nissan Leaf	24 kWh	40%	90%	6 hr	2 kW
3	Tesla Model S	85 kWh	50%	90%	5 hr	6.8 kW
2	Chevy Volt	16 kWh	20%	90%	4 hr	2.8 kW

Simulation studies are carried out in accordance with the various operation conditions and control modes previously outlined, that is:

Case 1) The WPCF is connected to an external AC grid with normal wind and load variations;

Case 2) The charging rate of the low priority PHEVs is reduced temporarily during the peak demand period;

Case 3) During very low wind speeds and high peak load demand, the ESU is required to charge the PHEVs;

Case 4) The worst case scenario wherein the ESU is completely discharged during the peak load period. In this case few PHEVs are not completely charged.

5.5.1 Case 1

Figure 5.15. shows the simulation results for Case 1, and Table 5.4 lists the main operation events. At time t = 0 s, PHEV-1 enters the charging facility and

starts charging with a load demand of 4.4 kW as shown in Figure 5.15 (c). The wind speed is 7.2 m/s and the wind turbine generates approximately 5 kW as shown in Figure 5.15 (a) and (b) respectively. Since the system is grid-connected the DC bus voltage is controlled by the G-VSC at the reference voltage level of 400 V as shown in Figure 5.15 (d). From Figure 5.15. and Table 5.4, the following events can be observed:

Table 5.4: Main operation events for Case 1

Events	Operation Condition	Time (S)
1	PHEV-1 starts charging	0
2	PHEV-2 starts charging	1.5
3	PHEV-1 leaves the facility and PHEV-3 starts charging	3
4	Wind Speed increases from 7.2 m/s to 8.6 m/s	3.5
5	PHEV-4 starts charging	4
6	PHEV-4 leaves the parking lot and the wind speed reduces to 8.2 m/s	16
7	PHEV-3 leaves the charging facility	18
8	Wind speed reduces to 7.7 m/s	19
9	PHEV-2 leaves the charging facility	19.5

Event 1 : PHEV-1 starts charging.

Event 2 : PHEV-2 starts charging. DC link voltage reduces momentarily due to the increase in PHEV load demand. As shown in Figure 5.15 (f) the supplementary power flows from the grid to the charging facility.

Event 3, 4, 5 : Events 3, 4 and 5 represent the variation in PHEV load demand and the wind speed. At t = 3.5 s the wind speed increases from 7.2 m/s to 8.6 m/s which results in a momentary increase in DC link voltage. Since $P_{PHEV} > P_{Wind}$ power continues to flow from the grid to the charging facility.

Event 6, 7 : PHEV-4 and PHEV-3 are completely charged and they leave the charging facility. Due to the decrease in PHEV load demand there is a momentary increase in DC link voltage as shown in Figure 5.15 (d).

Event 8, 9 : At t = 19 s wind speed reduces to 7.7 m/s. PHEV-2 is completely charged at t = 19.5 s. The DC link voltage momentarily increases to a very high value due to the negligible load demand. The charging facility now operates in Mode-2 and represents a grid-connected wind energy system. From Event 1 to Event 8 the variation in DC link voltage is within the threshold limits i.e., 360 V $< V_{DC-link} <$ 440 V and therefore the operation of the charging facility is in Mode-1.

5.5.2 Case 2

The operation of the charging facility during the peak load period is studied in this case and Figure 5.16 and Table 5.5 show the simulation results and the main operation events, respectively. At time t = 0 s, PHEV-1 starts charging with a load demand of 4.4 kW as shown in Figure 5.16 (c). The wind speed is 7.2 m/s and the wind turbine generates approximately 5 kW as shown in Figure 5.16 (a) and (b) respectively. The surplus power generated by the wind turbine (0.6 kW) is delivered to the grid by the G-VSC as shown in Figure 5.16 (g). During the peak demand period, the charging of the PHEV with the lowest priority order is terminated first followed by the PHEV in the next priority order. The priority order of the PHEVs is described in Table 5.3 and the associated control strategy has been described in Section 4.4.2. According to Figure 5.16 and Table 5.5, the following events can be observed.

Events 1 to 5 : Events 1 to 5 represent the variation in PHEV load demand and wind speed. As shown in Figure 5.16 (d) the variation in the load and wind speed causes momentary change in the DC link voltage. Initiation of PHEV charging during events 2, 3 and 5 results in a dip in DC link voltage (due to the increase in PHEV load demand). The control on the G-VSC detects the dip in DC link voltage and increases the power flow from the grid to the charging facility and therefore maintains the DC link voltage level at the reference value of 400 V.

Events 6, 7 : At time t = 7 s the load demand on the distribution transformer

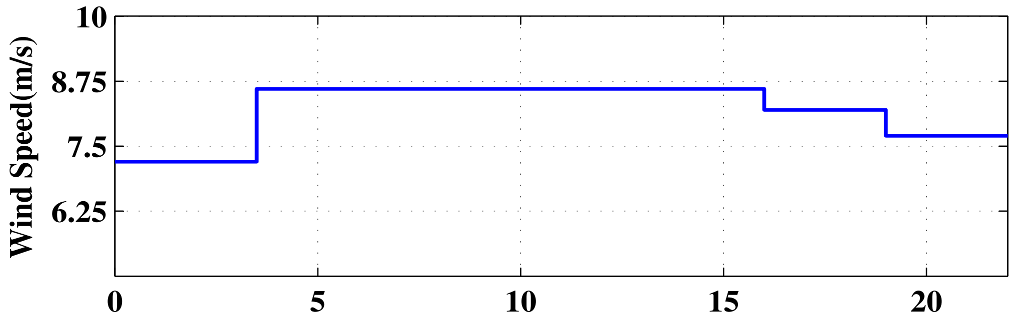
Wind Speed(m/s)
10
8.75
7.5
6.25
0
5
10
15
20

(a)

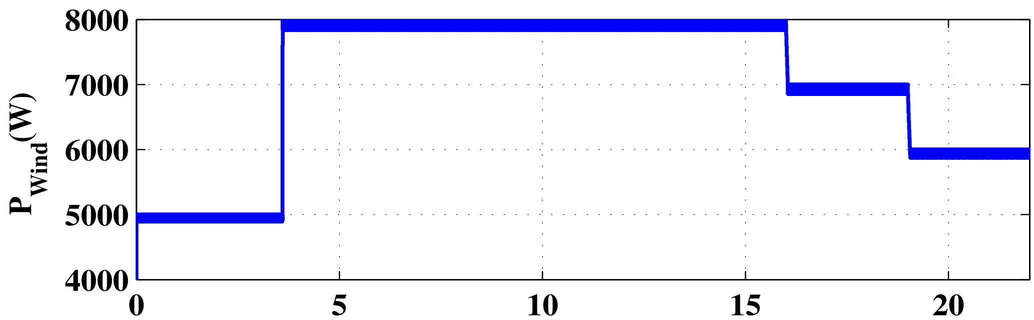
P_{Wind}(W)
8000
7000
6000
5000
4000
0
5
10
15
20

(b)

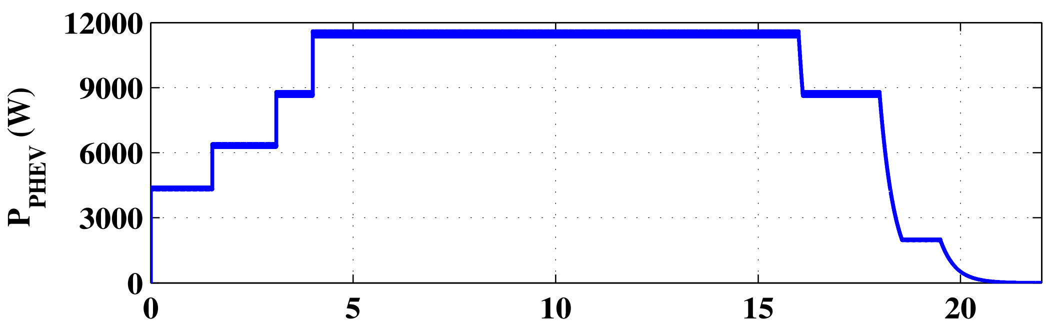
P_{PHEV} (W)
12000
9000
6000
3000
0
0
5
10
15
20

(c)

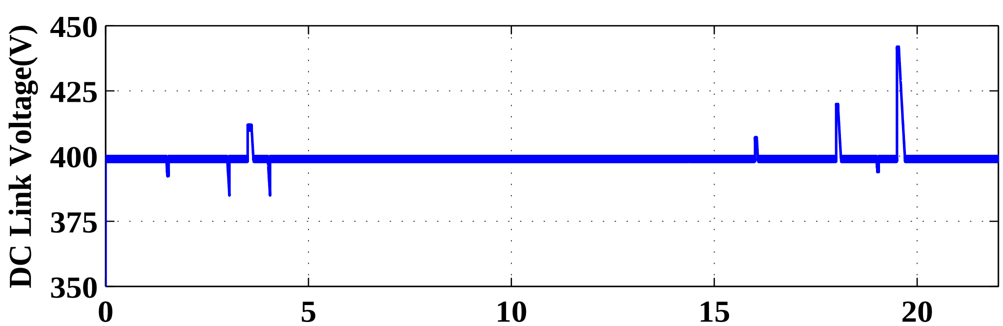
DC Link Voltage(V)
450
425
400
375
350
0
5
10
15
20

(d)

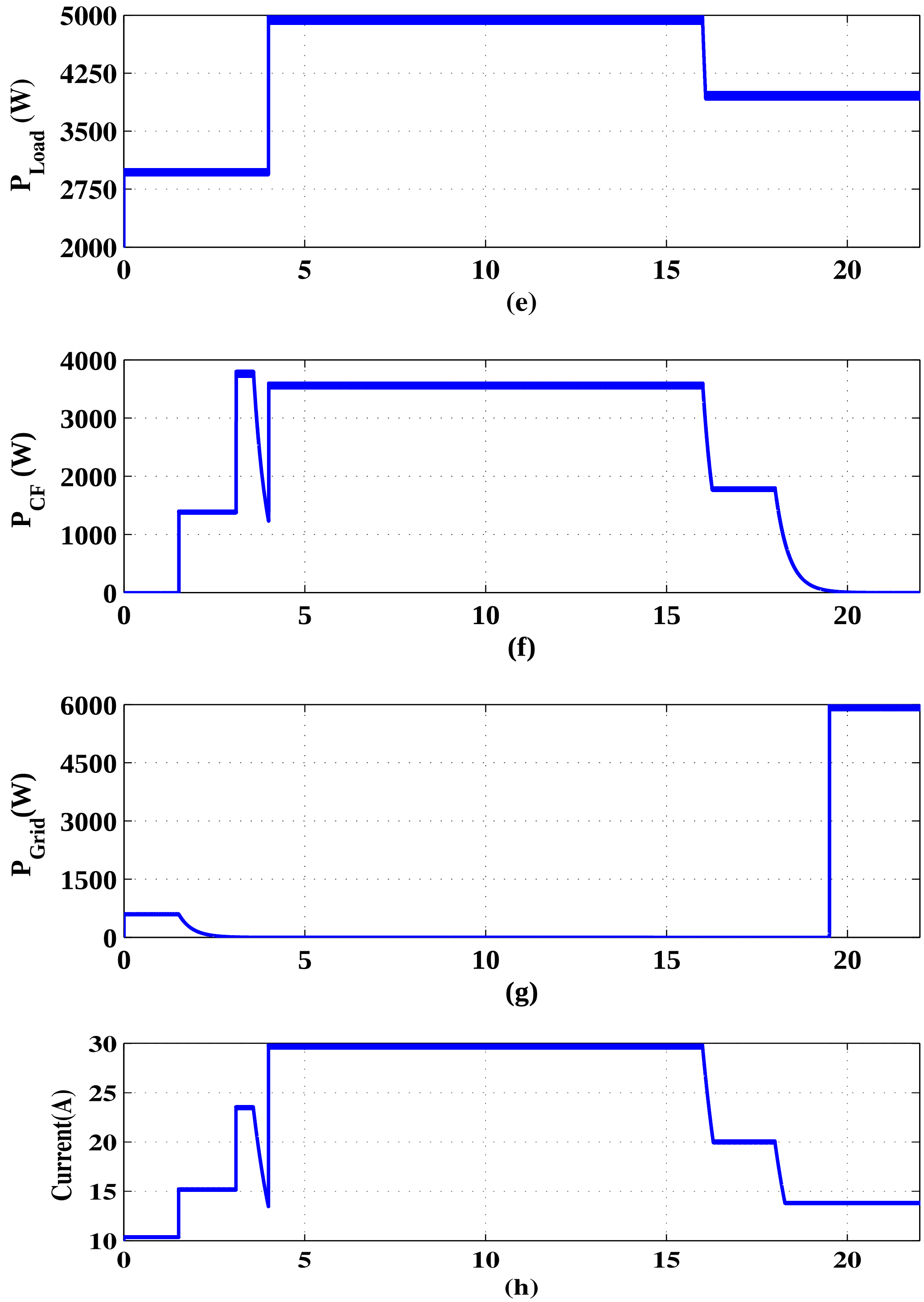

Figure 5.14: WPCF operation during Case 1. (a) Wind speed. (b) wind Power. (c) PHEV load demand. (d) DC link voltage (e) Load demand. (f) Power from the grid to WPCF. (g) Power delivered to the grid. (h) Load current.

exceeds its rating of 15 kVA. It can be seen from Figure I_{DMD} exceeds $I_{DMD-max}$ (41.5 A). In general the distribution transformers are designed to withstand the peak load demand for few seconds before the overload relay trips. In order to reduce the demand on the distribution transformer the rate of charging of the PHEV in the lowest priority order is reduced following the control algorithm described in Section 5.4.2 (B). Accordingly the charging of PHEV-2 which is last in the priority order is terminated temporarily and the rate of charge of PHEV-3 is reduced from 6.8 kW to 5.3 kW. As shown in Figure 5.16 (h) and (c), the controller acts swiftly and the load demand (I_{DMD})falls below the threshold limits ($I_{DMD-max}$) in 0.5 s.

Events 8, 9 & 10 : At t = 16 s it can be seen from Figure 5.16 (e) that there is a drop in the load demand on the distribution transformer. Therefore the charging of the PHEVs which was earlier terminated or rate reduced is now resumed. Since PHEV-3 is at a higher priority order compared to PHEV-2 it is charged ahead of PHEV-2 and in order to meet the departure time its charging is promoted to level-1. Once PHEV-3 is completely charged at t = 18 s PHEV-2 is promoted to level-1 and it gets charged at t = 19.5 s. Since the charging of all the PHEVs has been accomplished the load demand in the charging facility is negligible. Therefore the DC link voltage momentarily increases to a very high value due to the negligible load demand. The charging facility now operates in Mode-2 and represents a grid-connected wind energy system.

5.5.3 Case 3

This case describes the operation and control of the ESU in the charging facility during the periods of low wind speed and high peak load demand. Figure 5.17 and Table 5.6 show the simulation results and the main operation events, respectively. Two PHEVs, Toyota Prius with a load demand of 4.4 kW and Tesla

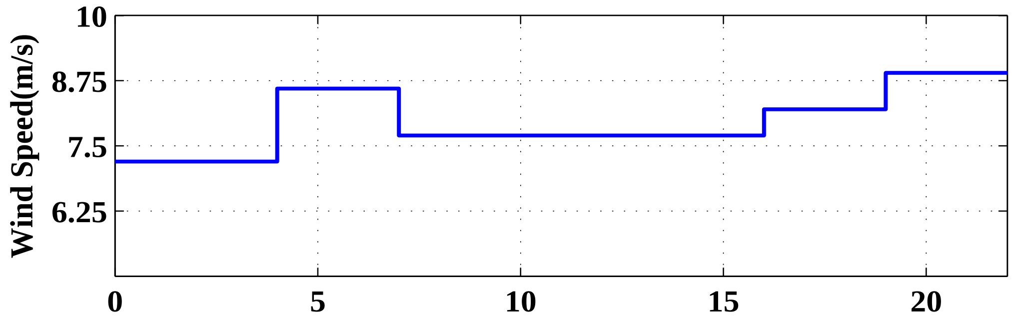
Wind Speed(m/s)
10
8.75
7.5
6.25
0
5
10
15
20

(a)

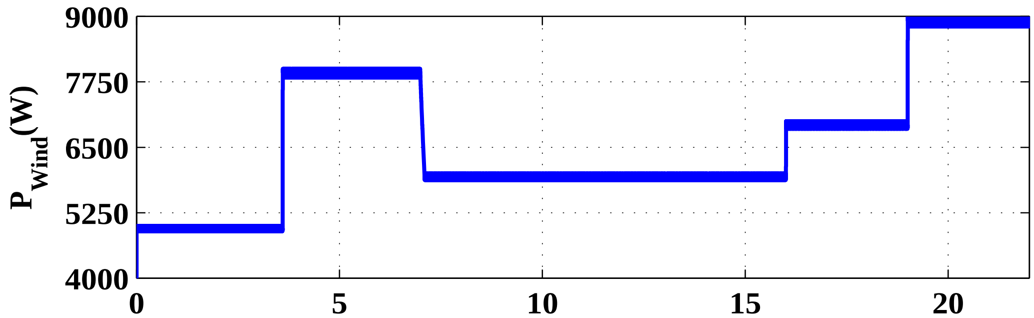
P_{Wind}(W)
9000
7750
6500
5250
4000
0
5
10
15
20

(b)

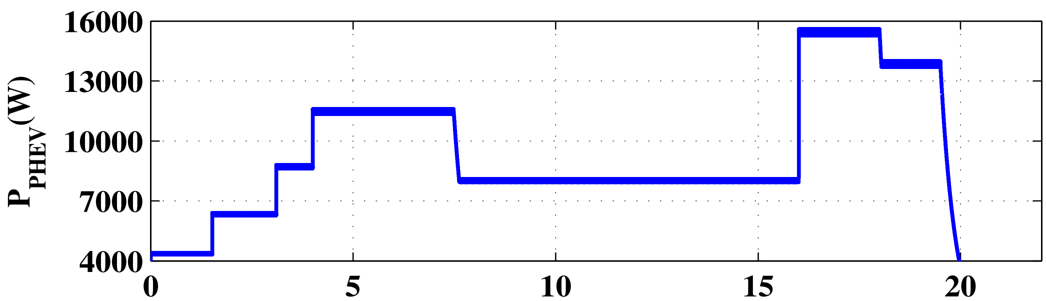
P_{PHEV}(W)
16000
13000
10000
7000
4000
0
5
10
15
20

(c)

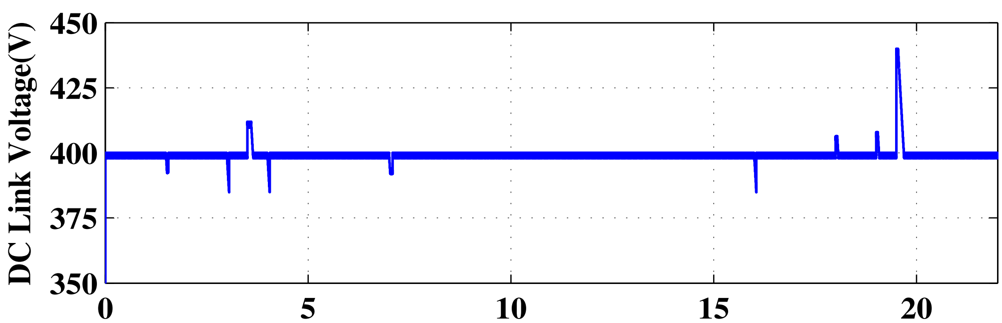
DC Link Voltage(V)
450
425
400
375
350
0
5
10
15
20

(d)

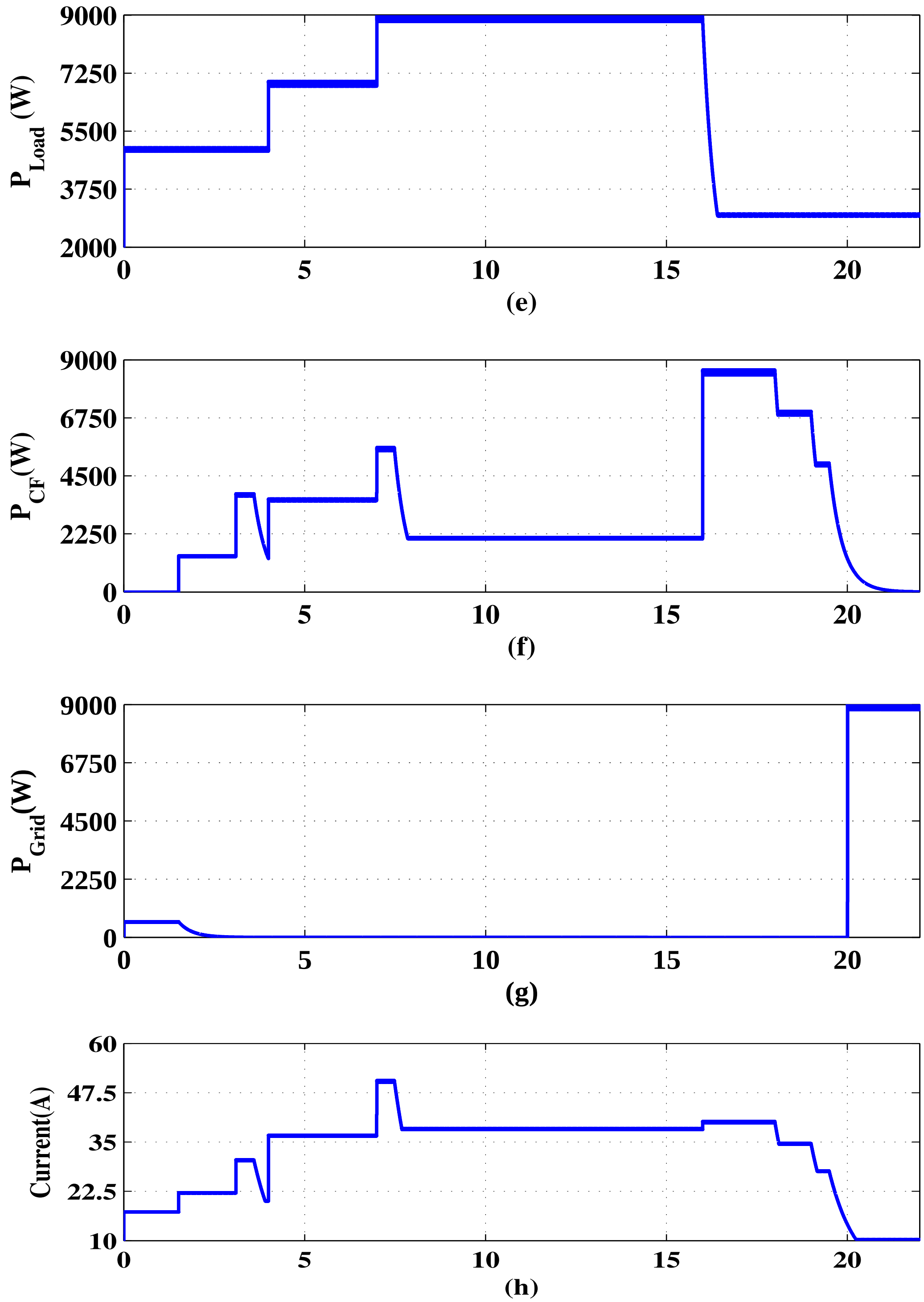

Figure 5.15: WPCF operation during Case 2. (a) Wind speed. (b) Wind power. (c) PHEV load demand. (d) DC link voltage (e) Load demand. (f) Power from the grid to WPCF. (g) Power delivered to the grid. (h) Load current.

Table 5.5: Main operation events for Case 2

Events	Operation Condition	Time (S)
1	PHEV-1 starts charging	0
2	PHEV-2 starts charging	1.5
3	PHEV-1 leaves the facility and PHEV-3 starts charging	3
4	Wind Speed increases from 7.2 m/s to 8.2 m/s	3.5
5	PHEV-4 starts charging	4
6	Load demand on the distribution transformer exceeds I_{Dmax}	7
7	Charging of PHEV-2 is stopped temporarily	7.5
8	PHEV-4 is charged completely. Priority level of PHEV-3 is promoted to level-1	16
9	PHEV-3 leaves the charging facility. Charging priority level of PHEV-2 is shifted to level-1	18
10	PHEV-2 leaves the charging facility	19.5

Model S with a load demand of 6.8 kW are considered. The arrival and departure times of the PHEVs is shown in Table 5.3. In the simulation the ESU starts discharging during the period of high peak load demand. The ESU starts charging once all the PHEVs are completely charged. According to Figure 5.17 and Table 5.6, the following events can be observed.

Table 5.6: Main operation events for Case 3

Events	Operation Condition	Time (S)
1	PHEV-1 starts charging	0
2	PHEV-1 leaves the facility and PHEV-2 starts charging	1.5
3	Wind Speed reduces to zero, load demand exceeds $I_{DMD-max}$	10
4	Charging rate of the PHEV-2 is reduced and ESU starts discharging	10.1
5	Load demand reduces ($I_{DMD} < I_{DMD-max}$)	13
6	PHEV-2 is charged completely. ESU starts charging	16.5
7	ESU is charged completely.	19

Events 1,2 : At time t = 0 s PHEV-1 starts charging. PHEV-2 starts charging at 1.5 s and PHEV-1 gets completely charged.

Event 3,4 : At time t = 10 s the power generated by the wind turbine reduces to zero and the load demand on the distribution transformer also exceeds its limts as shown in Figure 5.17 (a) and (b). This scenario demands the charging of the PHEV to be terminated but the presence of ESU facilitates the charging process without interruption. The ESU switches its control from standby mode to discharging mode in order to supply the PHEV load demand. The WPCF now operates in Mode - 3.

The power that can be delivered by the ESU (P_{ESU}) for a period of 1 hour can be calculated based on Equation 4.42 and the data given in Table 5.2 and it is obtained as 3.5 kW. Since $P_{PHEV} > P_{ESU}$ the rate of charging of PHEV - 2 is reduced until $P_{PHEV} = P_{ESU}$ based on the procedure described in Section 4.4.2 (B). Therefore from t = 10 s - 13 s the ESU acts as a source and its SOC decreases as shown in Figure 5.17 (e). PHEV-2 which was earlier charging in level - 3 now charges at level - 4. The battery capacity required to support the charging of PHEVs can be calculated by estimating the PHEV load demand during the peak load period. This can be done by means of in-dept probabilistic analysis which is beyond the scope of this dissertation.

Event 5 : As shown in Figure 5.17 (b) there is a drop in the load demand and increase in wind turbine power at t = 13 s. The ESU stops discharging and the PHEV load demand is now met by the wind turbine and the grid. The charging rate of PHEV-2 is now promoted to level - 2 as shown in Figure 5.17 (c) so as to charge it completely within the scheduled departure time.

Event 6,7 : At t = 16.5 s PHEV-2 is completely charged and it leaves the charging facility. The ESU which was in discharging mode during the peak load period now starts charging and its SOC increases as shown Figure 5.17 (e). Figure 5.17 (g) shows the charging power of the ESU. At t = 19 s the ESU is completely charged and the WPCF now operates in Mode - 2.

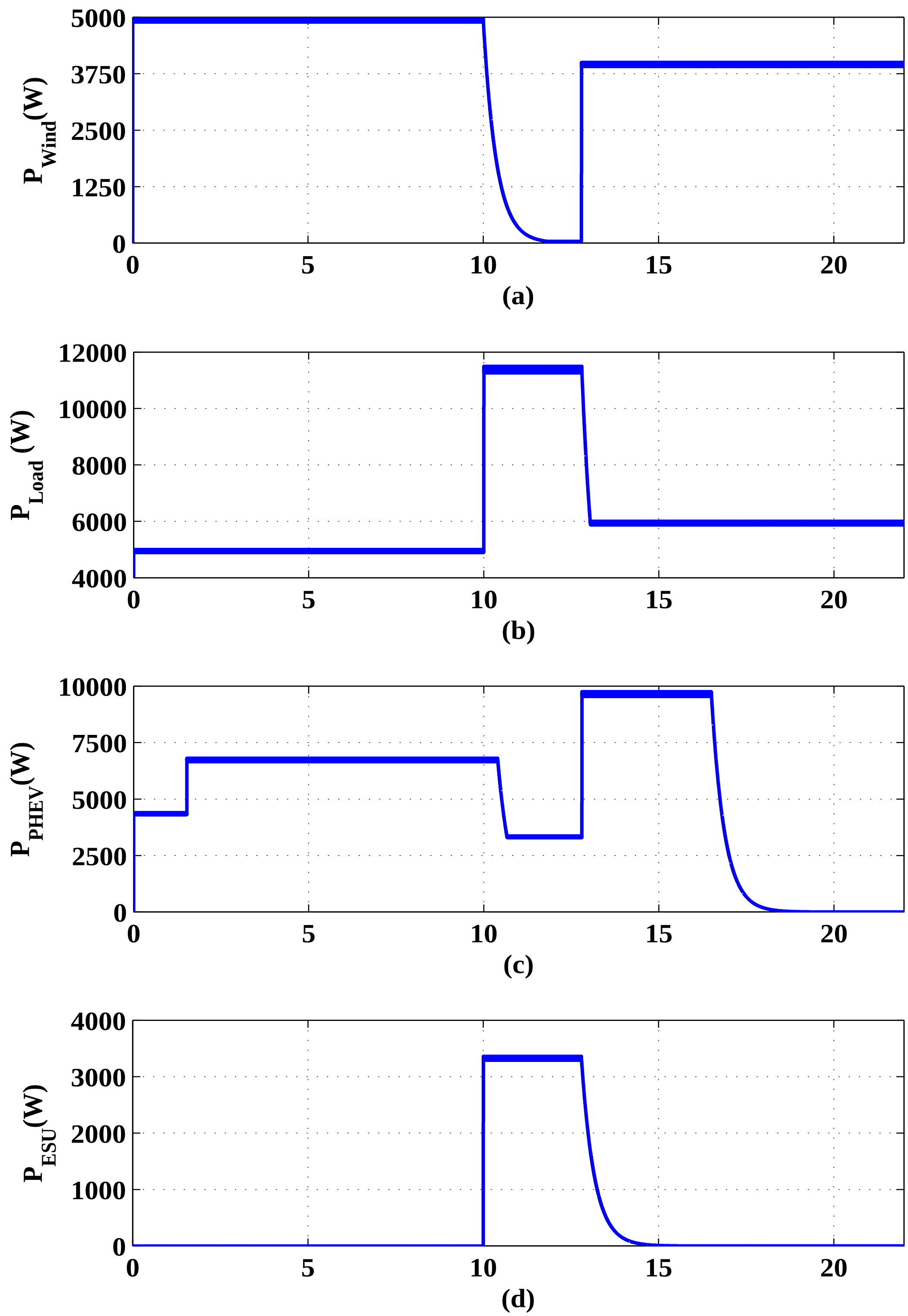

5000
3750
2500
1250
0
$P_{Wind}(W)$
0
5
10
15
20
(a)
12000
10000
8000
6000
4000
P_{Load} (W)
0
5
10
15
20
(b)
10000
7500
5000
2500
0
$P_{PHEV}(W)$
0
5
10
15
20
(c)
4000
3000
2000
1000
0
$P_{ESU}(W)$
0
5
10
15
20
(d)

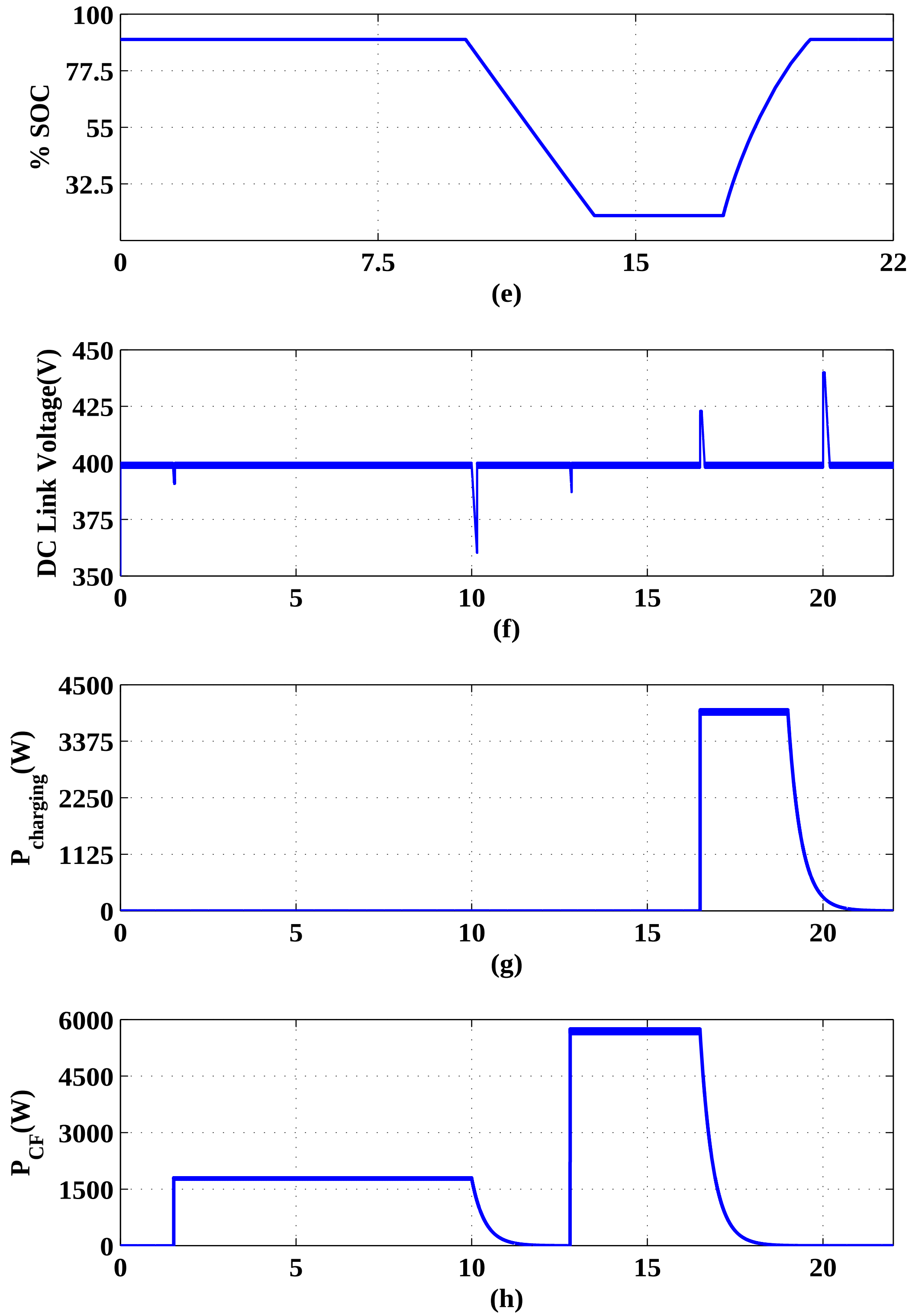

Figure 5.16: WPCF operation during Case 3. (a) Wind power. (b) Load demand. (c) PHEV load demand. (d) Power from the ESU (e) SOC of the ESU. (f) DC link voltage. (g) Charging power of the ESU. (h) Power from the grid to WPCF.

5.5.4 Case 4

This case describes the operation of the charging facility during the worst case scenario wherein the ESU is completely discharged during the peak load period with low wind speed. Figure 5.18 and Table 5.7 show the simulation results and the main operation events, respectively. Two PHEVs, Toyota Prius with a load demand of 4.4 kW and Tesla Model S with a load demand of 6.8 kW are considered. The arrival and departure times of the PHEVs is shown in Table 5.3. In the simulation the ESU is completely discharged during the period of high peak load demand. Hence the charging of the PHEV is temporarily terminated. According to Figure 5.18 and Table 5.6, the following events can be observed.

Events 1 - 4 : Events 1 - 4 are similar to the ones discussed in Case - 3. The ESU starts discharging at t= 10 s as shown in Figures 5.18 (d) and (e) and facilitates the charging of PHEV-2 during the period of peak load demand.

Event 5 : At t = 13 s the ESU is completely discharged and the peak load demand still exists. As shown in Figure 5.18 (e) the SOC of the ESU reduces to 20% at t = 13 s. Since the power generated by the wind turbine is almost negligible the charging of PHEV-2 is temporarily terminated at t = 13 s as shown in Figure 5.18 (c).

Event 6 : At t = 15 s the power generated by the wind turbine increases and the utility load demand falls below the threshold limits as depicted in Figures 5.18 (a) and (b). Therefore the charging of PHEV-2 now resumes. In order to meet the departure deadline it is promoted Level - 1 charging. It has to be noted that PHEV-2 started charging at t = 1.5 s and since its duration of stay is 5 hrs (i.e., 15 s) it departs at t = 16.5 s.

As per Equation (4.42) the power required to charge the PHEV from t = 15 s until its departure time of 16.5 s is around 22 kW. It can be seen from Figure

5.18 (a) that the power generated by the wind turbine is around 4 kW. The supplementary power of 18 kW has to be delivered by grid but the distribution transformer is rated at 15 kVA (12 kW considering 0.8 pf load). Since the utility load is around 6 kW the maximum power that can be delivered by the grid to the charging facility is 6 kW (12 - 6). Hence PHEV-2 is cannot be charged completely. As shown in Figure 5.18 (g) the SOC of the PHEV is around 80% by the time it departs the charging facility. Accordingly the customers are priced at a lower rate for charging.

Events 7, 8 : At t = 16.5 s PHEV-2 leaves the charging facility. This is evident from the momentary increase in DC link voltage as shown in Figure 5.18 (f). Therefore the ESU now starts charging and once it is completely charged the power generated by the wind turbine is delivered to the grid. The charging facility now operates in Mode - 2.

Table 5.7: Main operation events for Case 4

Events	Operation Condition	Time (S)
1	PHEV-1 starts charging	0
2	PHEV-1 leaves the facility and PHEV-2 starts charging	1.5
3	Wind Speed reduces to zero, load demand exceeds $I_{DMD-max}$	10
4	Charging rate of the PHEV-2 is reduced and ESU starts discharging	10.1
5	ESU is completely discharged	13
6	Load demand reduces ($I_{DMD} < I_{DMD-max}$). Charging of PHEV-2 is resumed	15
7	PHEV-2 leaves the charging facility with 80 % SOC. ESU starts charging.	16.5
8	ESU is charged completely.	19

5.6 Experimental Evaluation

To verify the proposed control scheme for WPCF, experimental tests based on a scale-down version have been carried out in the laboratory. Figure 5.18

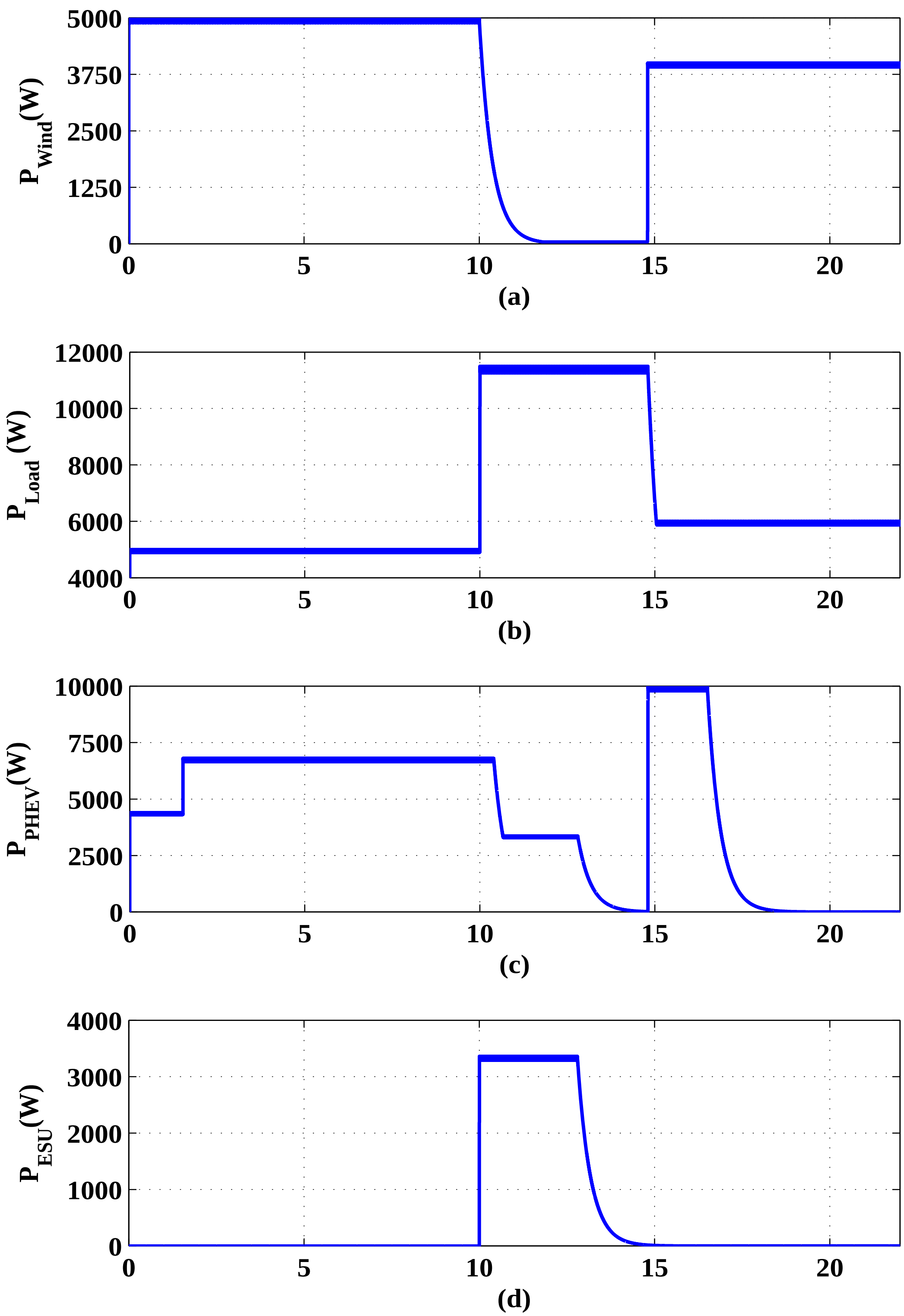

P_{Wind}(W)
5000
3750
2500
1250
0
0
5
10
15
20
(a)
P_{Load} (W)
12000
10000
8000
6000
4000
0
5
10
15
20
(b)
P_{PHEV}(W)
10000
7500
5000
2500
0
0
5
10
15
20
(c)
P_{ESU}(W)
4000
3000
2000
1000
0
0
5
10
15
20
(d)

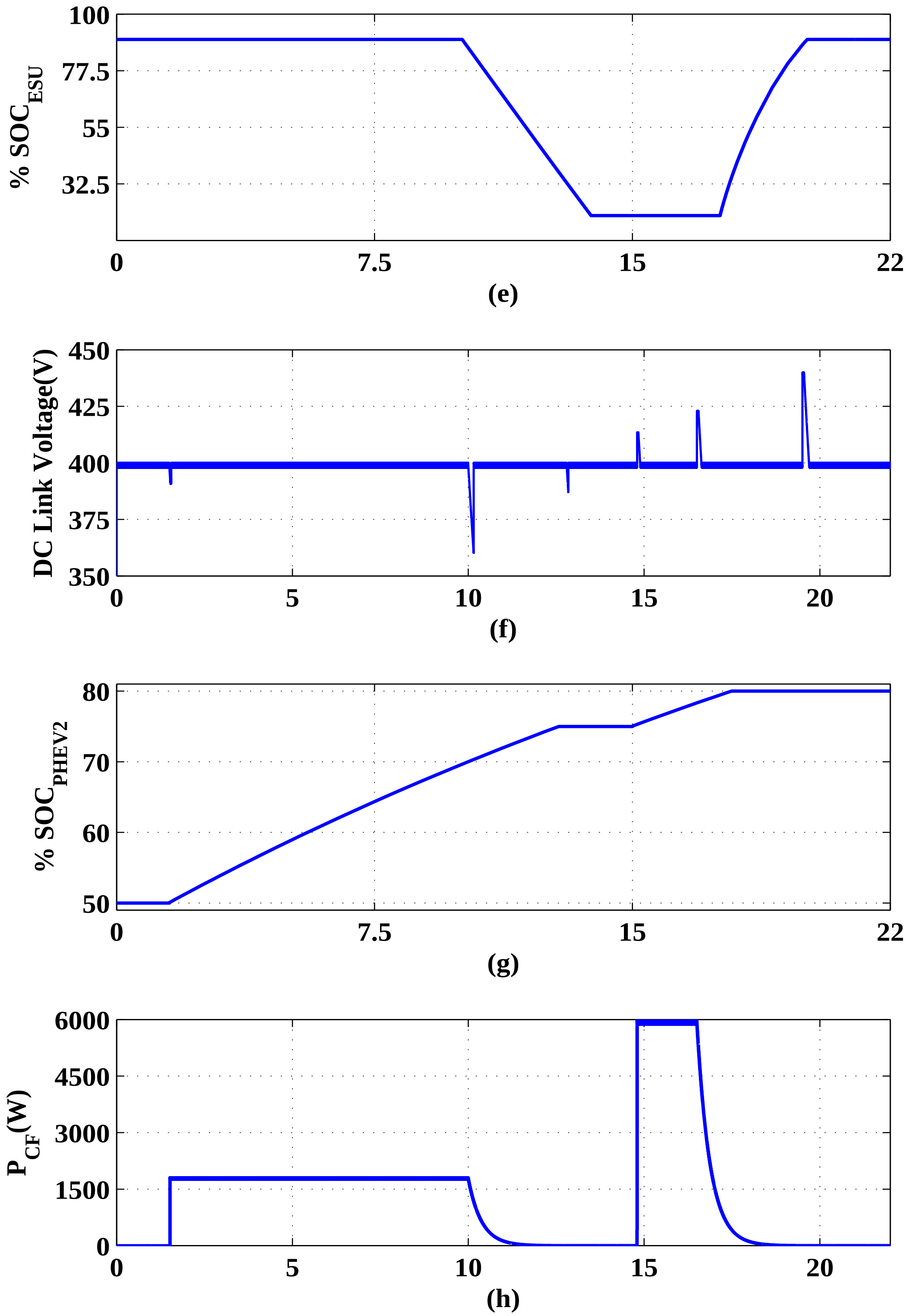

Figure 5.17: WPCF operation during Case 4. (a) Wind power. (b) Load demand. (c) PHEV load demand. (d) Power from the ESU (e) SOC of the ESU. (f) DC link voltage. (g) SOC of PHEV-2. (h) Power from the grid to WPCF .

shows the experimental setup of the system. As shown in the figure the setup consists of an emulated wind turbine, 3-phase diode bridge rectifier, high voltage (HV) DC/DC boost converter by TI, power pole boards in buck and buck-boost configuration from Hirel. Two batteries are used which function as an ESU and PHEV respectively.

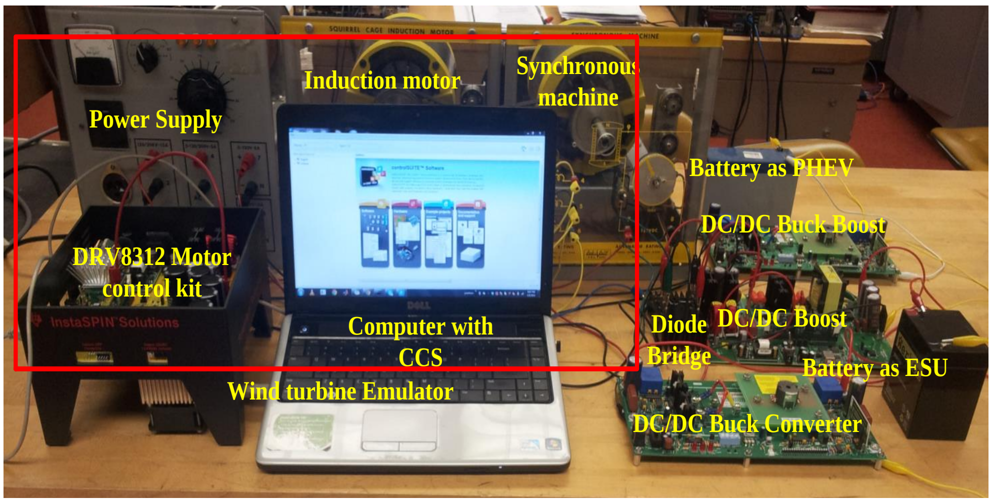

Figure 5.18: Lab scale implementation for experimental testing.

The conventional characteristics of a wind turbine are emulated by controlling a 3-phase induction motor with TI's HV motor control kit. A single DSP processor generates the required switching signals to control the DC/DC and DC/AC converters. The working of the emulator and other important components of the setup are described in the following sections.

Wind Turbine Test Bench System

In the proposed wind turbine test bench system (WTTBS) , the power-speed characteristics of a wind turbine are physically implemented by an induction motor drive. The shaft power P_m and speed ω_r of the induction motor represent the power and speed of the wind turbine rotor. The induction motor is coupled to a permanent magnet synchronous generator (PMSG) and it is fed by an inverter. The switching signals for the inverter are generated using Field oriented control technique (FOC).

The structure of the wind turbine emulator is depicted in Figure 5.19. A four-pole 1/4 hp/208 V squirrel-cage induction motor is used to emulate the wind turbine. The emulated power speed characteristics obtained for various values of the wind speed V_W are represented in Figure 5.20. A DSP based control system is developed to reproduce the turbine characteristics. The control is performed via a PC using code composer studio IDE. The measured shaft torque, rotor speed and wind speed are fed into the digital signal processor which generates the required current and frequency commands for the inverter. The inverter is present within the TI's high voltage motor control kit and the required switching signals are generated by C2000 TMS320F28069 DSP microcontroller.

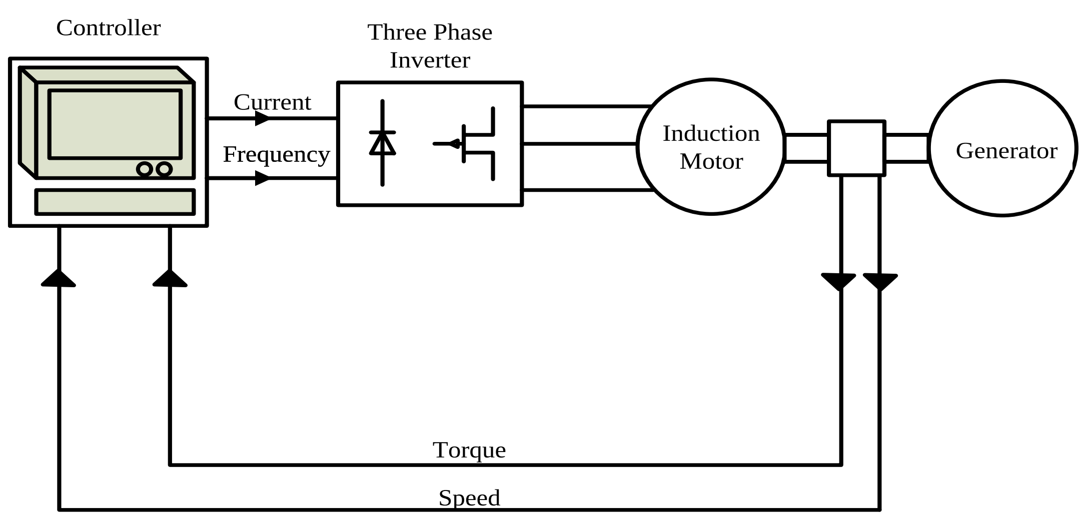

Figure 5.19: Structure of wind turbine test bench system.

Figures 5.21 and 5.22 depict the various stages present on the high voltage motor control kit to power the induction motor. The kit requires two inputs : 15 V DC power supply which powers the controller and the supporting cir-

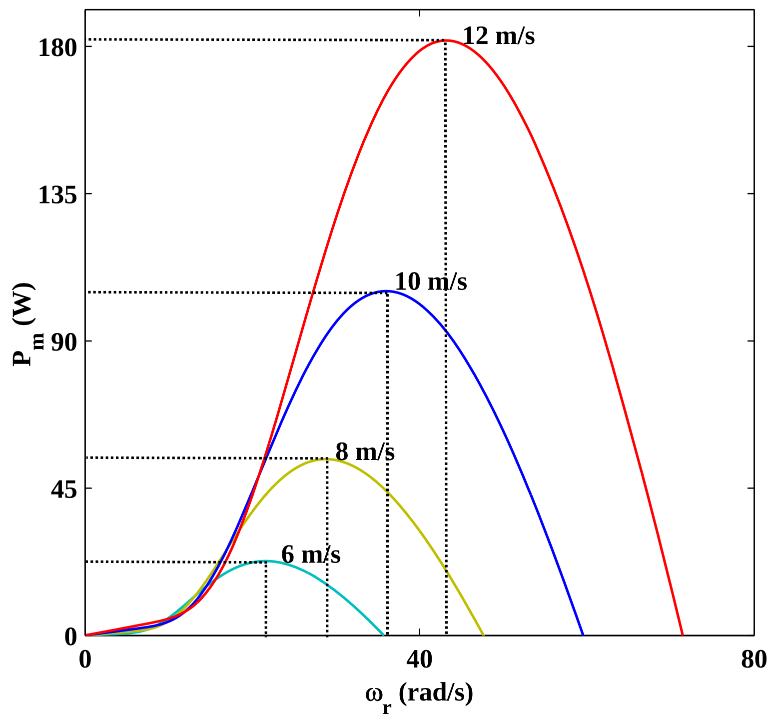

Figure 5.20: Power characteristics of wind turbine test bench system.

Figure 5.21: HV motor control kit.

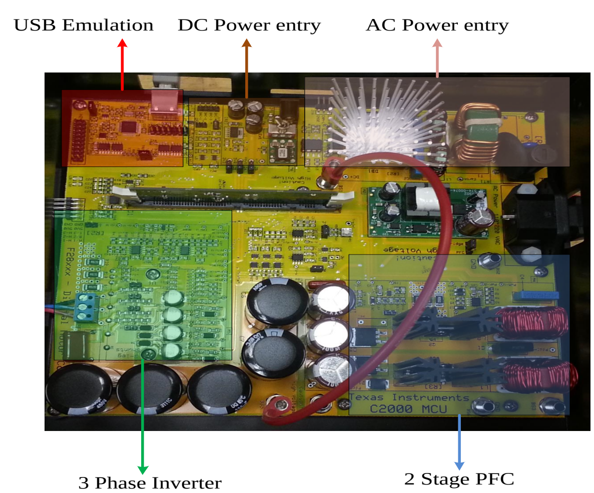

Figure 5.22: Power stages in the HV kit.

cuitry and a 120 V AC input to run the motor. As shown in Figure 5.21, the TMS320F28069 control card is embedded within the motor control kit. The required wind speed profiles and FOC logic are programmed into the control card through CCS IDE. Field oriented control of induction motor provides robust and cost effective method to replicate the static and dynamic characteristics of wind turbine system. To simplify the working of WTTBS a look up table is created for various values of wind speed. As shown in Table 5.8 for each value of wind speed a particular value of rotor speed and torque are generated. The rotor speed and the torque vary according to the load conditions.

Table 5.8: Rotor speed and torque for various wind speeds

Wind Speed	ω_{opt}**[rad/s]**	**Torque[N-m]**	$P_{mech,max}$**[W]**
6	20	1.125	22.5
8	28	1.71	48
10	36	3	110
12	44	4.14	182

5.7 Experimental Results

Experimental tests have been carried out in terms of transient-performance between different modes and the results are provided. The nominal DC link voltage is set at 100 V. Based on the allowable threshold voltage limits V_{S-1} and V_{S-2} are chosen as 90 V and 110 V respectively. A 12 V 5 Ah lead acid battery is used as the PHEV and it is charged at the rate of 60 W/hr. Figures 5.23 through 5.26 explain the experimental results for the various modes of operation.

Figure 5.23 shows the transition from Mode-1 to Mode-3. As shown in the figure a wind speed command of 8 m/s is given to the emulator and it generates a power 48 V as per Table 5.8. Since the battery is charged at 60 W/hr, the supplementary power of 12 W is provided by the grid. A sudden decrease in wind speed to 0 m/s shifts the control to Mode-3 wherein the DC/AC G-VSC functions as a rectifier.

Figure 5.24 describes the inversion operation during Mode-1. An increase in wind speed command from 6 m/s to 10 m/s increases the generated power by the emulator to 110 W. The additional power of 50 W is delivered to the grid. The current flowing to the grid can be seen in the figure. The grid current reduces to zero once the wind speed falls to 8 m/s since there is no surplus power.

Figure 5.26 shows the transition from rectification mode to inversion mode once the buck converter is tuned off. During the time when the buck converter is on (i.e., the battery is charging) the required power is delivered by the wind turbine and the grid. As shown in the figure when the buck converter is turned off (as shown in Figure 5.26) the G-VSC switches its operation from rectifier mode to inverter mode.

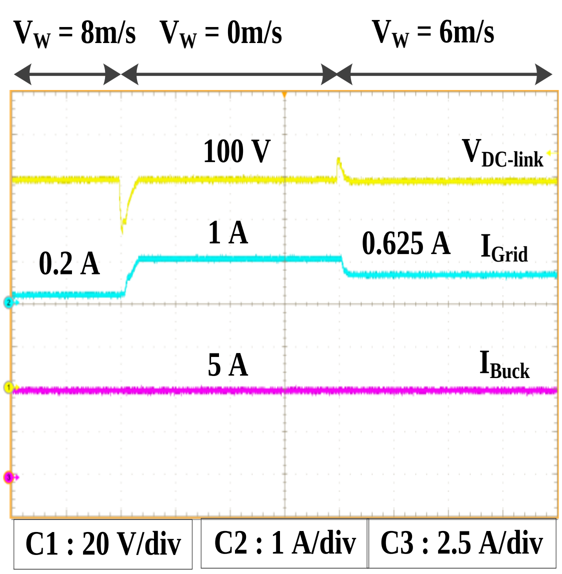

Figure 5.23: Mode-1 to Mode-3.

The transition from Mode-1 to Mode-2 is shown in Figure 5.25. It can be seen

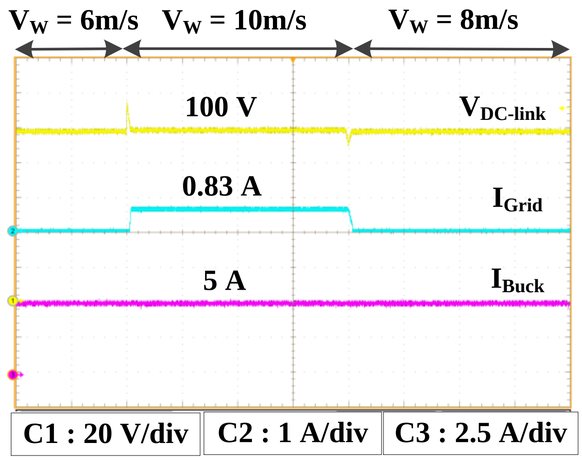

Figure 5.24: Grid inversion during Mode-1.

from the figure that the DC link voltage increases beyond 110 V when the buck converter is turned off. This is similar to the case wherein the PHEV leaves the charging facility once it is completely charged. The power generated by the wind turbine is now delivered to the grid.

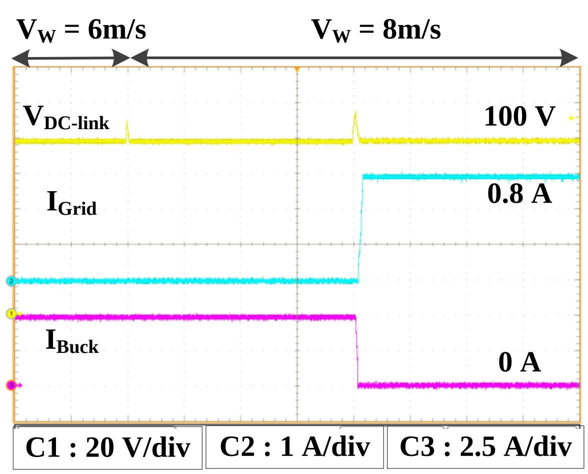

Figure 5.25: Mode-1 to Mode-2.

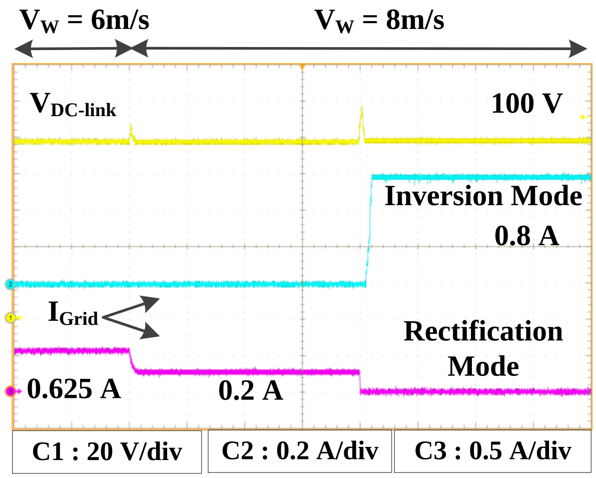

Figure 5.26: Transition from rectification to inversion.

5.8 Summary

This chapter proposed a distributed control strategy based on DC link voltage sensing for a charging facility featuring small scale wind turbine. Based on the change in DC link voltage levels various operating modes are considered. The proposed control strategy is simple, unique and enables maximum utilization of wind power for charging the PHEVs. The feasibility and effectiveness of the proposed control strategy has been validated both by the simulations as well as experimental results.

Chapter 6 Conclusions and Future Work

This dissertation proposes a new architecture and control for Plug-in Hybrid Electric Vehicle (PHEV) charging facilities integrated with photovoltaic (PV)/wind. The problem being the increase in load on the distribution transformer due to the future high penetration of PHEVs. This work poses an immediate need to investigate ways to reduce the stress imposed on the distribution network. The proposed architecture and control for PHEV charging facilities will provide the flexibility to charge the vehicle from a renewable source of energy, thus mitigating the impact on the distribution transformer.

A comprehensive solution for the posed problem involved -

- Development of a robust controller logic based on DC link voltage sensing to charge the PHEVs.
- Verifying the feasibility of the proposed system with the help of MATLAB-Simulink.
- Developing a DSP based laboratory prototype of the Power Conditioning Unit (PCU) and validating the proposed control strategy.

Several case studies are considered including worst case scenarios such as low power from PV/wind during peak load conditions. From the case studies it can be concluded PHEVs can be charged during the daytime without replacing the existing distribution transformers with the one's with higher kVA rating . Thus the proposed PV/wind based charging facilities provide a economically viable solution for the utilities. Also, it is important to note that PV/wind harbors a great advantage, in that the extra energy can be injected into grid, which can be used to balance the PV/wind turbine installation costs.

Future Work

Probabilistic Analysis

In the proposed control algorithm several assumptions are made regarding the size of the PV, arrival and departure times of the PHEVs and their initial SOC when they arrive at the charging facility. These quantities, despite their randomness, are crucial parameters when the energy within this system is to be managed and controlled.

In order to emmulate a real world charging scenario in public parking facilities, various models have to developed as an attempt to model these uncertain quantities using regression techniques based on historical data or statistical techniques based on probability distribution functions (pdfs). The proposed controller can be made real-time by updating the load data of the distribution transformer from the utility every 15 min. The rating of the ESU can be estimated by considering the variation in the PV/wind generation during the peak load period.

LVDC Microgrid

The proposed control strategy based on DC link voltage sensing can be extended to low voltage DC (LVDC) microgrids. Figure 6.1 shows one such example, which represents the electrical layout of remote telecom DC distribution. As shown in the figure the renewable energy resources such as the PV/wind are connected to DC bus through power electronic converters. Nevertheless, their last conversion stage is ordinarily based on a DC/DC converter. Therefore the concept of DC link Voltage sensing can be applied for effectively managing the direction of power flow.

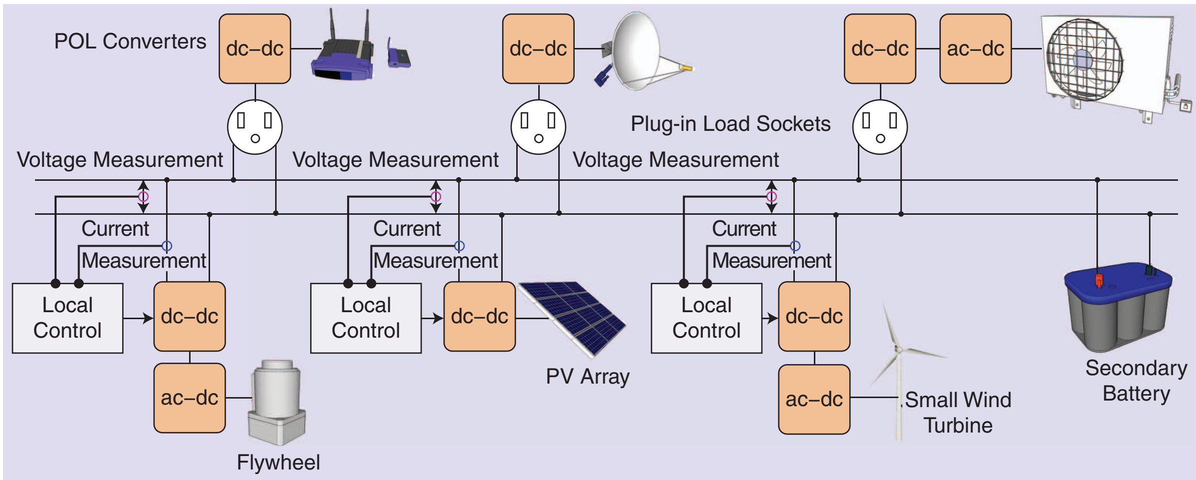

Figure 6.1: The electrical layout of a remote telecom DC distribution system.

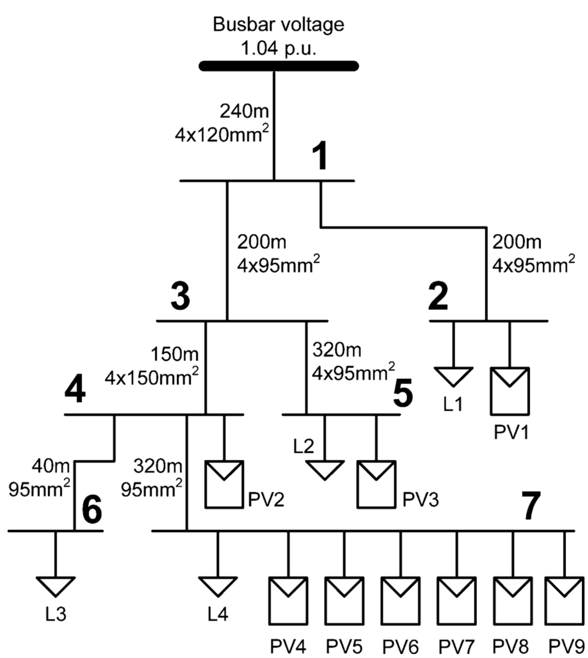

Figure 6.2: Single-line diagram of the Belgian LV grid feeder.

Optimal Location of PV/Wind Based Charging Facilities

This work has integrated the PV/wind system with the PHEVs present in public charging facilities. This concept can be further extended to a LV feeders as shown in Figure 6.2 with PV/wind penetration. Optimal location of PV/wind energy conversion systems can be determined through stability and sensitivity analysis. Voltage magnitude problems posed by high penetration of PV on the distribution network can be mitigated though the concept of V2G wherein the PHEVs act as voltage regulators.

References

[1] R. Lasseter, A. Akhil, C. Marnay, J. Stephens, J. Dagle, R. Guttromson, A. Meliopoulous, R. Yinger, and J. Eto, "Integration of Distributed Energy Resources: The CERTS Microgrid Concept," April 2002. [Online]. Available: http://certs.lbl.gov/CERTS_P_DER.htm

[2] M. Ehsani, Y. Gao, S. Gay, and A. Emadi, *Modern Electric, Hybrid Electric, and Fuel Cell Vehicles*. Boca Raton, FL: CRC Press, 2005.

[3] J. Larminie and J. Lowry, *Electric Vehicle Technology Explained*. New York: Wiley, 2003.

[4] S. Wirasingha and A. Emadi, "Pihef: Plug-in Hybrid Electric Factor," *IEEE Transactions on Vehicular Technology*, vol. 60, no. 3, pp. 1279–1284, March 2011.

[5] "International Energy Outlook 2011. U.S. Energy Information Administration (EIA) and International Energy Agency; 2011."

[6] R. Schmidt, "Information Technology Energy Usage and our Planet," in *Eleventh Intersociety Conference on Thermal and Thermomechanical Phenomena in Electronic Systems*, May 2008, pp. 1255–1275.

[7] "Nearly 22 Million Electric Vehicles Will be Sold from 2012 to 2020," April 2013. [Online]. Available: www.navigantresearch.com/newsroom/nearly-22-million-electric-vehicles-will-besold-from-2012-to-2020

[8] Y. Li, "Scenario-Based Analysis on the Impacts of Plug-in Hybrid Electric Vehicles' (PHEV) Penetration into the Transportation Sector," in *IEEE International Symposium on Technology and Society*, June 2007, pp. 1–6.

[9] SAE, "SAE Electric Vehicle and Plug-in Hybrid Electric Vehicle Conductive Charge Coupler. SAE Standard j1772," 2012.

[10] M. Yilmaz and P. Krein, “Review of Battery Charger Topologies, Charging Power Levels, and Infrastructure for Plug-in Electric and Hybrid Vehicles,” *IEEE Transactions on Power Electronics*, vol. 28, no. 5, pp. 2151–2169, May 2013.

[11] S. Hadley, “Evaluating the Impact of Plug-in Hybrid Electric Vehicles on Regional Electricity Supplies,” in *IREP Symposium on Bulk Power System Dynamics and Control - VII. Revitalizing Operational Reliability*, Aug 2007, pp. 1–12.

[12] Q. Yan and M. Kezunovic, “Impact Analysis of Electric Vehicle Charging on Distribution System,” in *North American Power Symposium (NAPS)*, Sept 2012, pp. 1–6.

[13] R. Moghe, F. Kreikebaum, J. Hernandez, R. Kandula, and D. Divan, “Mitigating Distribution Transformer Lifetime Degradation Caused by Grid-Enabled Vehicle (GEV) Charging,” in *IEEE Energy Conversion Congress and Exposition (ECCE)*, Sept 2011, pp. 835–842.

[14] A. Masoum, S. Deilami, P. Moses, and A. Abu-Siada, “Impacts of Battery Charging Rates of Plug-in Electric Vehicle on Smart Grid Distribution Systems,” in *IEEE PES Innovative Smart Grid Technologies Conference Europe (ISGT Europe)*, Oct 2010, pp. 1–6.

[15] K. Qian, C. Zhou, M. Allan, and Y. Yuan, “Load Model for Prediction of Electric Vehicle Charging Demand,” in *International Conference on Power System Technology (POWERCON)*, Oct 2010, pp. 1–6.

[16] M. Rutherford and V. Yousefzadeh, “The Impact of Electric Vehicle Battery Charging on Distribution Transformers,” in *Twenty-Sixth Annual IEEE Applied Power Electronics Conference and Exposition (APEC)*, March 2011, pp. 396–400.

[17] P. Papadopoulos, S. Skarvelis-Kazakos, I. Grau, L. Cipcigan, and N. Jenkins, “Predicting Electric Vehicle Impacts on Residential Distribution Networks

with Distributed Generation," in *IEEE Vehicle Power and Propulsion Conference (VPPC)*, Sept 2010, pp. 1–5.

[18] S. Agah and H. Abyaneh, "Distribution Transformer Loss-of-Life Reduction by Increasing Penetration of Distributed Generation," *IEEE Transactions on Power Delivery*, vol. 26, no. 2, pp. 1128–1136, April 2011.

[19] L. Jian, H. Xue, G. Xu, X. Zhu, D. Zhao, and Z. Shao, "Regulated Charging of Plug-in Hybrid Electric Vehicles for Minimizing Load Variance in Household Smart Microgrid," *IEEE Transactions on Industrial Electronics*, vol. 60, no. 8, pp. 3218–3226, Aug 2013.

[20] C. F. Tuffner FK, "Utilizing Electric Vehicles to Assist Integration of Large Penetrations of Distributed Photovoltaic Generation. Pacific Northwest National Laboratory," November 2012. [Online]. Available: http://www.pnnl.gov/main/publications/external/technical_reports/PNNL-22064.pdf

[21] U. Chukwu and S. Mahajan, "V2G Parking Lot with PV Rooftop for Capacity Enhancement of a Distribution System," *IEEE Transactions on Sustainable Energy*, vol. 5, no. 1, pp. 119–127, Jan 2014.

[22] T. Geiles and S. Islam, "Impact of PEV Charging and Rooftop PV Penetration on Distribution Transformer Life," in *IEEE Power and Energy Society General Meeting (PES)*, July 2013, pp. 1–5.

[23] S. Islam and T. Giles, "Distribution Transformer Life Optimisation in a Smart Feeder Embedded with Photovoltaic Power Generation," in *Seventh International Conference on Electrical Computer Engineering (ICECE)*, Dec 2012, pp. 953–957.

[24] M. Tabari and A. Yazdani, "A DC Distribution System for Power System Integration of Plug-in Hybrid Electric Vehicles," in *IEEE Power and Energy Society General Meeting (PES)*, July 2013, pp. 1–5.

[25] C. Hamilton, G. Gamboa, J. Elmes, R. Kerley, A. Arias, M. Pepper, J. Shen, and I. Batarseh, "System Architecture of a Modular Direct-DC PV Charging Station for Plug-in Electric Vehicles," in *Thirty-Sixth Annual Conference on IEEE Industrial Electronics Society*, Nov 2010, pp. 2516–2520.

[26] G. Gamboa, C. Hamilton, R. Kerley, S. Elmes, A. Arias, J. Shen, and I. Batarseh, "Control Strategy of a Multi-Port, Grid-Connected, Direct-DC PV Charging Station for Plug-in Electric Vehicles," in *IEEE Energy Conversion Congress and Exposition (ECCE)*, Sept 2010, pp. 1173–1177.

[27] D. Robalino, G. Kumar, L. O. Uzoechi, U. Chukwu, and S. Mahajan, "Design of a Docking Station for Solar Charged Electric and Fuel Cell Vehicles," in *International Conference on Clean Electrical Power*, June 2009, pp. 655–660.

[28] B. R. Alamri and A. R. Alamri, "Technical Review of Energy Storage Technologies When Integrated with Intermittent Renewable Energy," in *International Conference on Sustainable Power Generation and Supply*, April 2009, pp. 1–5.

[29] G. Carli and S. Williamson, "Technical Considerations on Power Conversion for Electric and Plug-in Hybrid Electric Vehicle Battery Charging in Photovoltaic Installations," *IEEE Transactions on Power Electronics*, vol. 28, no. 12, pp. 5784–5792, Dec 2013.

[30] Z. Rasinab and M. Rahmana, "Grid-Connected Quasi-Z-Source PV Inverter for Electric Vehicle Charging Station," in *International Conference on Renewable Energy Research and Applications (ICRERA)*, Oct 2013, pp. 627–632.

[31] Y. Gurkaynak and A. Khaligh, "Control and Power Management of a Grid Connected Residential Photovoltaic System with Plug-in Hybrid Electric Vehicle (PHEV) Load," in *Twenty-Fourth Annual IEEE Applied Power Electronics Conference and Exposition*, Feb 2009, pp. 2086–2091.

[32] A. Nagarajan and W. Shireen, "Grid-Connected Residential Photovoltaic Energy Systems with Plug-in Hybrid Electric Vehicles (PHEV) as Energy Storage," in *IEEE Power and Energy Society General Meeting*, July 2010, pp. 1–5.

[33] R. M. Oviedo, Z. Fan, S. Gormus, and P. Kulkarni, "A Residential PHEV Load Coordination Mechanism with Renewable Sources in Smart Grids," *International Journal of Electrical Power and Energy Systems*, vol. 55, no. 0, pp. 511 – 521, 2014.

[34] Y. Gurkaynak, Z. Li, and A. Khaligh, "A Novel Grid-Tied, Solar Powered Residential Home with Plug-in Hybrid Electric Vehicle (PHEV) Loads," in *IEEE Vehicle Power and Propulsion Conference*, Sept 2009, pp. 813–816.

[35] L. Roggia, C. Rech, L. Schuch, J. Baggio, H. Hey, and J. Pinheiro, "Design of a Sustainable Residential Microgrid System Including PHEV and Energy Storage Device," in *Proceedings of the 2011-14th European Conference on Power Electronics and Applications (EPE 2011)*, Aug 2011, pp. 1–9.

[36] S. Sheng, C.-T. Hsu, P. Li, and B. Lehman, "Energy Management for Solar Battery Charging Station," in *IEEE Fourteenth Workshop on Control and Modeling for Power Electronics (COMPEL)*, June 2013, pp. 1–8.

[37] Z. Chen, N. Liu, X. Xiao, and J. Zhang, "Energy Exchange Model of PV-Based Battery Switch Stations Based on Battery Swap Service and Power Distribution," in *IEEE Energytech Conference*, May 2013, pp. 1–6.

[38] G.-Y. Choe, J.-S. Kim, B. kuk Lee, C.-Y. Won, and T.-W. Lee, "A Bi-Directional Battery Charger for Electric Vehicles Using Photovoltaic PCS Systems," in *IEEE Vehicle Power and Propulsion Conference (VPPC)*, Sept 2010, pp. 1–6.

[39] M. Vaidya, E. Stefanakos, B. Krakow, H. C. Lamb, T. Arbogast, and T. Smith, "Direct DC-DC Electric Vehicle Charging with a Grid-Connected Photovoltaic System," in *Twenty-Fifth IEEE Photovoltaic Specialists Conference*, May 1996, pp. 1505–1508.

[40] J. Schonberger, R. Duke, and S. Round, "Dc-Bus Signaling: A Distributed Control Strategy for a Hybrid Renewable Nanogrid," *IEEE Transactions on Industrial Electronics*, vol. 53, no. 5, pp. 1453–1460, Oct 2006.

[41] K. Sun, L. Zhang, Y. Xing, and J. Guerrero, "A Distributed Control Strategy Based on DC Bus Signaling for Modular Photovoltaic Generation Systems with Battery Energy Storage," *IEEE Transactions on Power Electronics*, vol. 26, no. 10, pp. 3032–3045, Oct 2011.

[42] C. Jin, P. Wang, J. Xiao, Y. Tang, and F. H. Choo, "Implementation of Hierarchical Control in DC Microgrids," *IEEE Transactions on Industrial Electronics*, vol. 61, no. 8, pp. 4032–4042, Aug 2014.

[43] G. Preetham and W. Shireen, "Photovoltaic Charging Station for Plug-in Hybrid Electric Vehicles in a Smart Grid Environment," in *IEEE PES Innovative Smart Grid Technologies (ISGT)*, Jan 2012, pp. 1–8.

[44] P. Goli and W. Shireen, "PV Integrated Smart Charging of Phevs Based on DC Link Voltage Sensing," *IEEE Transactions on Smart Grid*, vol. PP, no. 99, pp. 1–8, 2014.

[45] D. Chen and L. Xu, "DC Microgrid with Variable Generations and Energy Storage," in *IET Conference on Renewable Power Generation (RPG 2011)*, Sept 2011, pp. 1–6.

[46] D. B. Richardson, "Electric Vehicles and the Electric Grid: A Review of Modeling Approaches, Impacts, and Renewable Energy Integration," *Renewable and Sustainable Energy Reviews*, vol. 19, no. 0, pp. 247 – 254, 2013. [Online]. Available: http://www.sciencedirect.com/science/article/pii/S1364032112006557

[47] W. Kempton and J. Tomic, "Vehicle-to-Grid Power Implementation: From Stabilizing the Grid to Supporting Large-Scale Renewable Energy," *Journal of Power Sources*, vol. 144, no. 1, pp. 280 – 294, 2005.

[48] F. Mwasilu, J. J. Justo, E.-K. Kim, T. D. Do, and J.-W. Jung, "Electric Vehicles and Smart Grid Interaction: A Review on Vehicle to Grid and Renewable Energy Sources Integration," *Renewable and Sustainable Energy Reviews*, vol. 34, no. 0, pp. 501 – 516, 2014. [Online]. Available: http://www.sciencedirect.com/science/article/pii/S1364032114001920

[49] D. Tuttle and R. Baldick, "The Evolution of Plug-in Electric Vehicle-Grid Interactions," *IEEE Transactions on Smart Grid*, vol. 3, no. 1, pp. 500–505, March 2012.

[50] J. Traube, F. Lu, and D. Maksimovic, "Electric Vehicle DC Charger Integrated within a Photovoltaic Power System," in *Twenty-Seventh Annual IEEE Applied Power Electronics Conference and Exposition (APEC)*, Feb 2012, pp. 352–358.

[51] J. Mossoba, M. Kromer, P. Faill, S. Katz, B. Borowy, S. Nichols, L. Casey, D. Maksimovic, J. Traube, and F. Lu, "Analysis of Solar Irradiance Intermittency Mitigation using Constant DC Voltage PV and EV Battery Storage," in

IEEE Transportation Electrification Conference and Expo (ITEC), June 2012, pp. 1–6.

[52] J. Traube, F. Lu, D. Maksimovic, J. Mossoba, M. Kromer, P. Faill, S. Katz, B. Borowy, S. Nichols, and L. Casey, "Mitigation of Solar Irradiance Intermittency in Photovoltaic Power Systems with Integrated Electric-Vehicle Charging Functionality," *IEEE Transactions on Power Electronics*, vol. 28, no. 6, pp. 3058–3067, June 2013.

[53] O. Sun, "Solar-Powered Electric Vehicle Charging Stations." [Online]. Available: http://www.onesuninc.com/chargingstations.php

[54] M. Solar, "Solar-Powered Electric Vehicle Charging Stations." [Online]. Available: http://www.meritbuilders.com/solar-charging-station

[55] SolarCity, "Solarcity to Make Solar-Powered Electric Vehicle Charging Available Across its Service Territory." [Online]. Available: http://www.solarcity.com

[56] Oakridge, "Solar-Assisted Electric Vehicle Charging Stations." [Online]. Available: http://info.ornl.gov/sites/publications/files/pub32842.pdf

[57] ORNL, "Solar-Assisted Electric Vehicle Charging Project." [Online]. Available: https://sustainability-ornl.org/Documents/RoadmapMeeting022311/Randy%20Memphis2.pdf

[58] EPRI, "Tennessee Valley Authority Smart Modal Area Recharge Terminal (SMART) Station Project," November 2012. [Online]. Available: http://www.epri.com/abstracts/pages/ProductAbstract.aspx?productId=000000000001026583

[59] J. Berst, "More EVs on the Road and More Headaches for Utilities," May 2011. [Online]. Available: http://www.smartgridnews.com

[60] EPRI, "Solar Photovoltaics Expanding Electric Generation Options," December 2007. [Online]. Available: http://mydocs.epri.com/docs/SEIG/1016279_Photovoltaic_White_Paper_1207.pdf

[61] "Smart Grid - Putting it All Together. a 2010 Reprint Journal from IEEE PES." [Online]. Available: http://ieee-pes.org/images/pdf/2010pe-SmartGrid-all.pdf?utm_source=pes3&utm_medium=web&utm_campaign=pesweb

[62] J. Huotari, "Solar-Assisted Electric Vehicle Charging Station Finished at Oak Ridge Lab," May 2011. [Online]. Available: http://www.oakridger.com/article/20110527/NEWS/305279998

[63] S. Bai, D. Yu, and S. Lukic, "Optimum Design of an EV/PHEV Charging Station with DC Bus and Storage System," in *IEEE Energy Conversion Congress and Exposition (ECCE)*, Sept 2010, pp. 1178–1184.

[64] P. Bauer, Y. Zhou, J. Doppler, and N. Stembridge, "Charging of Electric Vehicles and Impact on the Grid," in *Thirteenth International Symposium on MECHATRONIKA*, June 2010, pp. 121–127.

[65] A. Arancibia and K. Strunz, "Modeling of an Electric Vehicle Charging Station for Fast DC Charging," in *IEEE International Electric Vehicle Conference (IEVC)*, March 2012, pp. 1–6.

[66] D. Aggeler, F. Canales, H. Zelaya-De La Parra, A. Coccia, N. Butcher, and O. Apeldoorn, "Ultra-Fast DC-Charge Infrastructures for EV-Mobility and Future Smart Grids," in *IEEE PES Innovative Smart Grid Technologies Conference Europe (ISGT Europe)*, Oct 2010, pp. 1–8.

[67] P. Kulshrestha, L. Wang, M.-Y. Chow, and S. Lukic, "Intelligent Energy Management System Simulator for PHEVs at Municipal Parking Deck in a Smart

Grid Environment," in *IEEE Power and Energy Society General Meeting*, July 2009, pp. 1–6.

[68] J. Voelcker, "One Million Plug-in Cars by 2015," March 2011. [Online]. Available: http://spectrum.ieee.org/green-tech/advanced-cars/one-million-plugin-cars-by-2015

[69] S. Hadley, "Evaluating the Impact of Plug-in Hybrid Electric Vehicles on Regional Electricity Supplies," in *IREP Symposium on Bulk Power System Dynamics and Control - VII. Revitalizing Operational Reliability*, Aug 2007, pp. 1–12.

[70] A. Masoum, S. Deilami, P. Moses, and A. Abu-Siada, "Impacts of Battery Charging Rates of Plug-in Electric Vehicle on Smart Grid Distribution Systems," in *IEEE PES Innovative Smart Grid Technologies Conference Europe (ISGT Europe)*, Oct 2010, pp. 1–6.

[71] P. Denholm, M. Kuss, and R. M. Margolis, "Co-benefits of Large Scale Plug-in Hybrid Electric Vehicle and Solar PV Deployment," *Journal of Power Sources*, vol. 236, no. 0, pp. 350 – 356, 2013. [Online]. Available: http://www.sciencedirect.com/science/article/pii/S0378775312015534

[72] K. KOWALENKO, "Going Electric: Things to Consider," September 2011. [Online]. Available: http://theinstitute.ieee.org/technology-focus/technology-topic/going-electric-things-to-consider

[73] J. S. John, "Epri Plugs Smart Grid for Energy Savings," December 2008. [Online]. Available: http://www.greentechmedia.com/articles/read/epri-plugs-smart-grid-for-energy-savings-5308

[74] R. Lefevre, "Smart Grid Needs Energy Efficiency," July 2011. [Online]. Available: http://www.elp.com/articles/print/volume-89/issue-4/sections/smart-grid-needs-energy-efficiency.html

[75] U. D. of Transportation, "Summary of Travel Trends : 2009 Household Travel Survey." [Online]. Available: http://nhts.ornl.gov/2009/pub/stt.pdf

[76] R. W. Erickson and D. Maksimovic, "Fundamentals of Power Electronics, Second Edition, Springer," 2001.

[77] J. Huang, V. Gupta, and Y.-F. Huang, "Scheduling Algorithms for Phev Charging in Shared Parking Lots," in *American Control Conference (ACC)*, June 2012, pp. 276–281.

[78] P. Kadar and A. Varga, "Photovoltaic EV Charge Station," in *IEEE Eleventh International Symposium on Applied Machine Intelligence and Informatics (SAMI)*, Jan 2013, pp. 57–60.

[79] P.-E. Dziadek, W. Feucht, A. Mittnacht, H.-G. Kula, and H. Frank, "Eco-Friendly Application of EVs for Home-to-Work and Home-to-Education Transports," in *IEEE International Conference on Industrial Technology (ICIT)*, Feb 2013, pp. 705–709.

[80] S. Mesentean, W. Feucht, A. Mittnacht, and H. Frank, "Scheduling Methods for Smart Charging of Electric Bikes from a Grid-Connected Photovoltaic-System," in *Fifth European Symposium on Computer Modeling and Simulation (EMS)*, Nov 2011, pp. 299–304.

[81] S. Mesentean, W. Feucht, H.-G. Kula, and H. Frank, "Smart Charging of Electric Scooters for Home to Work and Home to Education Transports from Grid -Connected Photovoltaic-Systems," in *IEEE International Energy Conference and Exhibition (EnergyCon)*, Dec 2010, pp. 73–78.

[82] A. Mohamed, V. Salehi, T. Ma, and O. Mohammed, "Real-Time Energy Management Algorithm for Plug-in Hybrid Electric Vehicle Charging Parks In-

volving Sustainable Energy," *IEEE Transactions on Sustainable Energy*, vol. 5, no. 2, pp. 577–586, April 2014.

[83] S. Cutler, B. Schmalberger, and C. Rivers, "An Intelligent Solar Ecosystem with Electric Vehicles," in *IEEE International Electric Vehicle Conference (IEVC)*, March 2012, pp. 1–7.

[84] N. S. Giges, "Wind-Powered Charging Stations Coming Soon," Oct 2012. [Online]. Available: https://www.asme.org/engineering-topics/articles/renewable-energy/wind-powered-charging-stations-coming-soon

[85] R. Kot, M. Rolak, and M. Malinowski, "Comparison of Maximum Peak Power Tracking Algorithms for a Small Wind Turbine," *Mathematics and Computers in Simulation*, vol. 91, no. 0, pp. 29 – 40, 2013.

[86] W. Short and P. Denholm, "Preliminary Assessment of Plug-in Hybrid Electric Vehicles on Wind Energy Markets," April 2006. [Online]. Available: http://www.nrel.gov/docs/fy06osti/39729.pdf

[87] D. Dallinger, S. Gerda, and M. Wietschel, "Integration of Intermittent Renewable Power Supply Using Grid-Connected Vehicles - A 2030 Case Study for California and Germany," *Applied Energy*, vol. 104, no. 0, pp. 666 – 682, 2013.

[88] K. Mets, F. De Turck, and C. Develder, "Distributed Smart Charging of Electric Vehicles for Balancing Wind Energy," in *IEEE Third International Conference on Smart Grid Communications (SmartGridComm)*, Nov 2012, pp. 133–138.

[89] O. Sagosen and M. Molinas, "Large Scale Regional Adoption of Electric Vehicles in Norway and the Potential for Using Wind Power as Source," in *International Conference on Clean Electrical Power (ICCEP)*, June 2013, pp. 189–196.

[90] J. Basilio and S. Matos, “Design of PI and PID Controllers with Transient Performance Specification,” *IEEE Transactions on Education*, vol. 45, no. 4, pp. 364–370, Nov 2002.

[91] O. Tremblay, L.-A. Dessaint, and A.-I. Dekkiche, “A Generic Battery Model for the Dynamic Simulation of Hybrid Electric Vehicles,” in *IEEE Vehicle Power and Propulsion Conference*, Sept 2007, pp. 284–289.